GEOLOGY OF THE INTERMOUNTAIN WEST
an open-access journal of the Utah Geological Association
ISSN 2380-7601

Volume 13 ***2026***

THE GEOLOGIC GLORY OF THE LOWER JURASSIC NAVAJO SANDSTONE, SOUTHERN UTAH

Thomas C. Chidsey, Jr.

GEOLOGY OF THE INTERMOUNTAIN WEST

an open-access journal of the Utah Geological Association

ISSN 2380-7601

Volume 13 ***2026***

Production

Cover Design and Desktop Publishing
Douglas A. Sprinkel

Cover

Spectacular cross-bedding with secondary alteration and banding in the eolian Lower Jurassic Navajo Sandstone, Yant Flat, about 30 miles (50 km) northeast of St. George, Washington County, southwestern Utah. Photograph courtesy of Tyler Knudsen, Utah Geological Survey.

Become a member of the UGA to help support the work of the Association and receive notices for monthly meetings, annual field conferences, and new publications. Annual membership is $30 and annual student membership is only $5. Visit the UGA website at www.utahgeology.org for information and membership application.

The UGA board is elected annually by a voting process through UGA members. However, the UGA is a volunteer-driven organization, and we welcome your voluntary service. If you would like to participate please contact the current president or committee member corresponding with the area in which you would like to volunteer.

Utah Geological Association formed in 1970 from a merger of the Utah Geological Society, founded in 1946, and the Intermountain Association of Geologists, founded in 1949. Affiliated with the American Association of Petroleum Geologists.

GEOLOGY OF THE INTERMOUNTAIN WEST
an open-access journal of the Utah Geological Association
Volume 13 ***2026***

The Geologic Glory of the Lower Jurassic Navajo Sandstone, Southern Utah

Thomas C. Chidsey, Jr.
Utah Geological Survey, Emeritus
Sandy, UT 84094, USA; tomchidsey@gmail.com

ABSTRACT

The eolian Lower Jurassic Navajo Sandstone is a "glorious" geologic formation famous for its spectacular cross-bedding, magnificent cliffs, rounded sandstone domes, and countless beautiful canyons in southern Utah. The Navajo is a favorite of many geologists and is a large part of what makes southern Utah a favorite destination for tourists, outdoor enthusiasts, geology students, and researchers.

The Navajo Sandstone was deposited in a hot, arid setting as part of a great Sahara-like eolian erg landscape of huge dunes with interdune oases, wadis, and sand sheets. The sand was originally sourced, in part, from the northern Appalachian region and Canadian highlands far to the east and northeast, transported by sand-laden river systems along a circuitous route (north, northwest, west, and then south) to the western part of the continent, deposited in a large delta system, and then during times when parts of the delta dried, was blown into the Utah area from the north and northwest. Navajo bedding types and sedimentary structures include those found in modern sand dunes such as tabular, wedge, and textbook-quality trough cross-bedding; wind ripples; grainfall, grainflow, and avalanche deposits; and soft-sediment deformation.

The formation is called the Navajo Sandstone in central and southern Utah, northern Arizona, and western Colorado and New Mexico, and is age-equivalent to the upper part of the Nugget Sandstone in northern Utah and western Wyoming. The Navajo ranges in thickness from a depositional pinchout to 2300 feet [0–700 m]. It is separated from overlying Middle Jurassic Carmel/Temple Cap Formations by the J-1 unconformity that represents a hiatus of 10 million years.

The Navajo sandstone beds are friable and composed of clean, fine- to medium-grained, frosted, subrounded to subangular, moderately to well-sorted quartz sand. Sandstone beds are locally bleached by iron-reducing hydrocarbons, weak acids, or hydrogen sulfide. At least eight subfacies, three eolian dune and five non-eolian interdune, have been identified in the Navajo deposits. In two subfacies, thin-bedded sandy microbial (algal) boundstone and wackestone composed of limestone or dolomitic limestone were deposited in interdunal oases.

The Navajo Sandstone has a number of unique features. These include weirdly shaped iron- and manganese-rich diagenetic pipes and columns, beautiful alcoves and hanging gardens, weathered-out iron concretions (Moki marbles) that serve as an analog to "blueberries" found on Mars, unusually contorted bedding formed by soft-sediment deformation, honeycomb (tafone) weathering, and weathered out deformation bands.

The Navajo Sandstone serves as a reservoir for both hydrocarbons and carbon dioxide (CO_2) in central and east-central Utah. Covenant oil field in the central Utah thrust belt has produced almost 34 million

Citation for this article.
Chidsey, T.C., Jr., 2026, The geologic glory of the Lower Jurassic Navajo Sandstone, southern Utah: Geology of the Intermountain West, v. 13, p. 95–162, https://doi.org/10.31711/giw.v13.pp95-162.

barrels of oil since its discovery in 2004. The Navajo is also a significant disposal unit for produced water at Covenant and Drunkards Wash (a large field producing coalbed methane from the Cretaceous Ferron Formation off the northwest flank of the San Rafael Swell. Cores from the Navajo reservoir in Covenant field display many of the same dune and interdune subfacies and other eolian characteristics described from outcrops in the San Rafael Swell to the east. In addition to an oil and gas reservoir, the Navajo is a major aquifer for culinary water supplied to the growing St. George metropolitan area in southwestern Utah and for the Navajo Nation in the Four Corners area in southeastern Utah.

Finally, the Navajo Sandstone has great potential for the geologic storage/sequestration of CO_2 that could be captured from coal-fired power plants in the Castle Valley/eastern Wasatch Plateau area. The Navajo is also being investigated for storage of CO_2 produced as a waste product at a proposed iron ore processing plant in the Iron Springs mining district at the eastern margin of the Basin and Range Province in southwestern Utah.

INTRODUCTION

The Lower Jurassic Navajo Sandstone is perhaps the most well-known lithostratigraphic formation in southern Utah and creates some of the greatest scenery on Earth. The Navajo is represented by the magnificent cliffs and canyons in Utah's five renowned national parks (known as the "Mighty Five"), as well as in national monuments, recreational areas, and other public lands on the Colorado Plateau in the southern part of the state. The Navajo is most famous for massive cross-stratified sandstone beds representing an ancient dune sea or erg—a classic example of an eolian depositional environment.

When one thinks of the eolian Navajo Sandstone, the spectacular cross-bedded exposures in Zion National Park in southwestern Utah immediately come to mind, including such iconic features as The Great White Throne and Checkerboard Mesa (Figures 1A and 1B) (Biek et al., 2024). Farther west are incredible Navajo outcrops capped with Pleistocene basalt flows in Snow Canyon State Park near St. George (Figure 1C). In Capitol Reef National Park in south-central Utah one of the more prominent features is Navajo Dome composed of the Navajo (Figure 1D). The Navajo also forms the flanks of many large Laramide orogenic uplifts (latest Cretaceous through Eocene) such as the San Rafael Swell in east-central Utah (Figure 2) and the Circle Cliffs uplift farther to the south. Hanging valleys in the Navajo are the sites of beautiful waterfalls (e.g., Lower Calf Creek Falls [Figure 3A] in the Grand Staircase-Escalante National Monument in south-central Utah), alcoves and hanging gardens (Figure 3B), and potholes (also called waterpockets) often filled with water and teaming with life (Figure 3C). Magnificent examples of rock arches develop in the Navajo such as Corona Arch and inspiring Rainbow Bridge, the fourth largest sandstone arch in the United States having an interior height of 245 feet (74.7 m) and a 234-foot span (71.3 m) (Wilbur, 2007), in southeastern and south-central Utah, respectively (Figures 4A and 4B). "The Wave" in the Paria Canyon-Vermilion Cliffs Wilderness Area in Arizona along the border with Utah displays amazing deformed eolian features (Figure 5). Glen Canyon Dam that creates Lake Powell also in southern Utah and northern Arizona, is anchored in the Navajo (Figure 6). For the outdoor adventurer, some of Utah's most unique and popular trails are through or on top of the Navajo, such as the terrifying Angels Landing Trail in Zion National Park (Figure 7A) and the biker's challenging Slickrock Trail near the town of Moab in southeastern Utah (Figure 7B). The Navajo is not without its geologic hazards, specifically rock falls from exfoliation along surface fractures (Figure 8).

This paper describes many facets of the Navajo Sandstone that geologists, geotourists, outdoor enthusiasts, and sightseers from all over the world come to Utah to study and enjoy the glorious scenery created by this amazing formation. The following sections summarize the general Navajo characteristics, paleogeography, petrography, eolian depositional environments, stratigraphy, bedding and sedimentary structures, unique features, qualities as a reservoir for hydrocarbons and nat-

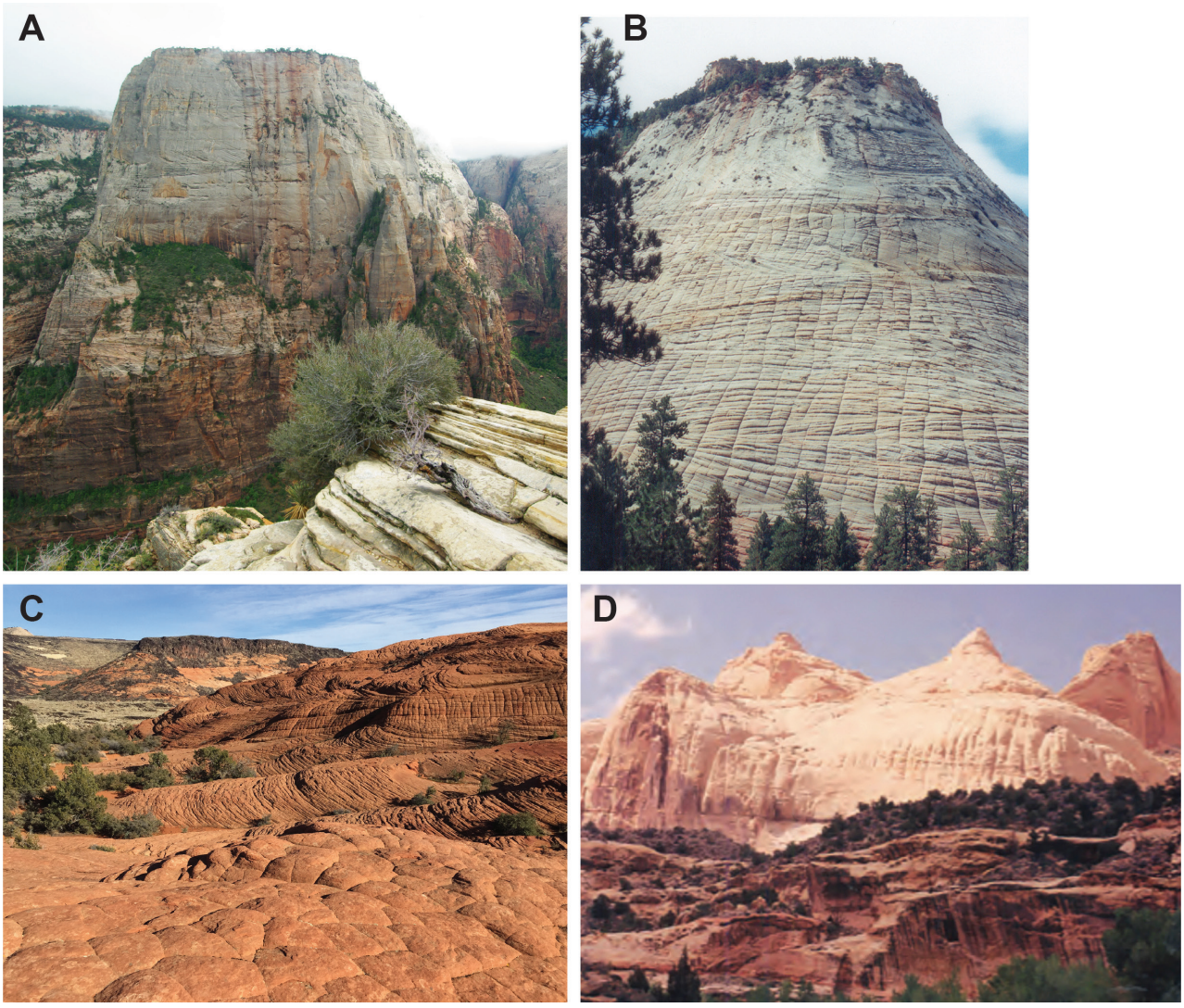

Figure 1. Examples of "glorious" features carved in the Lower Jurassic Navajo Sandstone in Utah. (A) The Great White Throne, and (B) Checkerboard Mesa (displaying combined cross-bedding and jointing), Zion National Park. Photographs of Zion National Park courtesy of Adam McKean, Utah Geological Survey, and from Biek et al. (2024), respectively. (C) Snow Canyon State Park. Photograph courtesy of Michael D. Vanden Berg, Utah Geological Survey. (D) Navajo Dome, Capitol Reef National Park. Photograph from Morris et al. (2024).

ural carbon dioxide (CO_2) production and as an aquifer for produced water disposal and culinary water storage, and finally, potential carbon sequestration to slow the warming of the planet.

GEOLOGIC OVERVIEW

General Description

Navajo Sandstone commonly weathers into vertical to rounded cliffs, alcoves, domes, and knobs of cross-bedded sandstone that epitomize what is called Utah's "slickrock" country. The Navajo ranges in thickness from 0 to 2300 feet (0–700 m) (Hintze and Kowallis, 2021). The sandstone is friable and weakly cemented, fine- to medium-grained, and contains little or no matrix material. Sand grains are composed primarily of clear quartz, which are subrounded to rounded, moderately to well sorted, and frosted, indicative of an eolian environment. Most grains are imperfectly rounded having spherical, discoidal, or lentiform shapes, which are covered with various amounts of quartz overgrowths

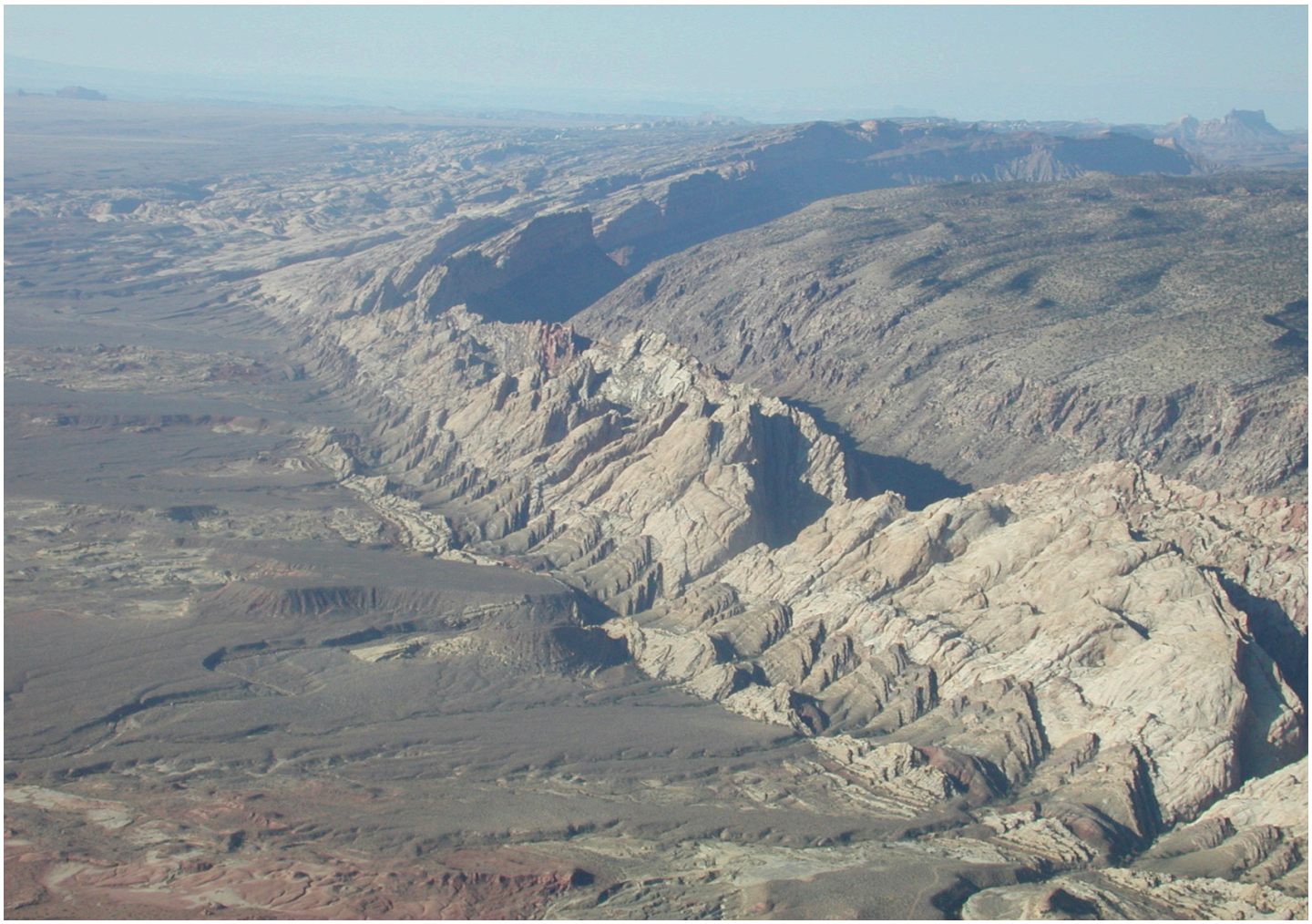

Figure 2. East-dipping Navajo Sandstone (massive pale-tan cliffs and slick rock) on the east flank of the Laramide-age San Rafael Swell, east-central Utah.

and pressure solution features (Freeman and Visher, 1975; Doelling and Davis, 1989). Consisting of over 90% quartz grains, most of the sandstone is classified as a quartz arenite. The sandstone does contain minor amounts of feldspar and some scattered heavy mineral grains, typically magnetite, as well as zircon, garnet, tourmaline, staurolite, and rare mica flakes and sphene (Gregory, 1948, 1950; Doelling and Davis, 1989; Chidsey et al., 2020). Calcite or dolomite are the main cementing agents, with varying amounts of secondary silica and iron oxide (Table 1; see **Dune and Interdune Subfacies in Outcrop** section).

The Navajo Sandstone also contains thin, horizontal, discontinuous beds of gray limestone and dolomitic limestone, very fine grained sandstone, and siltstone, which seem at odds with the extensive well-known and dominating, thick to massive, eolian cross-bedded sandstone. These deposits represent interdune oases, playas, or sabkhas (discussed in detail in later sections), matching the color of the surrounding eolian sandstone. Additionally, channel-form or wadi deposits occur in the Navajo. These rocks consist of a tan to reddish-orange, medium- to coarse-grained sandstone matrix containing rounded sandstone fragments or clasts and gray to dark-gray, subangular to subrounded dolomitic limestone clasts (Chidsey et al, 2024).

The main body of Navajo Sandstone is very uniform in terms of the rock yet has a wide variety of descriptive colors on outcrops – white, tan, buff, cream, yellow, yellowish-gray, gray, salmon, pink, orange, vermillion

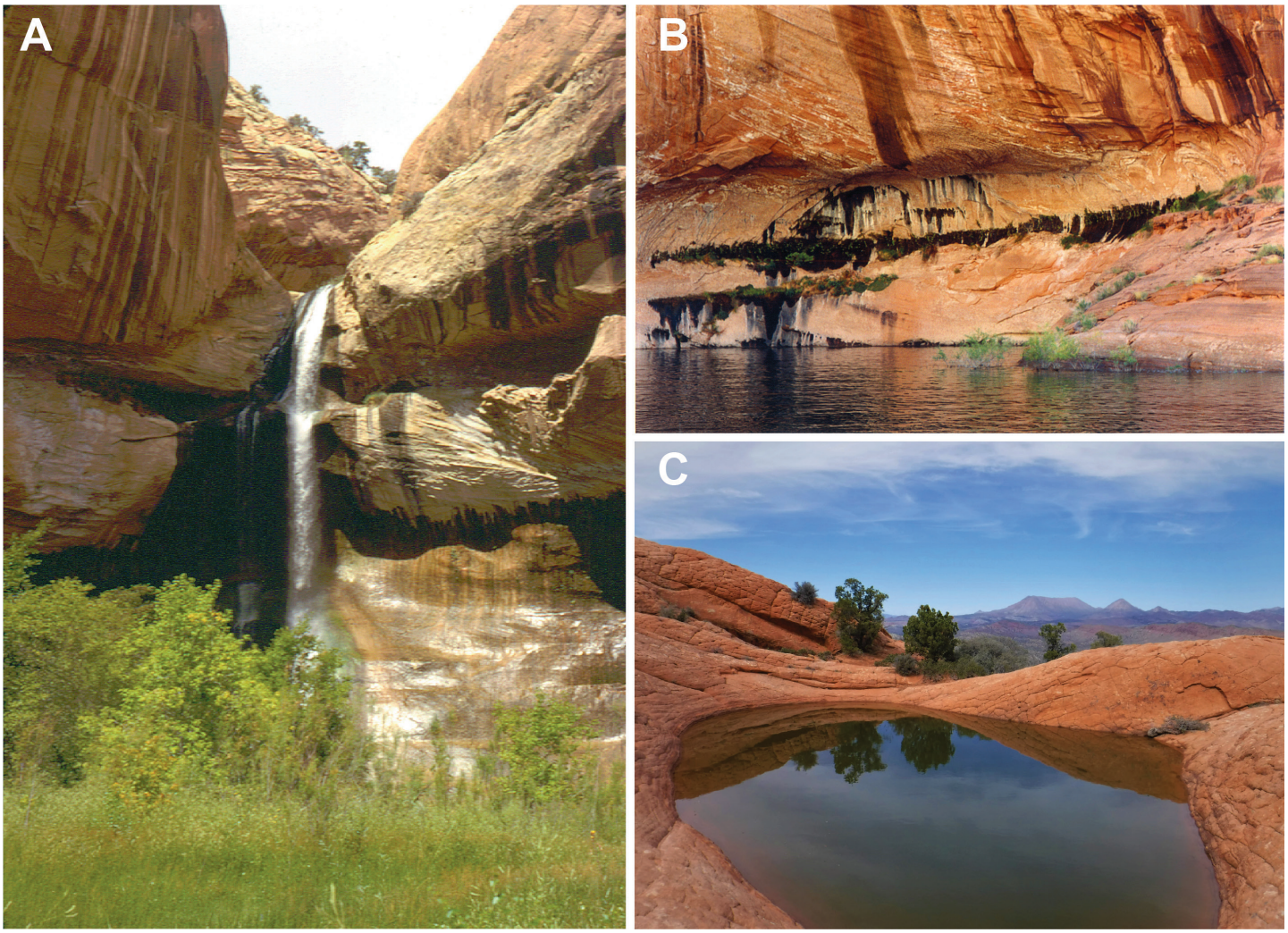

Figure 3. (A) Lower Calf Creek Falls in the Grand Staircase-Escalante National Monument in south-central Utah. Doelling et al. (2024). (B) Navajo alcove with a hanging garden in Rainbow Bridge National Monument. (C) Water pocket in the Navajo Sandstone, Red Mountain Wilderness Area, southwestern Utah. Water pockets often dry out between large rainstorms. Photograph courtesy of Jim Davis, Utah Geological Survey.

reddish-orange, light-reddish-brown, brown. These colors are due to the presence of varying amounts and oxidation states of hematite, goethite, and limonite in pores and cements. In Zion National Park, the Navajo is stained red from mudstone in the overlying Sinawava Member of the Temple Cap Formation. Sandstone beds are locally bleached (altered due to the removal of hematic cement that coats quartz grains) by iron-reducing hydrocarbons, weak acids (acidic water), or hydrogen sulfide migrating through the rocks as especially observed in Snow Canyon State Park and elsewhere (Beitler et al., 2005; Nielsen and Chan, 2009; Nielsen et al., 2009; Nielsen, 2010). Dense ironstone (concentration of hematitic and goethitic cement) also occurs in the Navajo when oxidizing (fresh) water migrates through the rock. Geochemical analyses of Navajo samples from the Snow Canyon area are shown in Table 2 (Willis and Hayden, 2015). Moderate-reddish-brown sandstone has 1% to 2% iron oxide. White, strongly bleached sandstone contains less than 0.5% iron oxides whereas very dark brownish-black ironstone contains up to 21% iron oxides and 5% manganese oxides (Willis and Hayden, 2015).

However, the most distinctive feature of the Nava-

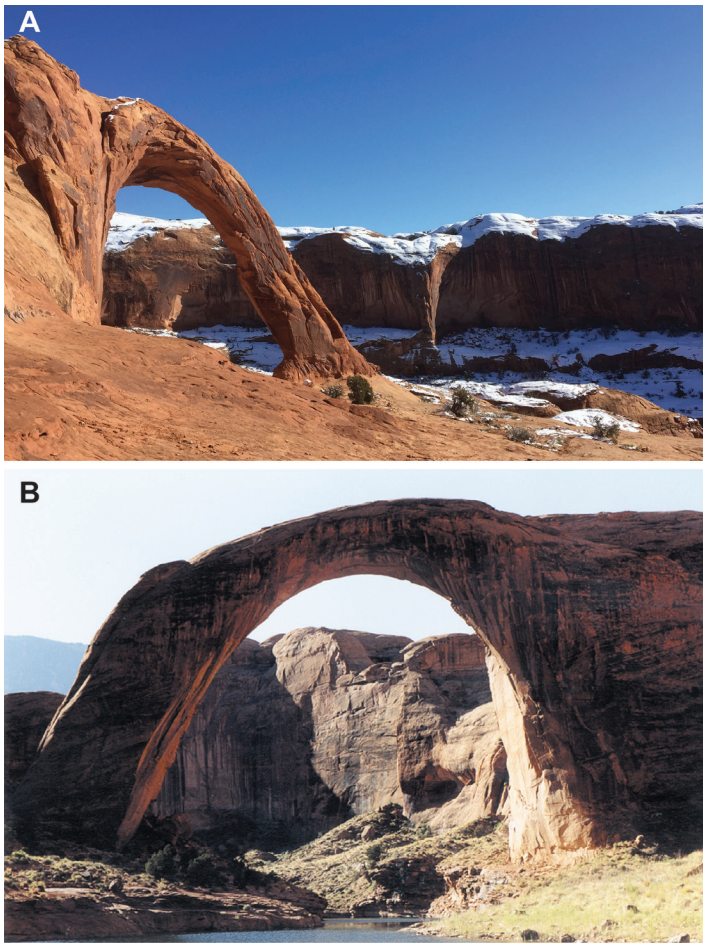

Figure 4. Sandstone rock arches developed in the Navajo Sandstone. (A) Corona Arch, southeastern Utah. Photograph courtesy of Greg McDonald, Utah Geological Survey. (B) Rainbow Bridge, Rainbow Bridge National Monument, south-central Utah.

jo Sandstone is its classic broad, sweeping, high-angle, cross-bedding; photographs of which can be found in many textbooks on sedimentary geology as representing an eolian depositional environment. The cross-beds are characterized by sets of large, high-angle troughs, reaching thicknesses up to 45 feet (14 m). These large-scale cross-beds that dominate the Navajo are etched out by weathering and are often highlighted by desert varnish (iron-manganese-oxide staining). Dips of cross-beds between set boundaries vary as much as 40° from the nearly horizontal structural attitude of the formation (Ahlbrandt and Frybreger, 1982). Contorted bedding and soft-sediment deformation, wind ripples, and small-scale trough cross-bedding are also abundant.

Leaching of calcite cement by rainwater has caused the outer 1 to 3 inches (2.5–7.6 cm) of the Navajo Sandstone to become softer and more friable (Dames & Moore, 1972). Stress-release exfoliation of this weaker, outer sandstone and frost wedging along joints lead to massive rock falls (Figure 8).

Paleogeography, Paleoclimate, and Sand Source

During the Early Jurassic (190 Ma) most of Utah was the site of a vast coast and inland dune field or erg deposited on a broad, flat plain in the southern part of the Western Interior Basin (Blakey, 1994; Peterson, 1994) (Figure 9). The Navajo/Nugget erg covered about 140,000 square miles (350,000 km^2) (Figure 9A) (Beitler et al., 2005) and began in latest Triassic time, lasting approximately 20 million years (Hintze and Kowallis, 2021). The erg extended from present-day Wyoming to as far south and far west as northern Arizona and southeastern California, respectively, depositing the Navajo Sandstone and age-equivalent rocks.

The Western Interior Basin was on the southwestern region of the North American craton, extending from northern Arizona and New Mexico north to the Canadian border (Peterson, 1994). The southwestern border of the basin and continent (now California) was bounded by a magmatic arc (Figure 9A), which resulted from subduction beginning during the Triassic (Dubiel, 1994; Marzoff; 1994; Peterson, 1994). The Western Interior Basin was structurally shallow and asymmetrical providing the accommodation space to receive and preserve massive amounts of eolian sand. Additionally, back-arc subsidence along the magmatic arc to the west and possible foreland basin subsidence adjacent to the early stages of what would become the Elko orogeny during the Middle Jurassic also contributed to the preservation of these thick Early Jurassic eolian deposits (Blakey, 1994; Thorman, 2011; Thorman et al., 2020).

A rapidly subsiding trough, the Utah-Idaho trough, was present on the west side of the Western Interior Basin from what is now southeastern Nevada through western Utah north into eastern Idaho (Peterson, 1994). The eastern side of the basin was a structural shelf that was disrupted in southeastern Utah by three ancestral

Figure 5. "The Wave" in the Navajo Sandstone in the Paria Canyon-Vermilion Cliffs Wilderness Area along the Utah-Arizona border. Photograph courtesy of Mario F. Caputo, Mt. San Antonio College.

Figure 6. Glen Canyon Dam, Arizona, which forms Lake Powell, is built into the Navajo Sandstone, Glen Canyon National Recreation Area, Utah and Arizona.

(Pennsylvanian to Permian) uplifts – the Uncompahgre, Monument (also referred to as the Piute platform), and Emery (Peterson, 1994; Hintze and Kowallis, 2021). These features influenced sedimentation and depositional thickness during the Early Jurassic. The Utah-Idaho trough provided accommodation space for as much as 2200 feet (670 m) of Navajo sand in southwestern Utah as found in Zion National Park, whereas 80 to

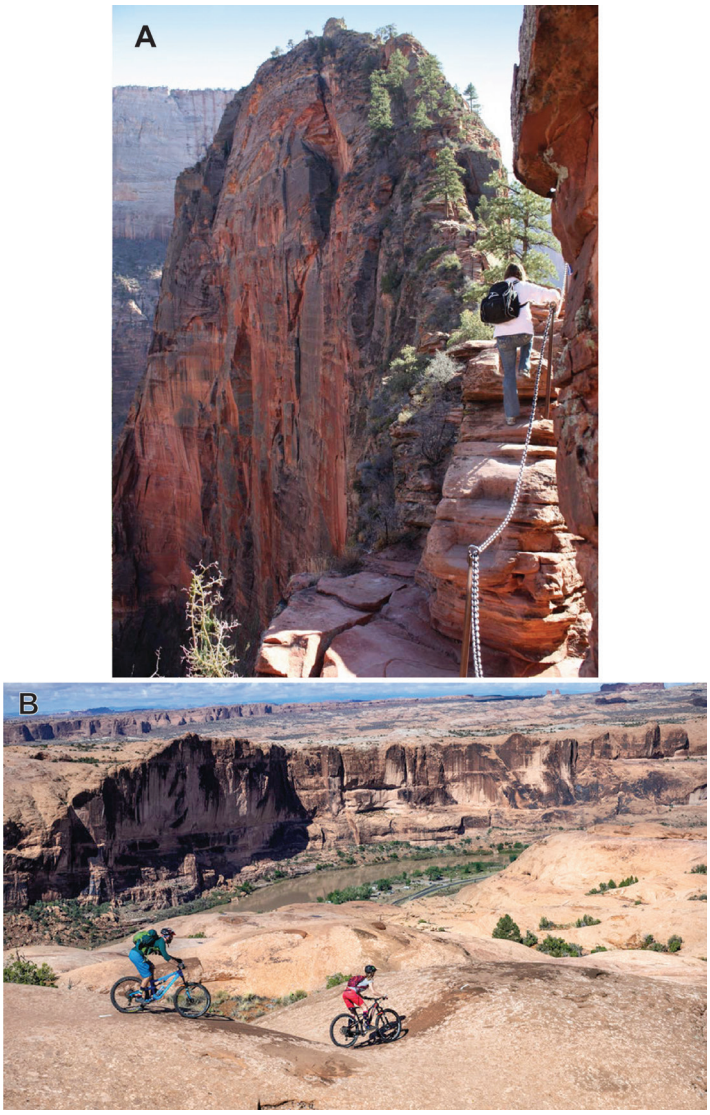

Figure 7. Popular trails through and on the Navajo Sandstone. (A) Angels Landing Trail in Zion National Park shown here with 2000-foot cliffs (610 m) on both sides. Photograph courtesy of Zion Ponderosa Ranch. (B) Bikers on the Slickrock Trail above the Colorado River and Arches National Park beyond. Photograph by Chuck McQuade, courtesy of Outdoor Alliance.

Figure 8. Rock fall of Navajo Sandstone in 1983, Rainbow Bridge National Monument, demonstrating the process of exfoliation and the dangers posed to visitors. The event was captured on film by Tom Tyler, a park visitor, who regularly went to Rainbow Bridge via Lake Powell, at full pool in 1983, and donated the photograph to the National Park Service. National Park Service poster photograph.

800 feet (24–240 m) are present in the shelf region to the east depending on proximity to the ancestral uplifts (Hintze and Kowallis, 2021); note that these thicknesses have also been likely affected by erosion of the Navajo Sandstone by the development of the J-1 unconformity discussed later.

The climate at the time of Navajo eolian sand deposition was hot and dry in the southern Western Interior Basin (Peterson, 1994; Blakey, 1994). Globally, the Earth was under a hothouse cycle in the Early Jurassic and North America was in the northern hemisphere of the Pangea supercontinent, which was beginning to break up. North America was also moving northward with Utah and the Western Interior Basin between 15° to 30° north latitude, the driest and hottest latitude zones where atmospheric circulation patterns favor erg

Table 1. Mineral compositions and porosity, in percent based on 300-point count analysis, from samples of Navajo subfacies collected from outcrops along the west flank of the San Rafael Swell in east-central Utah (Chidsey et al., 2020). See Figure 44 for location of study area.

Subfacies*	**LTC**	**STC**	**RWE**	**WAM**	**SAM**	**PDI**	**EID**
Minerals/Lithics/Porosity							
Monocrystalline Quartz	52.7	40.3	57.6	29	45	22.3	37.3
Undulating Quartz	20.3	16	14.2	22.3	24.5	12.6	11
Polycrystalline Quartz	1	6	0	0.7	0.7	1.3	0
Total Quartz	74	62.3	71.8	52	70.2	36.2	48.3
K Feldspar	3.3	2.3	2.6	4.7	3.3	6.3	2.3
Plagioclase	8	3.7	2.3	3	4.6	1.3	0
Total Feldspar	11.3	6	4.9	7.7	7.9	7.6	2.3
Clay	0	8.3	0	0	0	2.6	0
Heavy Minerals	0	0	0.7	3.7	0.7	0	0.7
Calcite (Cement)	0.3	0.3	3	33	2.7	51	44
Lithics	0	0.3	0	0	0	0.3	0
Porosity	14.3	18.7	18.5	3.7	18.5	2	4.7
TOTAL	99.9	95.6	98.9	100.1	100	99.7	100

*Subfacies abbreviations: LTC = large trough cross-bedded, STC = small trough cross-bedded, RWE = reworked eolian, WAM = wavy algal mat, SAM = sandy algal mat, PDI = poorly developed interdune, and EID = evolving interdune; no data was collected for the ephemeral fluvial channel (EFC) subfacies.

creation (Kocurek and Dott, 1983; Peterson, 1988, 1994; Parrish, 1993; Allen et al., 2000; Loope et al., 2001; Hintze and Kowallis, 2021); e.g., basically the same latitudes as the Sahara and Arabian Deserts of today. High temperatures persisted throughout the Jurassic even though the continent continued to move north (Parrish, 1993).

The magmatic arc and associated elevated terrain bordering the southern Western Interior Basin (figure 9A) may have produced a rain shadow that further affected the climate and helped create the right conditions for major erg development (Peterson, 1994; Blakey, 1994). Thus, the overall paleoclimate and paleogeography of the basin were idea for sand-flow paths and subsequent accumulations into dune fields and the even Navajo larger erg (Blakey, 1994).

In southeastern and southwestern Utah, lithofacies and facies associations (perennial and ephemeral fluvial, distal fluvial/playa, sabkha, and erg-margin and erg-center environments) and genetic stratigraphy studied by Sansom (1992) document the evolution of the Navajo erg. In the southeast, Early Jurassic facies were climatically controlled transitioning from a fully fluvial to fully eolian environment. This transition was rapid in some areas while gradual in others due to the flow of subsurface Pennsylvanian-age salt and the creation of salt-cored structures, which affected dune field accumulations (Sansom, 1992). In the southwest, the genetic succession transitions, due to eustatic control(?), from a distal fluvial to a sabkha and finally to an erg environment. The Navajo erg advanced and contracted in re-

Table 2. Geochemical analyses, rock descriptions, and location of Navajo Sandstone samples from the Snow Canyon area, southwestern Utah. From Willis and Hayden (2015).

Sample No.	SiO2	Fe2O3	MnO	Na2O	MgO	Al2O3	K2O	CaO	TiO2	BaO	Total
SC0302	90.09	0.49	0.01	0.88	0.16	2.89	0.14	0.25	0.07	0.05	95.03
WA0305	63.86	21.10	5.28	0.36	0.19	1.51	0.25	0.86	0.02	0.59	94.02
WA0306	67.79	18.05	0.05	0.80	0.18	2.53	0.33	0.85	0.06	0.07	90.71
WA0307	77.10	1.69	0.08	4.83	0.18	5.25	0.15	0.15	0.35	0.23	90.01

Sample No.	Desciption	Quadrangle	UTM 12 S mN (lat N)	UTM 12 S mE (long E)
SC0302	White, strongly bleached sandstone	Santa Clara	4125779 N (37.2494°)	266983 E (113.6272°)
WA0305	Glossy, very dark-brownish-black ironstone	Washington	4116385 N (37.1651°)	268031 E (113.6125°)
WA0306	Dull, very dark-brownish-black ironstone	Washington	4116385 N (37.1651°)	268007 E (113.6128°)
WA0307	Typical moderate-reddish-brown sandstone	Washington	4112875 N (37.1337°)	269023 E (113.6003°)

ICP method; datum NAD 27
Samples represent the variability of secondary alteration of the Navajo Sandstone caused by migration of reducing (acidic water) and oxidizing (fresh water) through the rock; samples range from highly bleached sandstone (removal of hematitic cement) to dense ironstone (concentration of hematitic and goethitic cement).

sponse changes in the fluvial systems along its southern margins (Blakey, 1994). It grew from a number of isolated smaller dune fields that coalesced as they enlarged with increased sand supply (Sansom, 1992).

Based on U-Pb isotopic dating of detrital zircon (DZ) grains (Dickinson and Gehrels, 2003, 2010; Rahl et al., 2003; Allred and Blum, 2022; Allred et al. 2023), the Navajo sand was originally sourced, in part, from the northern Appalachian region and Canadian highlands far to the east and northeast. The DZ U-Pb signature of detrital grains from different phases of the Appalachian orogenesis and orogenic system, which extended 3100 miles (5000 km) from eastern Canada to West Texas and Mexico, is dominated by Grenville (about 1250 Ma) and Appalachian (about 500 to 275 Ma) age groups (Allred and Blum, 2022; Allred et al., 2023). The grains with the Appalachian signature were likely transported by transcontinental, sediment-laden rivers to the late Paleozoic, western passive margin of Laurentia beginning in the Middle Pennsylvanian and continuing through the Triassic (Leary et al., 2020; Allred and Blum, 2022; Allred et al., 2023); this margin was an active depocenter since the Neoproterozoic (Stewart and Suczek, 1977). These postulated river systems followed a circuitous route north and north-northwest turning to the west and then south in the western part of the continent, possibly including sedimentary contributions along the way from present-day Arctic Canada and Greenland (Trettin, 1991; Beranek et al., 2010). Sediment transport west from the central and southern Appalachian orogenic system was probably precluded because: (1) during sea-level lowstands a large part of the eastern section of the continent drained into the Ouachita trough, a narrow Cambrian through Mississippian deep-water basin, and a foreland basin in the Pennsylvanian during the early stages of the Ouachita orogeny; (2) during sea-level highstands, most of the midcontinent was dominated by shallow-marine carbonate deposition; and (3) farther west, the Pennsylvanian through Permian Ancestral Rockies were an additional barrier (Allred and Blum, 2021).

Sand-rich sediments were deposited in a large delta system, and then during times when parts of the delta dried due to the arid climate, the sand was blown into the Utah area consistently from the north and northwest causing the sand to migrate southward with time (Blakey, 1994; Dickinson and Gehrels, 2003, 2009). This scenario is supported by regional analyses of the mean

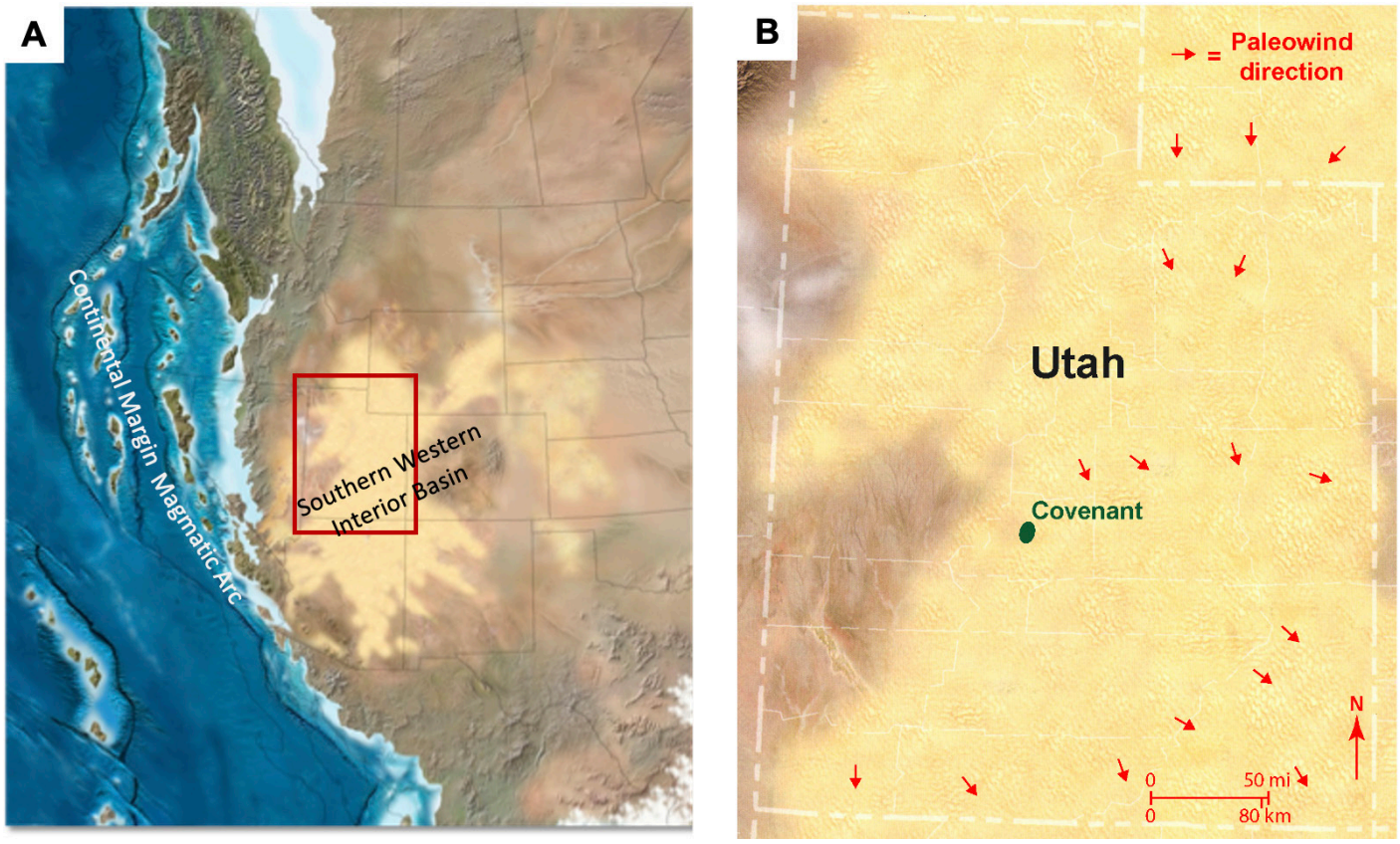

Figure 9. Paleogeography during the Early Jurassic (190 Ma) showing the Navajo erg. (A) Western U.S. regional paleogeography; brown outline shows the location of B. After Blakey (2013). (B) Utah paleogeography; arrows indicate dominant paleowind directions. Modified from Picard (1975) and Blakey and Ranney (2008). Note the location of Covenant oil field to be discussed later.

dip of Navajo dune foreset beds that indicate paleowind directions were dominantly from the north and northwest (Figure 9B) (Picard, 1975; Blakey, 1994; Peterson, 1994).

Depositional Environments: Modern and Ancient

Dunes and Interdunes

The Navajo Sandstone was deposited mostly as eolian dunes, but also includes interdune oases or ephemeral lakes, wadis, playa, sabkhas, and sand sheets (Blakey, 1994; Peterson, 1994). Navajo dunes were large (widths up to 2200 feet [670 m]) to small, straight-crested to sinuous, coalescing, transverse barchanoid ridges as suggested by the formation's large-scale cross-bedding. Navajo dunes tended to be stacked in sets with each set having cross-beds representing slightly different wind directions or deposition-wind-scour, followed by a new episode of deposition (Figure 10). Dune sets are often separated by generally thin, planar beds (with some crinkle bedding) composed of mud, silt, and very fine grained sand representing an interdune environment such a playa, sabkhas (some deposits contain evaporites) or mudflat. Tepee structures (sedimentary structures formed by evaporation of water and subsequent precipitation of minerals within sediment that causes expansion and buckling to form teepee-like shapes in peritidal environments [Wikipedia, 2026]) and mineral casts created by the growth of halite and other evaporite minerals further suggest the presence of playas (Sansom, 1992).

Modern analogs to the Navajo Sandstone include

Figure 10. Cross-bedding in five stacked sets in the Navajo Sandstone, Buckhorn Wash, San Rafael Swell, east-central Utah. View to the north-northeast. Dune foreset beds indicate a complexity occurred in paleowind directions within local areas. Here wind directions shifted from the north and northwest to from the south and southeast as shown between the cross-bedding sets. Photograph courtesy of Michael Chidsey, Sqwak Productions Inc.

the great ergs in the Sahara Desert with their giant dunes having widths over 2000 feet (600 m). However, a closer small modern analog can be found at the Little Sahara Recreation in west-central Utah (Figure 11). In this area prevailing winds blowing from the southwest have transported sand from a large delta built where the Sevier River drained into Pleistocene Lake Bonneville (Hamblin, 2004). The Little Sahara contains a wide variety of dune types, as well as interdune areas, analogous to those of the Jurassic erg represented by the Navajo. Figure 11 displays a moment in time for the Little Sahara dune field, and shows how rapidly eolian deposits change over a relatively short distance. Applied to a hydrocarbon reservoir or water aquifer, the Little Sahara demonstrates the potential for heterogeneity that can exist even in a massive sandstone such as the Navajo.

Oases

The Navajo Sandstone was deposited near sea level, and high paleo-water table conditions produced "oases"—ponds, lakes, and springs that filled some low depressions. The water table was a climatically controlled and thus fluctuated over time (Sansom, 1992; Peterson, 1994). Deposition occurred when springs and lakes existed for relatively long periods of time. Modern oases pockmark the Sahara. These bodies are spring-fed by shallow groundwater and are commonly surrounded by a thin belt of lush vegetation bounded immediately by large dunes (Figure 12A). Numerous ponds due to a high water table are found between gigantic dunes in the Alashan area of the Gobi Desert in northern China (Figure 12B) (Webster, 2002). Hundreds of shallow interdune ponds in between elongate dunes also occur in Lençóis Maranhenses National Park on the northeastern coast of Brazil (Figure 12C) where the water table is very close to the surface.

The Navajo Sandstone within the Glen Canyon National Recreation Area and other Navajo outcrops throughout southern Utah contain light-gray, thin-bed-

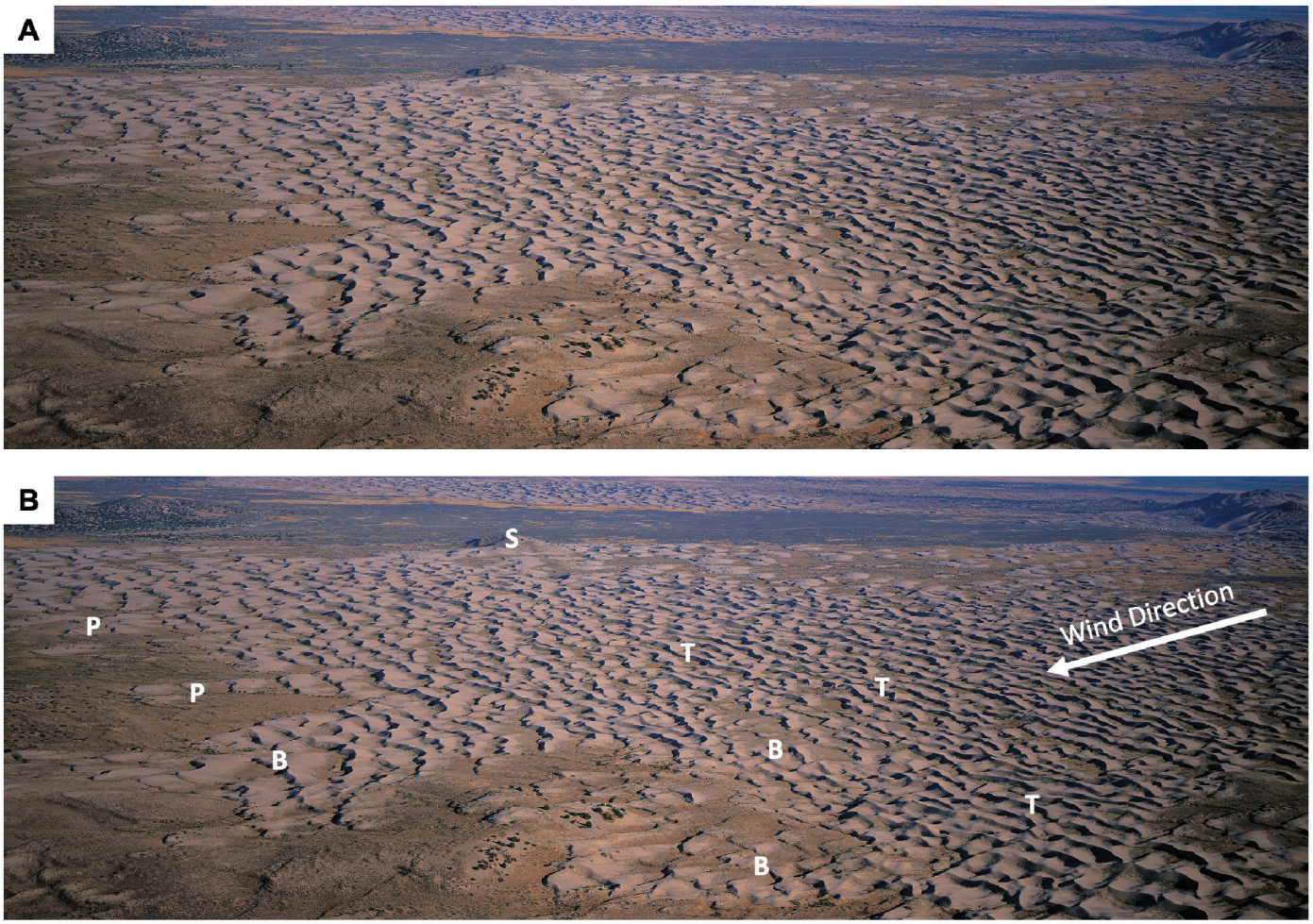

Figure 11. Modern dune field in the Little Sahara Recreation Area, west-central Utah; A unannotated, B annotated. Winds blowing from the southwest have transported sand from a now-exposed large delta built by the Sevier River into Pleistocene Lake Bonneville. The photograph shows a wide variety of dune types: low parabolic dunes with trailing arms (P), crescent-shaped barchan dunes (B), transverse dunes (T), and a large star dune (S). On the right the dunes are spaced closely together but in the center the dunes become more separated by interdune areas, and then on the left there are even larger areas of interdune deposits. After Hamblin (2004).

ded, lenticular carbonate beds interpreted to represent interdune oases deposits (Doelling and Chidsey, 2012; Parrish et al., 2017, 2019; Anderson et al., 2024) (Figure 13A). Many limestone beds also contain cryptalgalaminites (algal laminae) most likely created by coccoid blue-green algal or cyanobacterial processes as organic mats in shallow ponds and lakes of Navajo oases. Beds can be followed for thousands of feet or pinch out over short distances (Figure 13B). These deposits are laminated, 5- to 10-feet (1.5–3 m) thick and horizontally bedded (Figure 13C). The surfaces of the upper parts of these beds often display oscillation ripple marks and desiccation features such as mudcracks (Figure 13D) and salt casts. There are increases in soft-sediment deformation along the margins of limestone deposits due to fluid flow caused by the upward pressured of groundwater (Chan et al., 2023). Some oasis beds yield fossil plants including tree trunks, vertebrate and invertebrate fossils, and dinosaur tracks (Figure 14) and other trace fossils (Stokes, 1991; Santucci and Kirkland, 2010; Riese et al., 2011; Britt et al., 2016; Tran et al., 2025). Fresh groundwater at a shallow depth had to persist for prolonged periods of time, perhaps many thousands of years, to allow the lake or pond limestone deposits

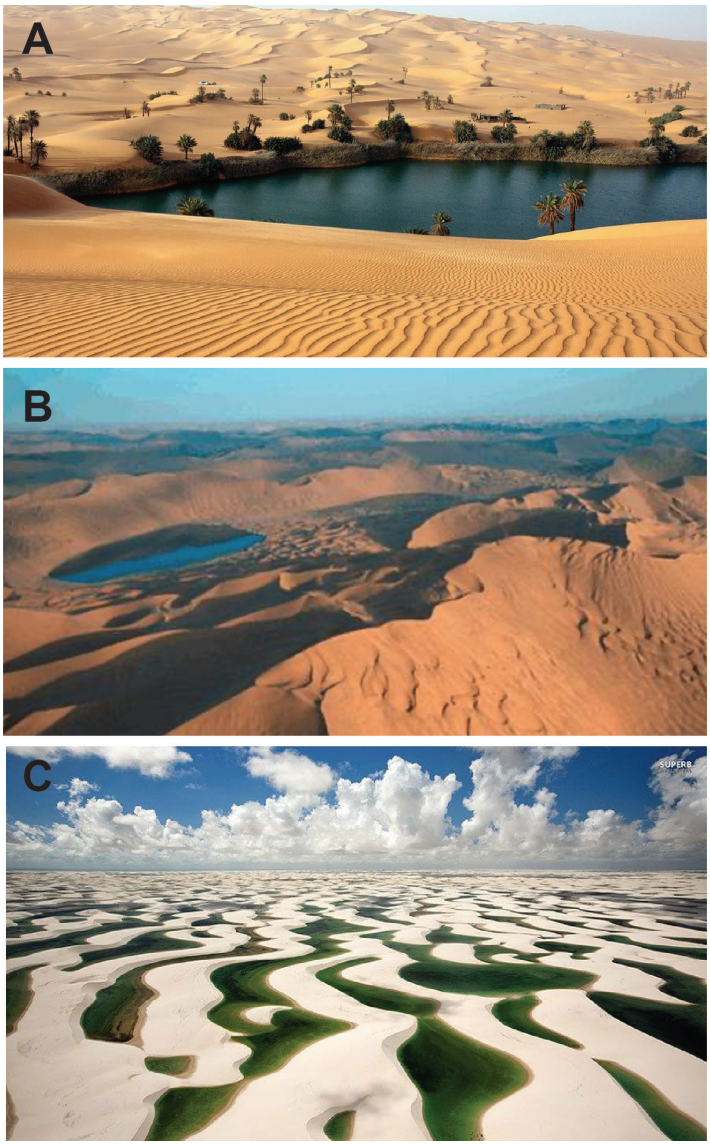

Figure 12. Navajo Sandstone interdune analogs. (A) Modern oasis in the Sahara Desert, Libya. Photograph courtesy of Shutterstock. (B) Numerous ponds between gigantic dunes in the Alashan area of the Gobi Desert in China. Modified from Webster (2002). (C) Dunes and lakes in Lençóis Maranhenses National Park, Brazil. Note the green color representing algal growth. Photograph courtesy of Misadventures.

of these oases to develop their observed thicknesses (Stokes, 1991; Anderson et al., 2024).

Wadis

In addition to oases, large deserts contain wadis. A wadi is a stream bed or channel in desert regions that is usually dry. It may be a steep-sided, boulder-laden ravine that is the site of torrential flooding during rainy seasons. They commonly occur in the Sahara and Middle East (Figure 15). Deposits representing wadis are also present in the Navajo Sandstone (Figure 16A) (Chidsey et al., 2012, 2024). They are channel-form and have abrupt and slightly irregular bases and tops. These deposits consist of clasts that vary from pea to small boulder size (Figure 16B). Some contain rip-up clasts imbricated and inclined in the upstream direction.

Sand Sheets

Sand sheets, represented by low-relief, poorly drained, vegetated or gravel pavement deposits, were also common in the Navajo/Nugget Sandstone (Lindquist, 1988). These areas acted as sand transport surfaces.

Bedding, Sedimentary Structures, and Bounding Surfaces

The Navajo Sandstone preserves most bedding types and sedimentary structures found in modern sand dunes. The Navajo is best known for its aforementioned cross-bedding, which includes tabular planar, wedge planar, and trough cross-bedding types, all associated with eolian deposition (Figure 17) (Ahlbrandt and Fryberger, 1982). Tabular planar cross-bedding is rectangular shaped consisting of a cross-bedded unit bounded above and below by planar bounding surfaces (Figure 18). It represents a single unit of deposition. Foresets, or cross-stratum, are also planar to abrupt or slightly concave in the wind direction at their bounding surfaces. Thicknesses range from several inches to 3 or more feet (1 m or more). Wedge planar cross-bedding is wedge-shaped having oblique bounding surfaces and foreset laminae (Figure 18). Trough cross-bedding, for which the Navajo is most famous consists of spoon-shaped (trough-shaped) top and bottom surfaces (see front cover photograph and Figure 10). Cross-bedded units have upward concave curved foresets within erosion scours elongated parallel to the wind direction. Each trough is an individual unit of deposition and can be 8 inches to 3 feet or more (20 cm to 1 m or more) thick.

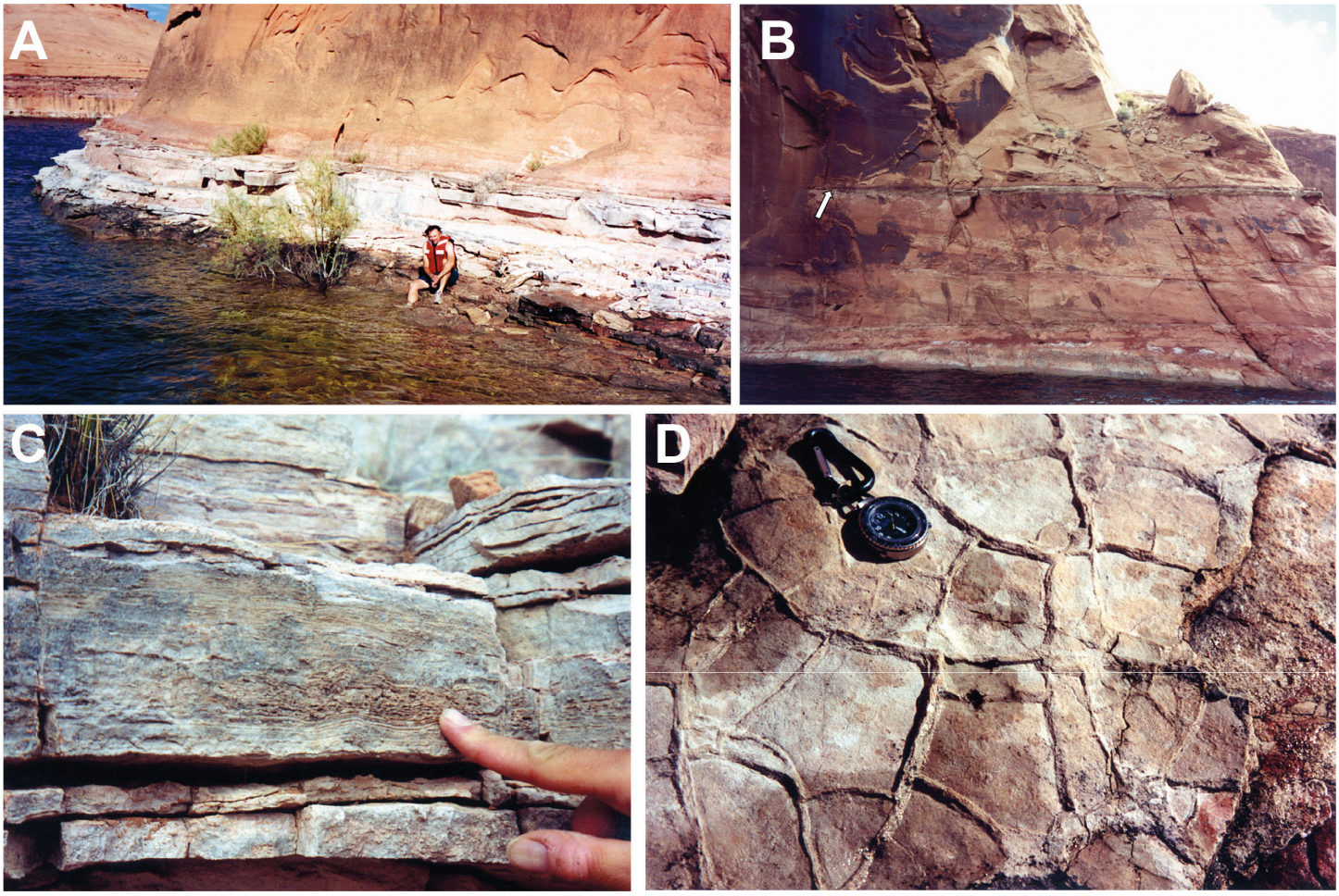

Figure 13. Oasis deposits in the Navajo Sandstone along Lake Powell, Glen Canyon National Recreation Area. (A) Typical limestone oasis deposit (below the high-water line a few feet above swimmer's head); the lake was at near full pool when this photograph was taken in 1999. (B) Rapid pinch-out of thin limestone bed (arrow). (C) Well-displayed algal laminae within limestone. (D) Mudcracks on top of a muddy limestone. From Anderson et al. (2024).

They occur in multiple sets which are in turn truncated downwind by additional troughs and by the overlying set of cross-beds (Neuendorf, et al., 2011; Geological Digressions, 2022).

Modern eolian sand dunes provide analogs (Figure 11) for recognizing the types of eolian deposits and sedimentary structures found within the Navajo Sandstone and its cross-bedding. The upper exposed surface of the rounded domes and knobs of the Navajo are often envisioned as a field of sand dunes frozen in time—however, this is not technically accurate. Whereas weathering and erosion of the upper surface does take advantage of preexisting weaknesses in the rock, these surfaces are erosional, not depositional, and seldom actually replicate paleotopographic surfaces in the Early Jurassic.

In terms of geomorphology (Figure 19A), a sand dune consists of a windward, gently inclined stoss slope from the base to the crest and a steeper leeward slope representing the sand's angle of repose. The leeward slope consists of the brink, which divides the top of the dune from a steep slipface. Blowing sand falls over the brink forming a cornice in a wind shadow. When the cornice grows too large and heavy, it collapses and the sand avalanches down the slipface to form an apron of sand at the base of the dune. The apron has a curved, concave up surface and the point between it and the slipface is the toe of the dune. The generally flat surfaces between dunes, the interdune areas, are dune migrating

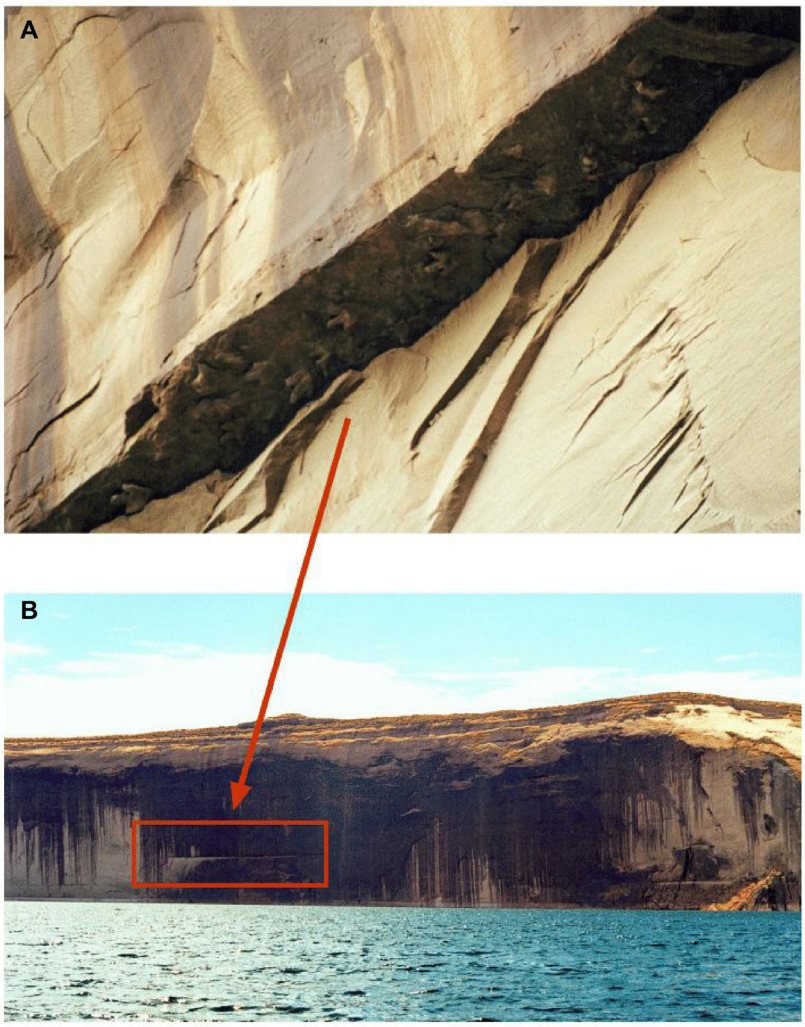

Figure 14. (A) Interdune dinosaur tracks (taken with a telephoto lens) containing at least 14 tracks from a tridactyl (three toed), theropod (bipedal) 20-foot-long (6-m) carnivorous dinosaur (*Eubrontes* sp.) (Lockley et al., 1998; Santucci and Kirkland, 2010; Tran et al., 2025), beneath an overhang in the Navajo cliff face called Tapestry Wall along Lake Powell (B), Glen Canyon National Recreation Area. Red box indicates location of the overhang on the Navajo cliff face. From Chidsey et al. (2012).

surfaces (Ahlbrandt and Fryberger, 1982; Neuendorf et al., 2011; Elder, unpublished date).

A sand dune described in genetic terms deals with how and what sedimentary structures or deposits formed (Figure 19B); i.e., what can be observed occurring in a modern dune and interpreted in Navajo outcrops and well cores. Wind ripples form on the dune crest or on the top beds of the windward surface; they may occur on interdune surfaces but are rarely preserved there. Wind ripples are straight-crested low ridges that extend for long distances perpendicular to the wind direction. The crests and troughs are rounded. However, unlike aqueous ripples, the crests tend to be composed of courser grains than the toughs. Grainfall and grainflow deposits occur on the dune leeside slipface. Grainfall deposits consist of very fine grained sand and silt that settle from the air where the wind loses its energy after crossing the dune crest. Slight differences in the size and mineral composition (e.g., quartz versus heavier iron-bearing minerals) of grainfall deposits can produce pinstripe laminations, a distinctive eolian dune feature. Grainflow deposits consist of a coarser-grained sand mass that moves down the steep dune slipface due to gravity. They are usually thicker than grainfall deposits. Avalanche deposits are found at the base of the dune where sand masses have avalanched down the slipface. They are loosely packed and have significant porosity and permeability (Ahlbrandt and Fryberger, 1982; Neuendorf et al., 2011). Wind ripples, grainfall and grainflow deposits, pinstripe laminations, and avalanche deposits are preserved in the Navajo Sandstone. Where the water table was high during the Early Jurassic these bedding features and sedimentary structures were destroyed by soft-sediment deformation leaving bedding

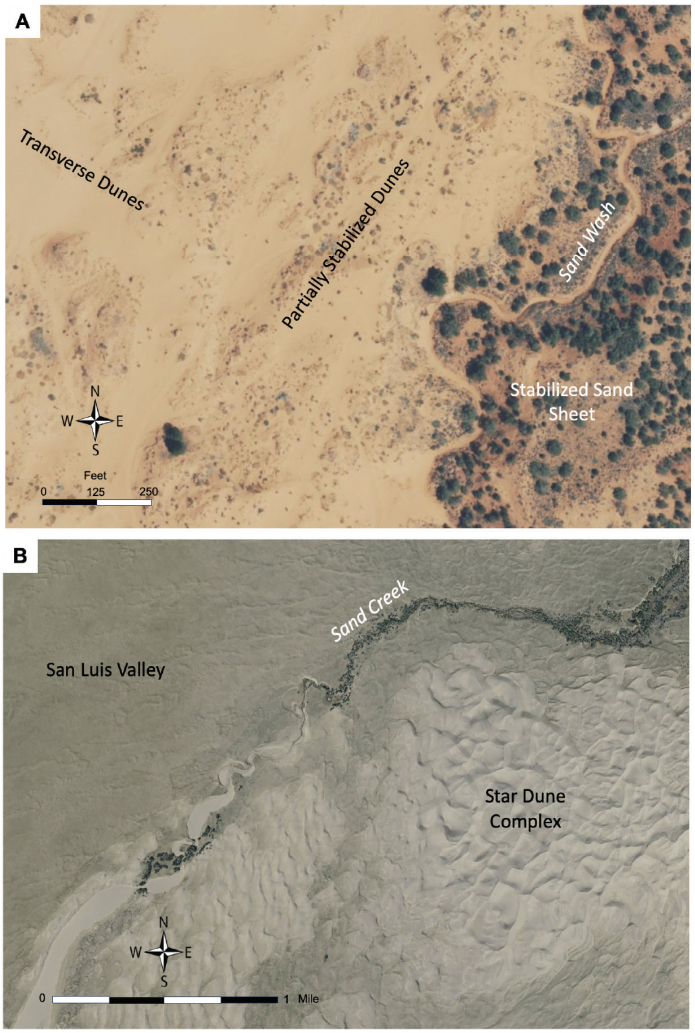

Figure 15. Modern wadis. (A) Aerial view of Sand Wash in Coral Pink Sand Dunes State Park, southwestern Utah. Google Earth image; geology from Ford et al. (2024). (B) Sand Creek in Great Sand Dunes National Park, south-central Colorado. Google Earth image. Fluvial sand and gravel deposited by Sand Wash and Sand Creek could eventually be covered and preserved by migrating dunes.

convoluted or massive and homogenous (Sanderson, 1974; Doe and Dott, 1980). They usually have low porosity and permeability in Navajo reservoirs and aquifers.

Bounding surfaces separate distinct sets of dune bedding, both in modern dunes and in Navajo outcrops (Figures 10, 18, and 19C). Within a dune, a set of cross-beds or foresets is bounded by upper and lower surfaces. Two or more adjacent sets are referred to as cosets (Figure 17). A first-order bounding surface, an interdune or migration surface, is generally horizontal and resistant to erosion. A second-order bounding surface, also called a superimposition surface, develops by the migration of one dune over another. A third-order bounding surface, referred to as a reactivation surface, occurs when the wind direction changes, causing deposition to cease, which is often followed by erosion. A reactivation surface forms when the original conditions and deposition resume above the surface (Elder, unpublished date). Hasiotis et al. (2021) used a sequence stratigraphic approach to define bounding surfaces in the Navajo Sandstone to identify an architectural hierarchy of genetically related sedimentary packages and the surfaces that bound them of both eolian and non-eolian parts of an erg system. They defined seven bounding surfaces and eight depositional units from small to large scale (the reader is encouraged to refer to their paper for details). Navajo bounding surfaces at depth often act as baffles or barriers to fluid flow.

STRATIGRAPHY

The Navajo Sandstone makes up the beautiful White Cliffs of the Grand Staircase, the colossal 10,000-foot-thick (3000-m) sequence of exposed sedimentary rocks that dip north 1° to 2° from the rim of the Grand Canyon, Arizona, about 80 miles (130 km) north to Bryce Canyon National Park in southern Utah (Figures 20A and 21). The dominating escarpment of the White Cliffs, between the Vermilion Cliffs below and the Gray Cliffs above, represents the third step of the Grand Staircase. The east-west-trending Grand Staircase is about 60 miles (100 km) long (Hamblin, 2004).

In 1879, the famous geologist/paleontologist Charles D. Walcott (1850–1927) was the first to measure and describe the entire section comprising the Grand Staircase, from the bottom of the Grand Canyon to the top of the Pink Cliffs near Bryce Canyon National Park (Walcott, 1879; Hintze and Yochelson, 2009). Walcott had already made a name for himself with the 1909 discovery of fabulous fossils in the Middle Cambrian Burgess Shale in the Canadian Rockies of British Columbia, Western Canada; he later became the third director of the U.S. Geological Survey. Walcott's 1879

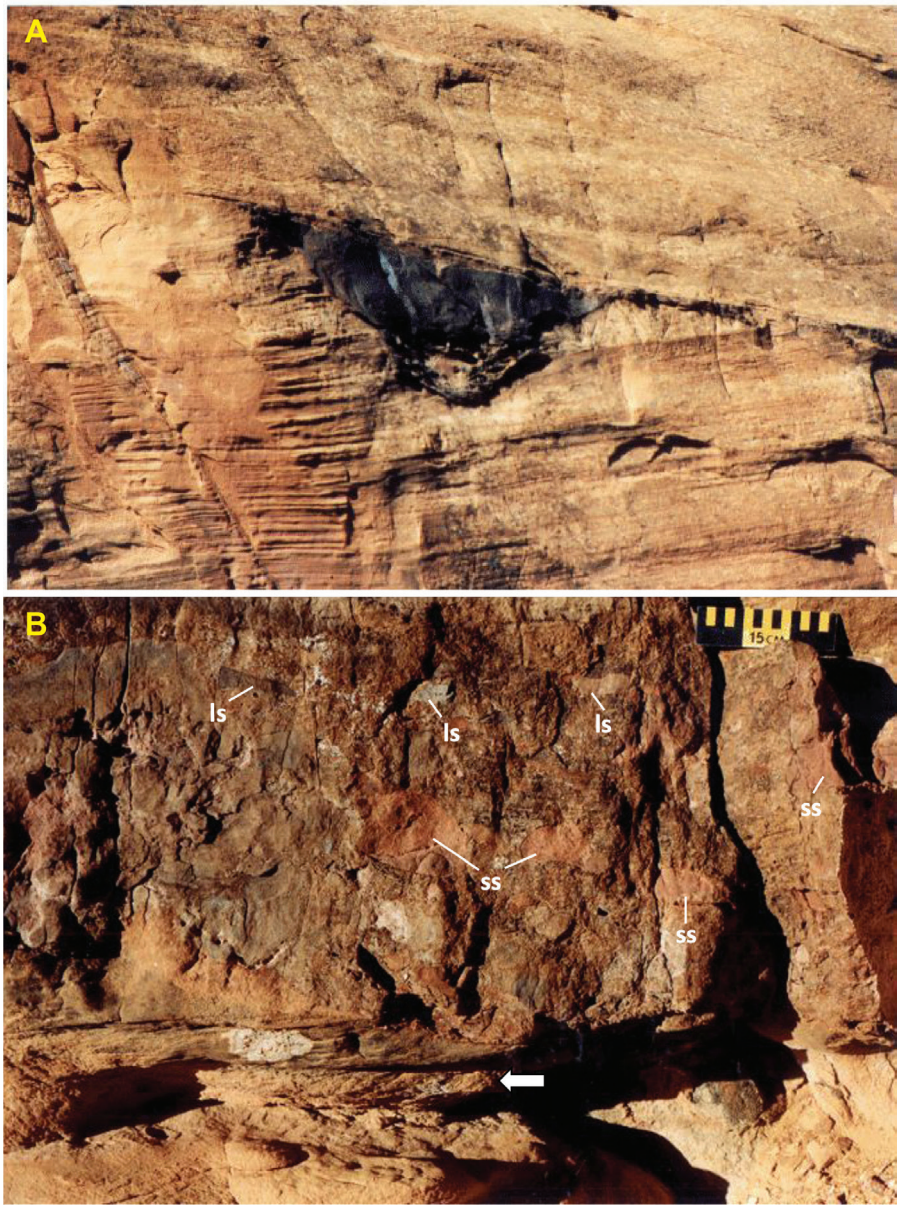

Figure 16. Wadi deposits in the Navajo Sandstone, Rainbow Bridge National Monument. (A) Wadi channel filled with strongly cemented sand; channel deposit is about 5 feet (1.5 m) thick (taken with a telephoto lens). (B) Wadi "pudding stone" consisting of sandstone (ss) and dolomitic limestone (ls) rip-up clasts in a medium- to coarse-grained sandstone matrix. Note horizontal stratification and small-scale cross-beds (arrow) at base of photograph. After Chidsey et al. (2024).

route through the Grand Staircase followed Kanab Creek from its junction with the Colorado River in the Grand Canyon, beginning with Cambrian Muav Limestone, to its northern headwaters on the Paunsaugunt Plateau, ending with the Eocene Claron Formation. Along Kanab Creek through the White Cliffs, he measured and described what would later be established as the Navajo Sandstone in sections 7 and 17, T. 41 S., R. 6 W., SLBL&M, Kane County, Utah. Walcott's Navajo section is presented below as published, slightly modified, in Cross (1908, p. 105) and Doelling and Davis (1989, p. 47):

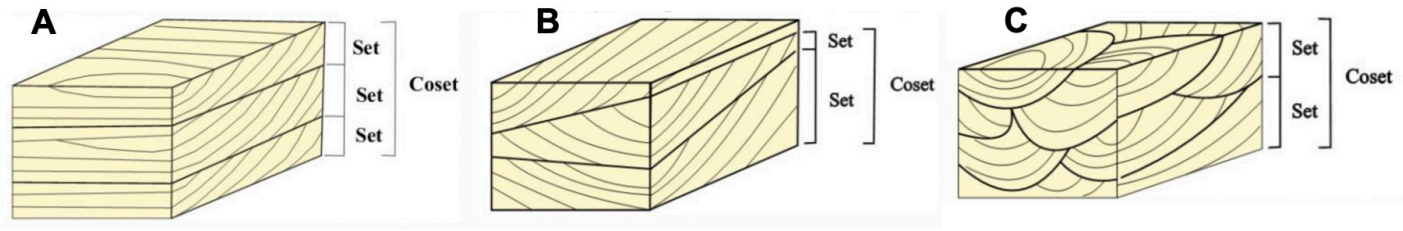

Figure 17. Types of cross-bedding. (A) tabular planar, (B) wedge planar, and (C) trough. After various online geology courses.

Unit 1. White cliff sandstone (i.e., the White Cliffs), massive, cross-bedded, light gray, broken into five principal belts by horizontal lines of bedding, 585 feet (178 m).

Unit 2. Vermilion sandstone, cross-bedded, friable, readily disintegrating, forming the foothills and slope to the more compact sandstone at the northern end of Vermilion Cliffs Canyon, 650 feet (198 m).

Unit 3. Gray and reddish-brown, cross-bedded sandstone, horizontal beds of varying thickness divide the mass into bands from 25 to 100 feet (8–31 m) thick, 300 feet (91 m).

Unit 4. Evenly bedded red sandstone; upper part an indurated, dark reddish-brown stratum; indurated layers alternate with more friable layers and shales beneath, 120 feet (37 m).

Unit 5. Massive gray sandstone, cross-bedded; upper part is a light gray massive friable bed, the entire mass is subdivided into six principal beds by sub-horizontal lines of bedding of a dark, more indurated sandstone, the beds are from 20 to 80 feet (6–24 m) thick, and may be seen on many steep escarpments along the canyon, 310 feet (95 m).

Walcott used rock color and topographic expression to define units 1 through 3 in the fairly homogeneous 1535-foot-thick (468-m) section of cross-bedded sandstone comprising the main body of the Navajo Sandstone (Doelling and Davis, 1989). The middle vermilion or pink sandstone is generally less resistant than the other two units. Units 4 and 5 fit the thickness and descriptions of the Tenney Canyon Tongue of the Kayenta Formation and the Lamb Point Tongue of the Navajo Sandstone (Doelling and Davis, 1989), discussed in the next section.

Gregory and Moore (1931) and (Doelling and Davis, 1989) argue against the use of color in subdividing the Navajo Sandstone. They reasoned that the lines dividing the color changes are commonly not exactly horizontal and cross the formation without regard to texture, stratification, or cross-bedding (Doelling and Davis, 1989). However, Biek et al. (2024) still divides the Navajo into three informal subunits in Zion Canyon National Park generally following Walcott's 1879 description, in ascending order, the brown, pink, and white subunits. The brown subunit is cliff-forming, likely more strongly cemented by iron oxide (hematite). The middle pink subunit is friable, porous, and uniformly colored by hematitic staining. The upper white subunit forms the massive high cliffs. The white color represents a change in oxidation state of the iron-bearing cementing minerals (iron oxide [hematite] to hydrated iron oxide [limonite] and oxyhydroxide [goethite]) (Chan and Parry, 2002; Nielsen et al., 2009; Biek et al., 2024). Biek et al. (2024) does recognize that the boundaries between these subunits are irregular rising and falling across sets of cross-beds.

There is no type section or type locality for the Navajo Sandstone; however, Walcott's measured section noted above could serve as the type section. It was named for the "Navajo Country" of southeastern Utah and northeastern Arizona (likely within Navajo Canyon) in the Navajo Nation, as described by Gregory (1917). The Navajo Sandstone was originally considered the upper

Figure 18. Tabular and wedge planar cross-bedding in the Navajo Sandstone, Buckskin Gulch area, Kane County, south-central Utah. View to the east. Dune foreset beds indicate dominant paleowind direction from the north. Photograph courtesy of Mark Milligan, Utah Geological Survey.

formation of the La Plata Group (Gregory, 1917) but was later reassigned to the Glen Canyon Group by Baker (1936). Walcott's 1879 Navajo section through the White Cliffs along Kanab Creek is considered a primary key reference section for the Navajo Sandstone in Utah's far south. About 140 miles (230 km) to the northeast in east-central Utah, another primary key reference section (a composite section) for the Navajo has been measured and described along the west flank of the San Rafael Swell in the Justensen Flats/Devils Canyon area just south of Interstate 70 (NW1/4SE1/4 section 2 and NW1/4NW1/4 section 10, T. 23 S., R. 9 E., SLBL&M) in Emery County, Utah (see Hanson, 2007; Dalrymple and Morris, 2007; Chidsey et al., 2020).

There are two drillholes that can serve as primary key subsurface reference sections for the Navajo Sandstone. The State 16-2 research well (renamed the State 16-2LN-CC, API No. 43-019-50089, after the horizontal leg was drilled; section 16, T. 22 S., R. 17 E., SLBL&M) was drilled on the northwest end of the northwest-southeast-trending Paradox fold and fault belt, Grand County, southeastern Utah. Excellent drill cuttings were recovered through the entire Navajo section at 10-foot (3 m) intervals from the top at 1660 feet (506 m) to the base at 2040 feet (622 m) (Chidsey, 2023). The Federal 17-3 well (API No. 43-041-30036;

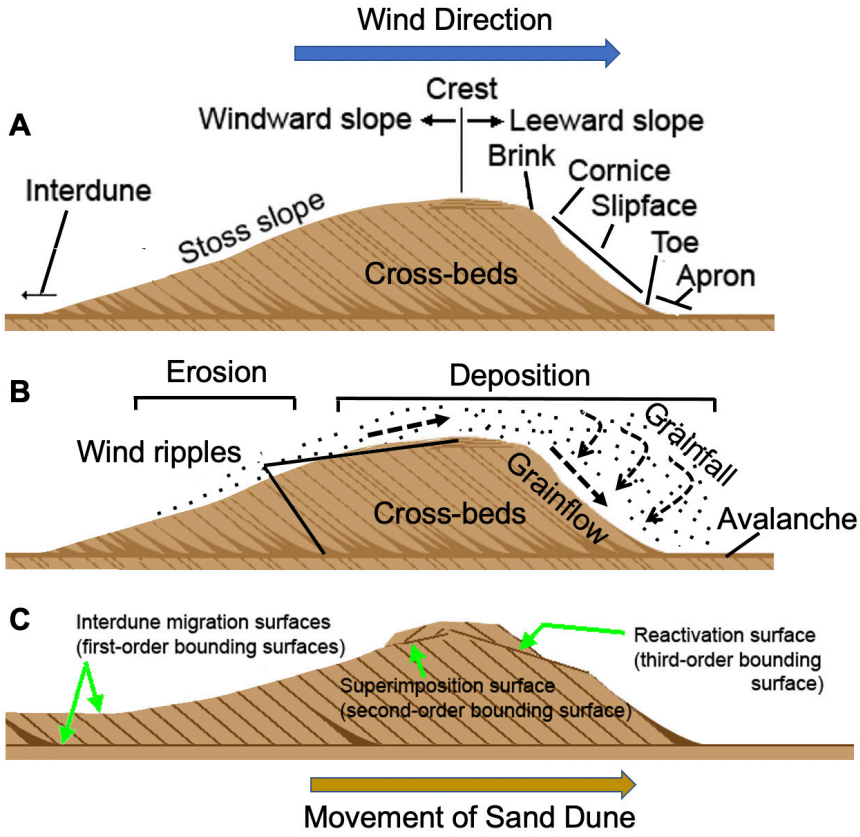

Figure 19. Diagrams of dune terminology. (A) Geomorphic terms. (B) Genetic terms. (C) Bounding surface types. Modified from Elder (date unknown) and Neuendorf et al. (2011).

NW1/4 SW1/4 section 17, T. 23 S., R. 1 W., SLBL&M) was drilled in Covenant oil field in the central Utah thrust belt, Sevier County, Utah. Although this well penetrated a structurally complex Mesozoic stratigraphic section, it cored a non-faulted upper Navajo reservoir section from the top of the formation at 6774 feet (2065 m) to 6294 feet (1918 m), as well as 35 feet (11 m) of the unconformably overlying Sinawava Member of the Middle Jurassic Temple Formation. This core has been used continually over the past 20 years for numerous research studies and as a teaching tool for student and industry groups because of its well-displayed reservoir properties and eolian facies. Both the cuttings and cores from the State 16-2 and Federal 17-3 wells, respectively, are publicly available at the Utah Geological Survey's Core Research Center in Salt Lake City.

REGIONAL CORRELATIONS

The Navajo Sandstone extends from the Grand Staircase to central Utah. Age-equivalent rocks to the Navajo include the upper part of the Nugget Sandstone in northern and northeastern Utah and southwestern Wyoming (Sprinkel et al., 2011b). The Aztec Sandstone exposed in the Mojave Desert of Nevada, Arizona, and California is considered correlative to the Navajo Sandstone. However, a U-Pb zircon date of 170 ± 3 Ma obtained from the Aztec Sandstone in the Cowhole Mountains of southeastern California indicated a Middle Jurassic age and correlative to the Temple Cap Formation (Busby et al., 2002; Sprinkel et al, 2011a). The Lower Jurassic Navajo Sandstone is unconformably capped by the Middle Jurassic Temple Cap Formation (Figures 22A and 22B). However, the Temple Cap is not present everywhere because it was deposited on an irregular surface (Peterson and Pipiringo, 1979; Doelling et al., 2013), e.g., some areas in the San Rafael Swell, Henry Mountains basin, and along the Waterpocket Fold in east-central and south-central Utah, where the Navajo is overlain by the Middle Jurassic Carmel Formation (Sprinkel et al., 2011a, 2024; Doelling et al., 2013).

The Temple Cap Formation in most of southwestern and central Utah is represented by a northeast- to

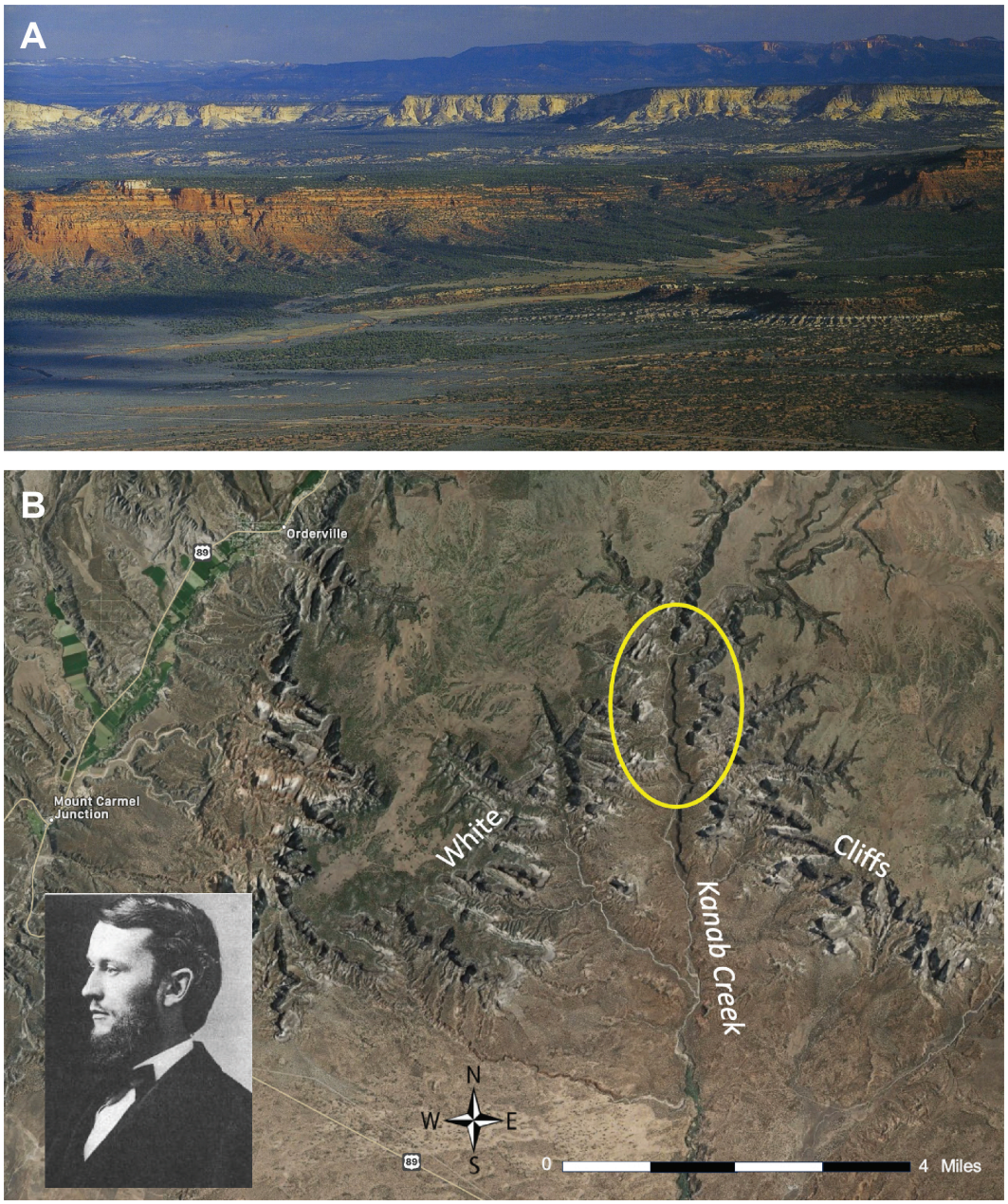

Figure 20. (A) The Grand Staircase with the imposing White Cliffs composed of the Navajo Sandstone. View north from Kaibab Plateau, Arizona. After Hamblin (2004). (B) Google Earth image showing location (yellow oval) along Kanab Creek of Charles D. Walcott's 1879 measured section and description of the Navajo Sandstone composing the White Cliffs of the Grand Staircase, Kane County, Utah. Inset: Charles D. Walcott in 1873. From Wikipedia (2025).

southwest-trending coastal dune field (the middle White Throne Member consisting of white cross-bedded sandstone) that intertongues with marine to marginal marine tidal flat and sabkha deposits (the lower Sinawava and upper Esplin Point Members consisting of reddish-brown mudstone, siltstone, and very fine grain sandstone) (Blakey, 1994; Peterson, 1994; Blakey and Ranney, 2008; Hartwick, 2010; Sprinkel et al., 2011a). The interbedded sandstone, siltstone, mudstone, limestone, and gypsum of the Carmel Formation represent restricted and marginal to marine depositional environments (Blakey and Ranney, 2008; Douglas A. Sprinkel, Utah Geological Survey, written communication, January 2013; Hintze and Kowallis, 2021). The Navajo Sandstone contact with the Temple Cap or Carmel Formations is usually sharp and distinct.

The Navajo Sandstone, and its tongues, are conformably underlain by the Lower Jurassic Kayenta Formation, which is characterized by distinct reddish-brown, blocky siltstone and fine-grained sandstone beds that form steep ledgy slopes. The Kayenta was deposited in an arid sandy braided river system with perenni-

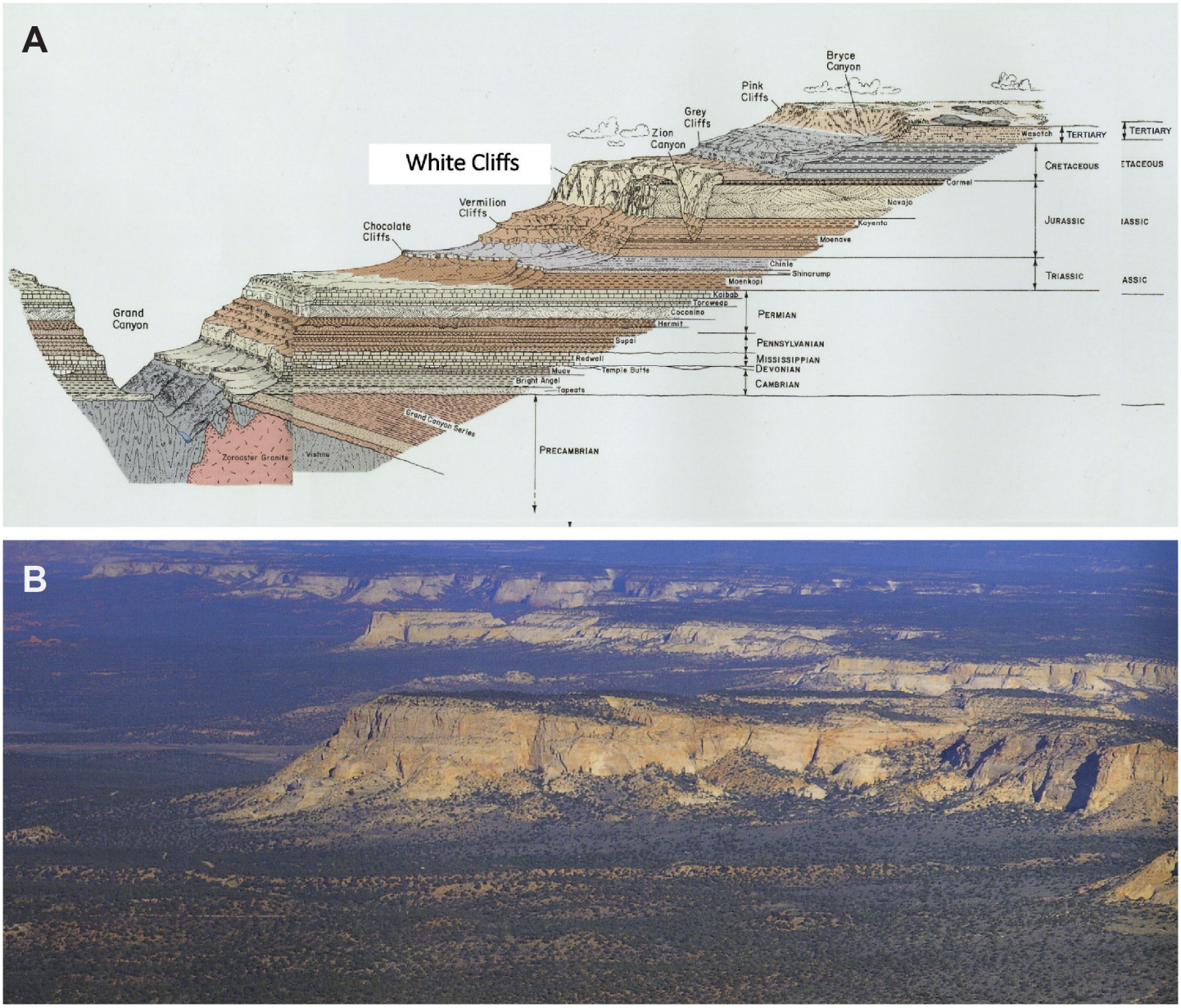

Figure 21. (A) Stratigraphy of the Grand Canyon and Grand Staircase; note the dominating White Cliffs composed of the Navajo Sandstone. (B) View of the White Cliffs looking west just north of the town of Kanab, Utah. The Navajo thickness ranges from about 1700 to 2200 feet (520–670 m) (Hintze and Kowallis, 2021). After Hamblin (2004).

al streams flowing west from the remaining Ancestral Rockies and the Appalachians far to the east (Lynds and Hajek, 2006; Blakey and Ranney, 2008).

Tongues of the Navajo Sandstone

The basal contact of the Navajo Sandstone with the Kayenta Formation is typically sharp and intertonguing (Doelling and Davis, 1989; Tuesink, 1989). Although five to as many as ten Navajo tongues may be present (Blakey, 1994), two are relatively thick and extensive enough to be named and mapped – the Lamb Point and Shurtz Tongues.

Lamb Point Tongue

As mentioned at the beginning of the **Stratigraphy** section, units 4 and 5 of Walcott's 1879 measured section

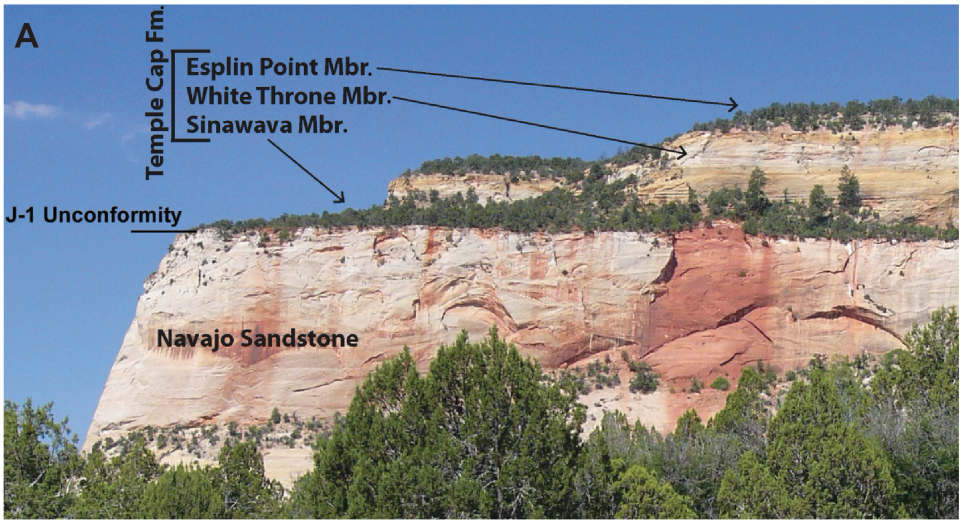

B

Age		Map Unit	Thickness feet (m)	Schematic Column
JURASSIC	San Rafael Group	Summerville Fm.	100-400 (30-120)	
		Curtis Fm.	30-250 (9-75)	J-3 unconformity
		Entrada Sandstone	300-800 (90-240)	gypsum
		Carmel Fm.	200-700 (60-210)	
		Temple Cap Fm.	0-60 (0-18)	J-1 unconformity
	Glen Canyon Gp.	Navajo Ss.	400-650 (120-200)	
		Kayenta Fm.	130-570 (45-90)	
		Wingate Ss.	240-420 (70-130)	scoured surface
Ŧ		Chinle Fm.	130-475 (40-145)	Ŧ-5/J-0 unconformity(?) Ŧ-4 unconformity

Figure 22. (A) Lower Jurassic Navajo Sandstone separated by the J-1 unconformity from the overlying Middle Jurassic Temple Cap Formation; view west at the east entrance of Zion National Park. The red staining on the Navajo cliff face was made by water running off of dark red-brown mudstone in the Sinawava Member of the Temple Cap. Photograph courtesy of Douglas A. Sprinkel, Utah Geological Survey. (B) Stratigraphic column of exposed part of the Triassic and Jurassic section along the western flank of the San Rafael Swell, east-central Utah, including age, thickness, and weathering profile. Modified from Hintze and Kowallis (2021).

probably represent the Tenney Canyon Tongue of the Kayenta Formation and the Lamb Point Tongue of the Navajo Sandstone of modern stratigraphic terminology. The Lamb Point overlies the main body of the Kayenta and is separated from the main body of the Navajo by the reddish-brown, slope-forming, shaly to thin-bedded, fine-grained sandstone of the Tenney Canyon in Kane County north of the border with Arizona topping the Vermillion Cliffs (Figure 21) (Doelling and Davis, 1989).

The Lamb Point Tongue of the Navajo Sandstone was measured and described by Doelling and Davis (1989) in Cottonwood Canyon in the SW1/4 section 15, T. 43 S., R. 7 W., SLBL&M, Kane County, Utah, between the town of Kanab and Coral Pink Sand Dunes State Park 8 miles (13 km) to the west; as a side note, the source of the dune sand in the park is the Navajo. Their section should be considered a primary key reference or type section for the Lamb Point. It is repeated below as published, with slight modifications:

> Unit 5. Sandstone, tan, medium-grained, eolian cross bedded with occasional contorted cross-beds, cliff-former, 48.8 feet (14.9 m).
>
> Unit 4. Sandstone, like unit 5, but slope and ledge-forming, 64.0 feet (19.5 m).
>
> Unit 3. Covered slope (tan sand from ledges and

cliff above), 80.4 feet (24.5 m).

Unit 2. Covered slope (fine-grained orange-brown sand), 65.7 feet (20.0 m).

Unit 1. Sandstone, orange, medium-grained, friable, cross-bedded with angles up to 36°, cross-bed sets up to 25 feet (7.6 m) thick, massive, cliff-former, 74.1 feet (22.6 m).

Total Lamb Point Tongue: 333.0 feet (102 m).

Outcrops of the Lamb Point Tongue pinch out about 18 miles (29 km) west of the reference section in the eastern part of Zion National Park (Biek et al., 2024) and 20 miles (32 km) east, they merge with the main body of the Navajo Sandstone where the overlying Tenney Canyon Tongue pinches out (Doelling and Davis, 1989).

The Lamb Point consists of white to tan to gray, fine- to medium-grained, friable, sandstone with minor reddish-brown siltstone and gray limestone. Sand grains are rounded to subrounded and frosted mainly composed of quartz (90%), chert (5%), and feldspar (5%), weakly cemented by carbonate cement (Doelling and Davis, 1989). Like the main body of the Navajo, the Lamb Point is characterized by spectacular cross-bedding.

Shurtz Tongue

Another more localized tongue of the Navajo Sandstone, the Shurtz Tongue, is present about 50 miles (80 km) northwest of the Lamb Point Tongue in the canyons and ridges east and south of Cedar City in Iron County, Utah. It is named for well-exposed outcrops in Shurtz Canyon about 6 miles (10 km) south of Cedar City in the SE1/4SE1/4 section 10, T. 37, R. 11 W., SLBL&M (Rowley et al., 2006), which has been designated as the type location (Averitt et al., 1955). The Shurtz Tongue overlies the main body of the Kayenta Formation and is separated from the main body of the Navajo Sandstone by the ledgy to slope-forming, reddish-brown, thin- to thick-bedded, mudstone, siltstone, and fine-grained sandstone of the Cedar City Tongue of the Kayenta (Knudsen, 2024). The Shurtz rapidly thins south from 345 to 62 feet (105–19 m) over a distance of 8 miles (13 km), pinching out southward toward the town of Kanarraville; northward the outcrops are cut off by faulting (Averitt et al., 1955; Averitt, 1962; Biek and Hayden, 2016; Chandonia and Hogan, 2023).

The Shurtz Tongue, similar to the main body of the Navajo Sandstone, consists of reddish-orange, medium-grained, cross-bedded sandstone (Averitt and Threet, 1973). However, cross-bedding is generally at a smaller scale than the main body of the Navajo above and significantly more planar (Knudsen, 2024). In addition, the depositional environment for the Shurtz was more of a coastal dune field and sabkha than the classic Navajo erg (Knudsen, 2024).

The Age of the Navajo Sandstone and the J-1 Unconformity

The exact age of the entire Navajo Sandstone in southern Utah is unknown. Volcanic ash beds and fossils are rare and thus prevent a direct date (Willis and Hayden, 2015); note: an incomplete skeleton of *Seitaad*, an Early Jurassic genus of sauropodomorph dinosaur, was collected from the Navajo near Comb Ridge in southeastern Utah (Sertich and Loewen, 2010) and tracks from the large theropod ichnogenus *Eubrontes* and associated ichnofauna have also been reported from numerous Navajo locations in Utah (Lockley et al., 2026). However, the minimum age of the Navajo Sandstone is constrained by ash beds present in the overlying Temple Cap Formation, which yielded $^{40}Ar/^{39}Ar$ isotopic ages ranging from about 173 to 171 Ma or lower most Middle Jurassic (Aalenian) (Kowallis et al., 2001; Sprinkel et al., 2009; Doelling et al., 2013). In addition, Sprinkel et al. (2011a) reported that an ash bed in the Gypsum Spring Formation at Devils Slide in northern Utah's Weber Canyon, yielded a date of 184.6 ± 0.2 Ma (Ar/Ar sanidine) and 183.2 ± 0.49 Ma (U-Pb zircon). The lower part of the Gypsum Spring age is older than the oldest Temple Cap age (Sprinkel, et al., 2024). This suggests the top of the Navajo is about 185 Ma (Pliensbachian). The maximum age of the Navajo is constrained by diagnostic palynomorphs in the underlying Whitmore Point Member (upper member) of the Moenave Formation placing it in the lowermost Lower Jurassic (Hettangian or 201.4 to 199.5 Ma) (Cornet and Waanders, 2006). However, recent U-Pb geochronology

from carbonate beds 213 to 295 feet (65–90 m) above the base of the Navajo near Moab in southeastern Utah, indicate an age of 200.5 ± 1.5 Ma (Hettangian) to 195.0 ± 7.7 Ma (Sinemurian) (Parrish et al., 2019). Thus, the age of the Navajo is bracketed as young as Pliensbachian (192.9–184.2 Ma) to Sinemurian (199–192.9 Ma) or as old as Hettangian (201.3–199.3 Ma). Willis and Hayden (2015) suggest that the upper beds of the Navajo are probably older than 184 Ma (Pliensbachian).

The Navajo Sandstone and Temple Cap/Carmel Formations are separated by the J-1 unconformity, a major regional unconformity (Pipiringos and O'Sullivan, 1978; Peterson and Pipiringos, 1979). The J-1signaled the end of Early Jurassic eolian deposition due to a likely combination of major tectonic, climatic, and eustatic events (Blakey, 1994). It represents a period of major erosion beginning when erg accumulation ceased (Sansom, 1992) and paleotopographic development producing a hiatus of over 10 million years between the Early and Middle Jurassic, as determined by radiometric age data from volcanic ash-fall beds and palynomorph assemblages (Sprinkel et al., 2009, 2011a, 2011b, 2024). Extensive outcrop work, regional well correlations, and the aforementioned age dating of the Middle Jurassic (Temple Cap Formation) throughout Utah conducted by Sprinkel et al. (2011a, 2024) and Doelling et al. (2013) led to a better definition of the J-1. The J-1 is indicated in outcrop by (1) a distinct truncation of windblown cross-beds in the Navajo, (2) slight changes in color to darker brownish-red beds above the J-1, (3) a sparse lag of small—less than 0.1 inch (0.2 cm)—angular chert fragments (Figure 23A), (4) a network of polygonal desiccation cracks filled with sand from the overlying Temple Cap (Figure 23B), (5) brecciation zones, (6) carbonate nodules, (7) extensive bioturbation, and (8) weathering or bleaching that form alteration zones up to 30 feet (9 m) thick (Anderson et al., 2024). However, the J-1 can be very subtle in some areas. For example, the Navajo is slightly more enriched in barium and gallium and less variable in iron oxide than the overlying eolian White Throne Member of the Temple Cap (Figure 22A) based on discriminant analysis of X-ray fluorescence elemental data (Phillips, 2012; Phillips and Morris, 2013; Phillips et al., 2015).

The upper Navajo Sandstone contact with the Tem-

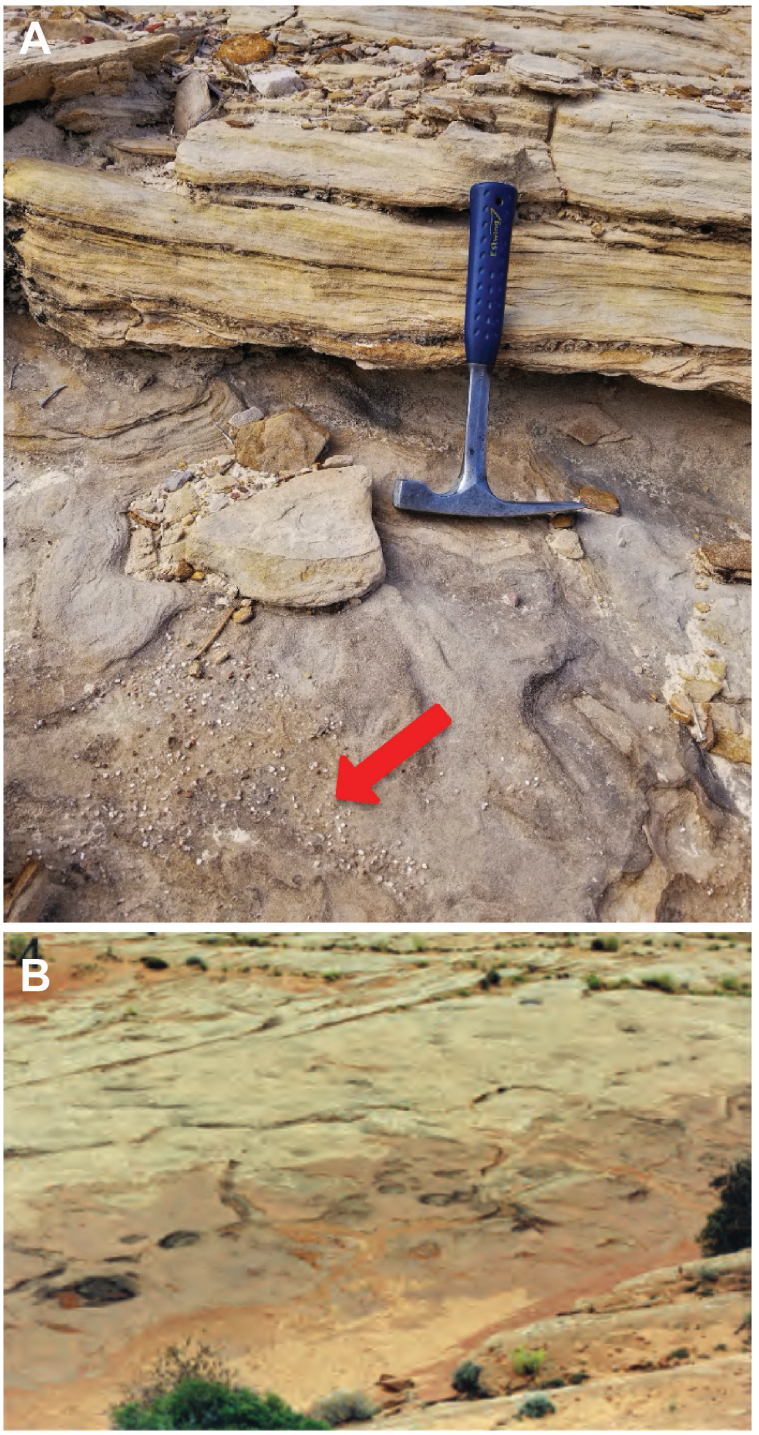

Figure 23. The J-1 unconformity on outcrops. (A) Angular chert granules (arrow), Black Dragon Wash, east flank of the San Rafael Swell, east-central Utah. Rock hammer for scale. Photograph courtesy of Douglas A. Sprinkel, Utah Geological Survey. (B) Shrinkage (desiccation) cracks, Glen Canyon National Recreation Area. From Anderson et al. (2024).

ple Cap Formation undulates with up to 200 feet (60 m) of topographic relief over long distances (Figure 24). This surface creates paleohighs and provides further evidence that the J-1 is a significant regional unconformity. The overlying Temple Cap in turn varies from 0 to 200 feet (0–60 m) thick due to deposition on the paleotopography developed by the J-1 at the Navajo contact (Sprinkel et al., 2011b, 2024; Doelling et al., 2013).

The Navajo Sandstone has a subtle but distinct characteristic geophysical log response; the overlying Sinawava Member of the Temple Cap Formation has a high gamma-ray profile recognized on other logs regionally (Figure 25). This well-defined gamma-ray change allows for easy identification of the Navajo top and correlation from well to well throughout southern Utah. Cores from Covenant field in the central Utah thrust belt

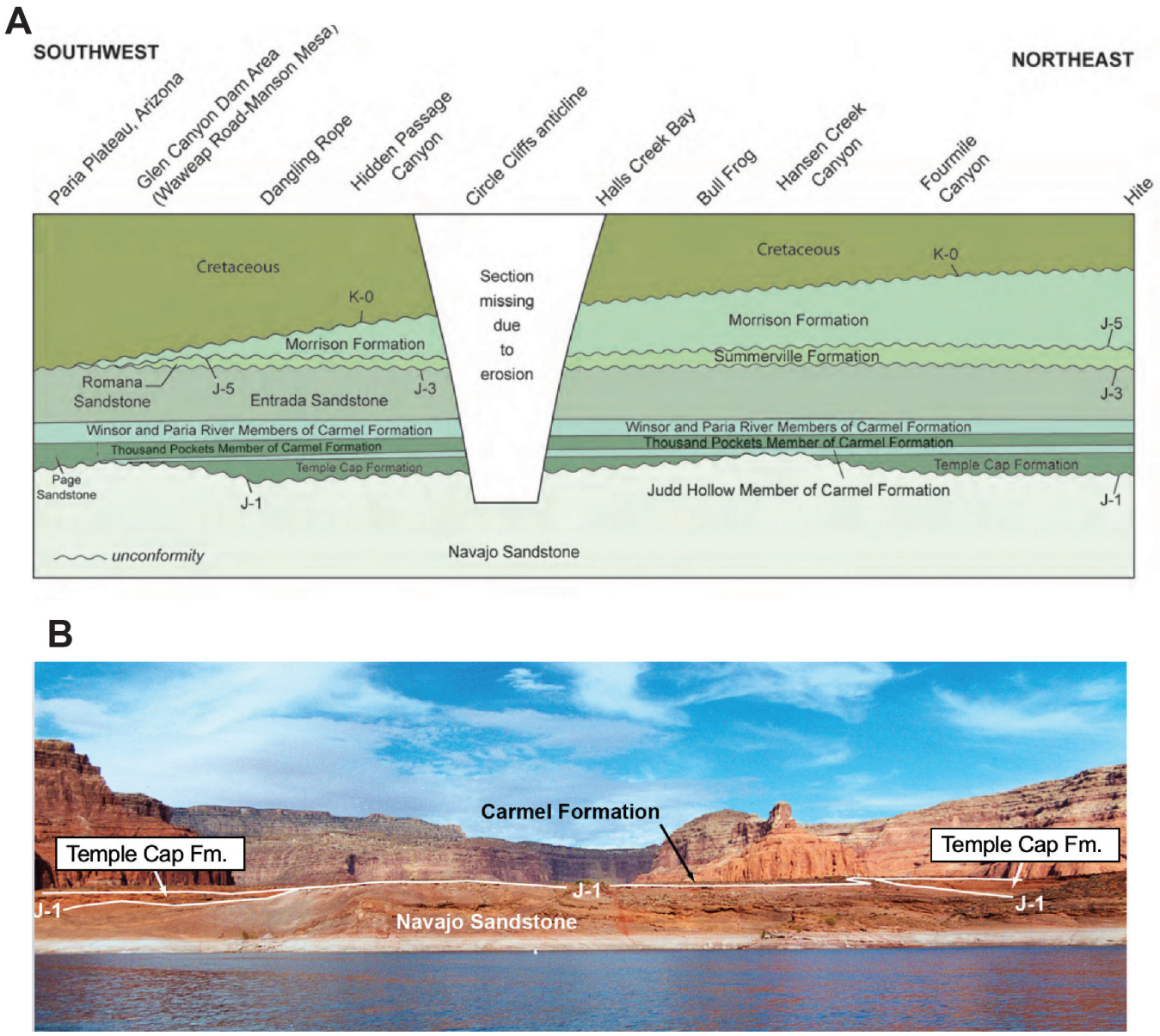

Figure 24. (A) Diagram showing the J-1 and other Jurassic unconformities and relationships southwest to northeast across Glen Canyon National Recreation Area. From Anderson et al. (2024). (B) J-1 unconformity at the Navajo/Temple Cap contact near Dangling Rope Marina, Glen Canyon National Recreation Area. Modified from Chidsey et al. (2012).

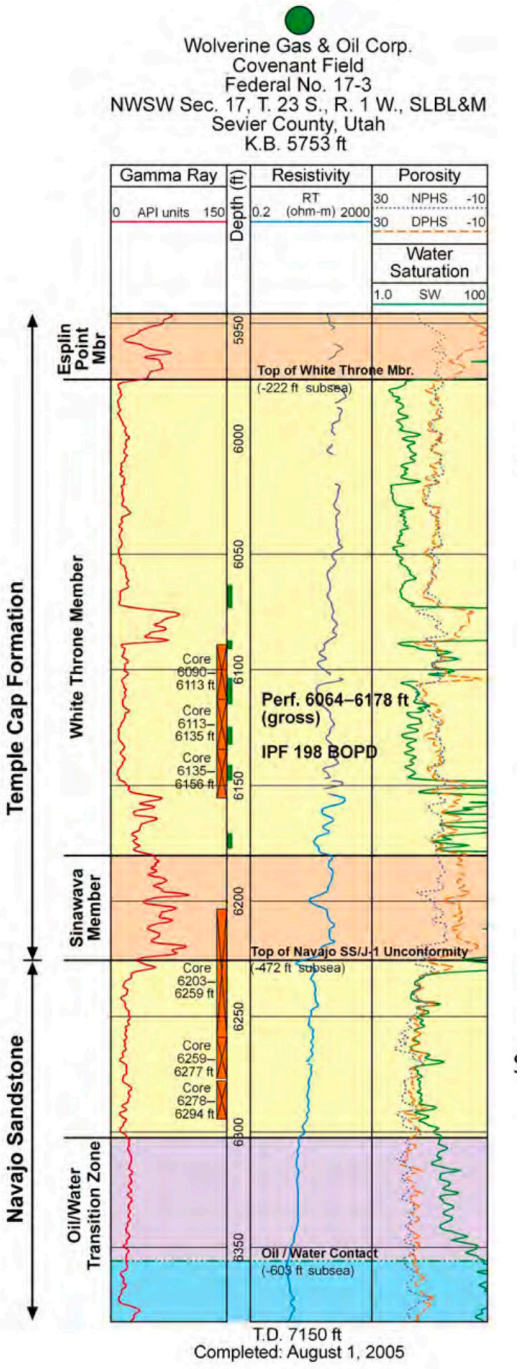

Figure 25. Federal No. 17-3 well log, Covenant field, central Utah thrust belt showing the true vertical depth (in feet) of the combined gamma ray, resistivity, and neutron-density log and the cored sections (vertical brown bars) of the Navajo Sandstone and Temple Cap Formation. The thin, vertical green bars indicate producing (perforated) intervals. See Figure 9 for approximate location of Covenant field. From Chidsey et al. (2020).

show that the contact between the red mudstone of the Sinawava and the underlying silty sandstone of the "Navajo Sandstone" is the most logical pick for the J-1 unconformity (see Figure 9 for approximate location of Covenant field). That contact is also easily identified on gamma-ray logs. However, the presence of marine glauconite below this lithologic contact implies that the J-1 unconformity is farther below and not at the base of the red mudstone of the Sinawava (Sprinkel et al., 2009, 2011a, 2011b, 2024; Chidsey et al., 2014; 2020; Chidsey and Sprinkel, 2016). Other possible candidates that could be the J-1 unconformity in Covenant core include (1) a small gravel lag that is overlain by very fine grained, massive sandstone (Figure 26A) and (2) a color change from the typical light and dark gray sandstone to bleached and pink-colored sandstone zones (Figure 26B) (Chidsey et al., 2020).

DUNE AND INTERDUNE SUBFACIES IN OUTCROP

A detailed study of the Navajo Sandstone outcrops and core in the San Rafael Swell and Covenant oil field in east-central and central Utah, respectively, was conducted by the Utah Geological Survey (UGS) and the Brigham Young University Department of Geological Sciences (Chidsey et al., 2020). This study focused on reservoir and aquifer characterization from the surface to the subsurface of the Navajo to expand the understanding of ancient erg systems. The study identified eight Navajo subfacies: three dune subfacies – large trough cross-bedded (LTC), small trough cross-bedded (STC), and reworked eolian (RWE); and five interdune subfacies – wavy algal mat (WAM), sandy algal mat (SAM), ephemeral fluvial channel (EFC), poorly developed interdune (PDI), and evolving interdune (EID). The lateral extent of each interdune facies varies greatly, ranging from a few tens of feet to miles and accounts for less than 10% of the Navajo section. However, these deposits create baffles and barriers to fluid flow, partitioning the Navajo reservoirs or aquifers.

The mineral composition (and percent) of these Navajo subfacies from outcrop samples collected as part of the 2020 study are shown in Table 1. The 300-point count analysis also determined porosity, which was generally higher than in cores.

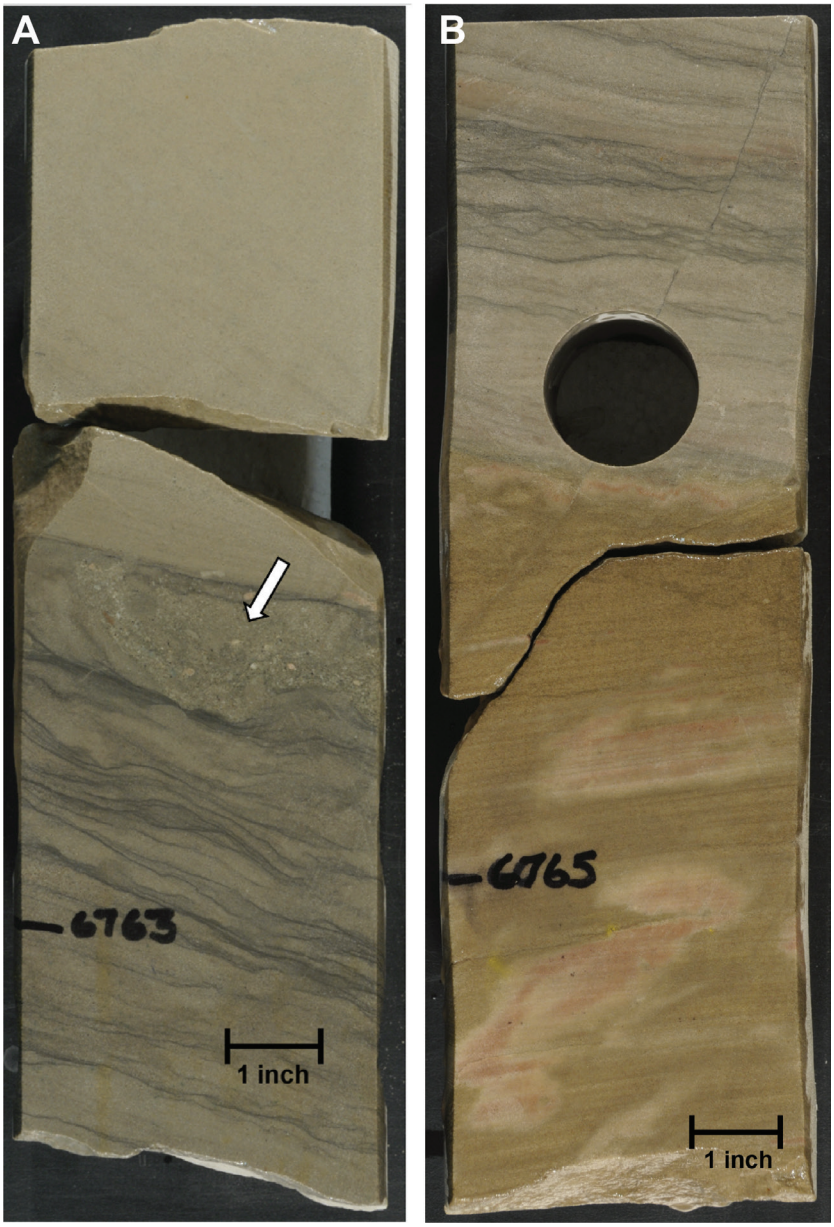

Figure 26. Possible candidates for the J-1 unconformity in core from the Federal 17-3 well, Covenant field. (A) Thin, very fine grained sandstone and siltstone displaying wavy laminations capped by a small gravel lag (arrow) that is overlain by very fine grained, massive (homogeneous) sandstone. The gravel lag may represent the J-1 unconformity or a small wadi deposit. Slabbed core from 6763 feet (2061 m). (B) Bleached and pink zones in low-angle, cross-bedding in fine-grained sandstone could be an indication of proximity to the J-1 unconformity. Slabbed core from 6765 feet (2062 m). From Chidsey et al. (2020).

Dune Subfacies Characteristics and Petrography

Dune subfacies LTC is characterized by 50-foot-thick (15 m) cross-beds and thick bedding, and consists of fine- to medium-grained, subangular to subrounded, well-sorted sand grains (Figures 27A and 27B). Petrographic analysis of outcrop samples yielded porosity and permeability values above 25% and 120 millidarcies (mD), respectively, indicating that the LTC has high reservoir and aquifer quality. Dune subfacies STC is characterized by 3-foot (1 m) cross-beds, thin to medium bedding, and consists of fine- to medium-grained, subrounded to subangular, moderately to poorly sorted sand grains (Figure 28). It has gradational upper contacts and occurs mostly in the lower Navajo Sandstone. The STC generally has good porosity but lower permeability than the LTC subfacies. Dune subfacies RWE is characterized by massive and contorted bedding attributed to a climatically controlled high water table (Sansom, 1992), is not laterally extensive, and consists of fine-grained, rounded to subrounded, moderately sorted sand grains (Figures 29A and 29B). The reservoir quality is poor for the most part.

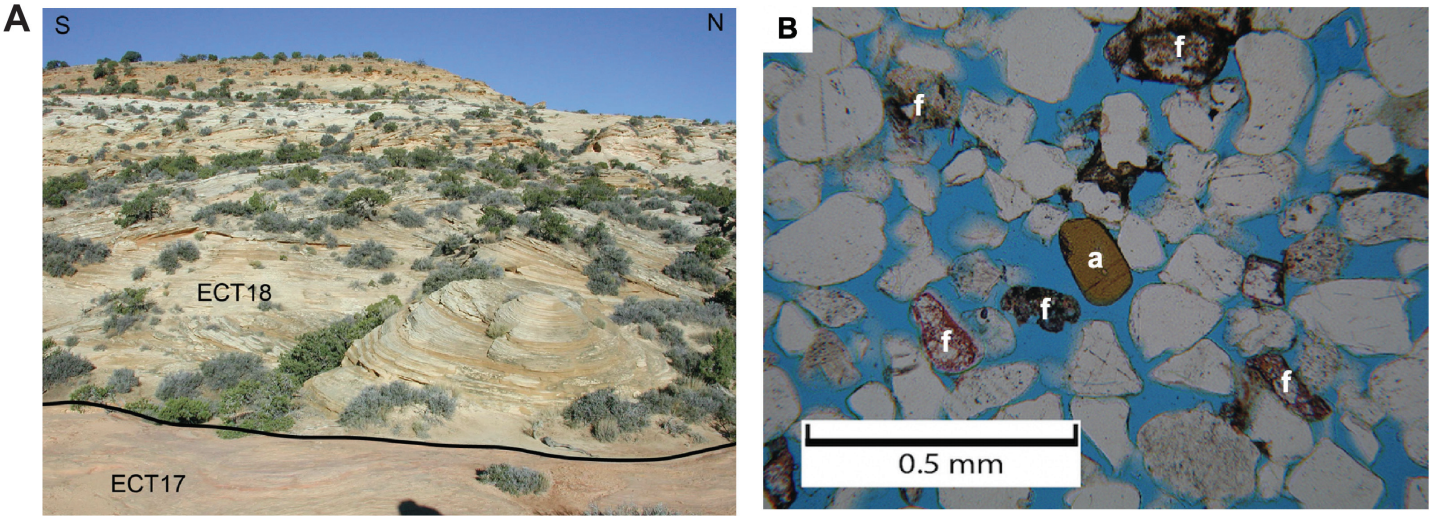

Figure 27. Lithologic and petrographic analysis of large trough cross-bedded (LTC) subfacies of the Navajo Sandstone in Eagle Canyon, west flank of the San Rafael Swell, east-central Utah. (A) Outcrop view, to the west, showing large trough cross-beds in unit ECT 18. (B) Photomicrograph from the lower part of section in A displaying excellent intergranular porosity (blue space), under plane-polarized light, in a matrix of mostly quartz grains and very few feldspar (f) and rare amphibole (a) grains. After Chidsey et al. (2020).

Figure 28. Small trough cross-bedded (STC) subfacies in the Navajo Sandstone, Eagle Canyon. Rock hammer for scale. From Chidsey et al. (2020).

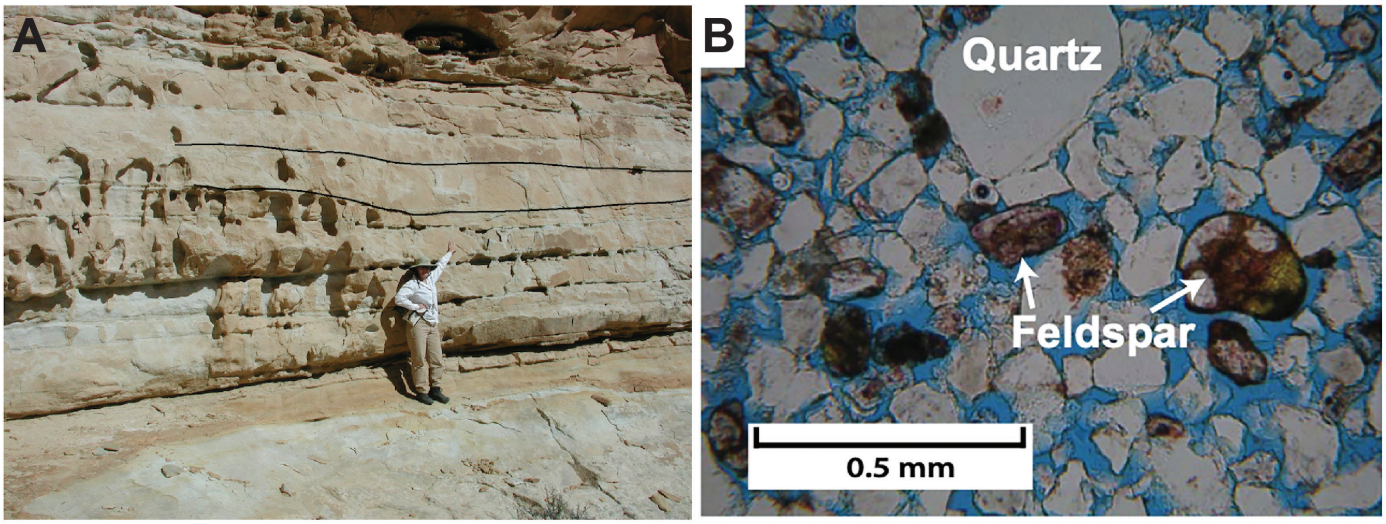

Figure 29. Lithologic and petrographic analysis of the reworked eolian (REW) subfacies in the Navajo Sandstone, Eagle Canyon. (A) Outcrop displaying lenticular channels. (B) Photomicrograph of REW subfacies displaying abundant porosity (blue space) between subrounded to subangular quartz grains, under plane-polarized light. The angularity of grains may be the result of breakage during reworking. From Chidsey et al. (2020).

Interdune Subfacies Characteristics and Petrography

Interdune subfacies WAM is characterized by laterally extensive, stromatolitic wavy laminae, desiccation features (mud cracks), disrupted bedding, and is very fine grained; fossils are lacking (Figure 30). Interdune subfacies SAM is characterized by thin planar and wavy laminae, which are not laterally extensive, and consists of very fine grained, well-sorted sand (Figure 31). Both WAM and SAM subfacies represent oases deposits. Interdune subfacies EID is characterized by massive to planar bedding, undulating contacts, and consists of very fine grained, subrounded to subangular, well- to moderately sorted sand (Figure 32). Interdune subfacies EFC is characterized by lens-shaped interbeds of planar and low-angle trough cross-beds, possible soft-sediment deformation, and bioturbation (Figure 33). It is associated laterally with large-scale convoluted bedding. Finally, interdune subfacies PDI is characterized by massive to planar beds of limited lateral extent, lacks any algal influence, and consists of fine grained, subrounded, well-sorted sand (Figure 34). Porosity and permeability analyses indicate that the interdunal subfacies represent barriers or baffles to fluid flow.

In addition to the interdune subfacies in the San Rafael Swell, thicker SAM Navajo oasis rocks along Lake Powell, described earlier, petrographically consists of sandy microbial (i.e., algal) stromatolitic to thrombolitic (clotted) boundstone and wackestone composed of limestone or dolomitic limestone (Figure 35). Small white quartz grains are presumably sand blown in by wind from nearby dunes. Such microbial structures could have easily formed in stressed environments that were intermittently desiccated. Salinity stresses, ranging from fresh to hypersaline waters, can promote these types of microbial mini-structures such as is likely occurring in the shallow interdune ponds in Lençóis Maranhenses National Park (Figure 12C).

STRANGE AND WONDEROUS FEATURES

The Navajo Sandstone is known for its strange and wonderous features. These include iron- and manganese-rich pipes and columns, alcoves and hanging gardens, weathered-out iron concretions, unusual soft-sediment deformation, honeycomb weathering, and spectacular deformation bands.

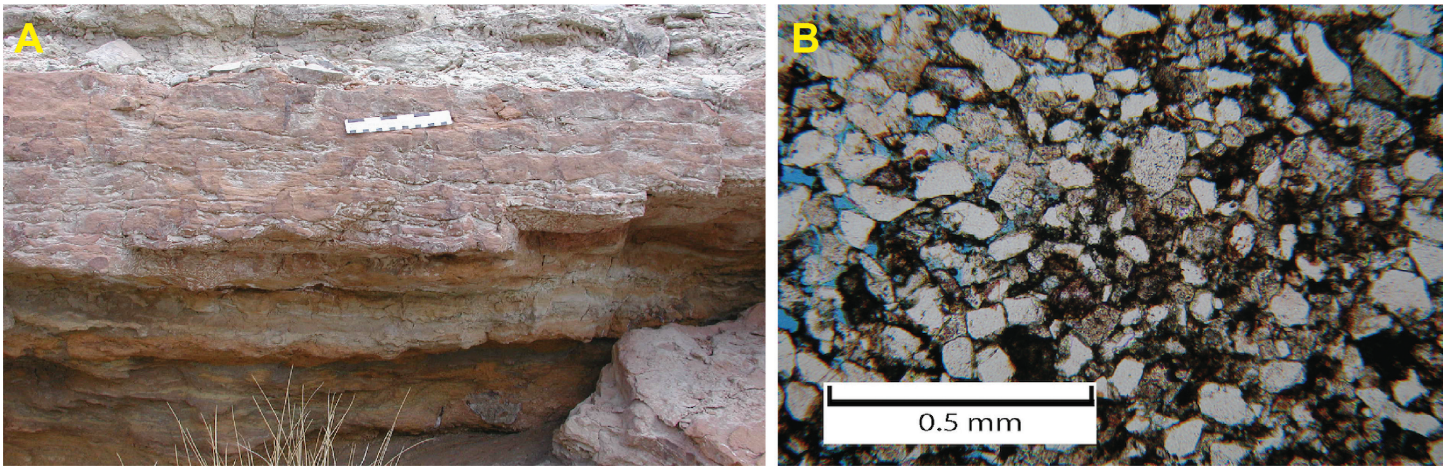

Figure 30. Lithologic and petrographic analysis of interdune wavy algal mat (WAM) subfacies in the Navajo Sandstone, Eagle Canyon. (A) Outcrop of the WAM subfacies; note wavy laminations. (B) Photomicrograph of WAM subfacies displaying quartz grains (light, angular) and the lack of porosity due to pervasive calcite cement and iron oxides (dark intergranular material), under plane-polarized light. Iron and manganese oxides make the calcite look dark in thin sections and give outcrops the dark red-brown color. From Chidsey et al. (2020).

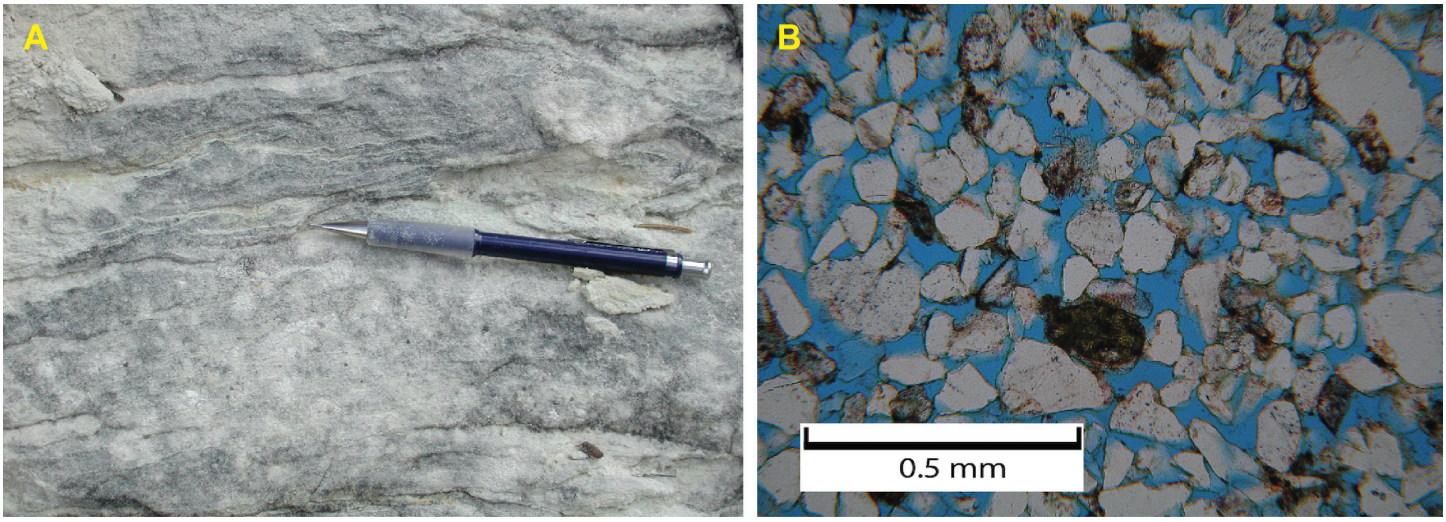

Figure 31. Lithologic and petrographic analysis of interdune sandy algal mat (SAM) subfacies in the Navajo Sandstone, Eagle Canyon. (A) Outcrop of interdune SAM subfacies displaying planar laminae. Mechanical pencil for scale. (B) Photomicrograph of SAM subfacies displaying abundant quartz grains and high porosity (blue space), under plane-polarized light. From Chidsey et al. (2020).

Iron- and Manganese-Rich Diagenetic Pipes and Columns

Weirdly shaped iron- and manganese-rich clusters or large groups of diagenetic pipes and columns are found weathered out in the upper part of the Navajo Sandstone northwest of Moab in southeastern Utah (Figure 36). They occur in thick, very porous and permeable sandstone of the Navajo in which hematite cement can compose up to 25% of the rock. These cylindrical structures are a few inches to over a foot in diameter and tens of inches to several feet high. They often appear to be planed off or broken; some are inclined. The pipes and columns have an outer, thick, hematite-cemented rind typically colored very dusky red, brownish-black, or black (Chan et al., 2000). Staining away from the core of the structures indicates fluid direction.

These iron- and manganese-rich pipes and columns

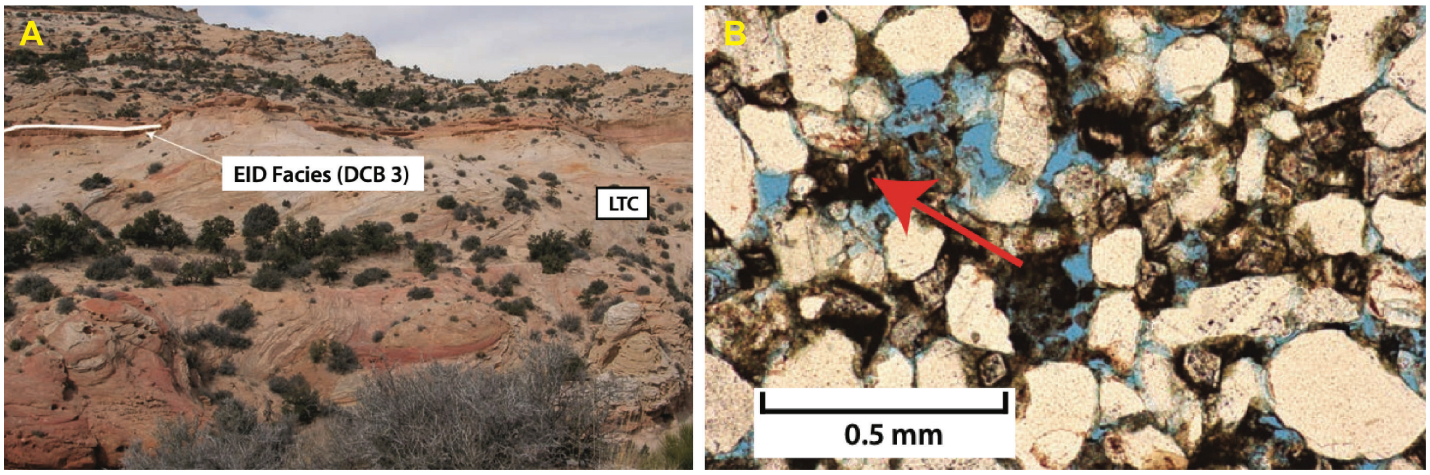

Figure 32. Lithologic and petrologic analysis of the evolving interdune (EID) subfacies, Devils Canyon/Justensen Flats area. (A) Outcrop view of the EID subfacies, which is variable in thickness, undulatory, and laterally extensive. (B) Photomicrograph displaying calcite cement and iron/manganese oxides (red arrow), under plane-polarized light, which provide the reddish color in outcrop. (See data in appendix of Willis and Hayden, 2015). From Chidsey et al. (2020).

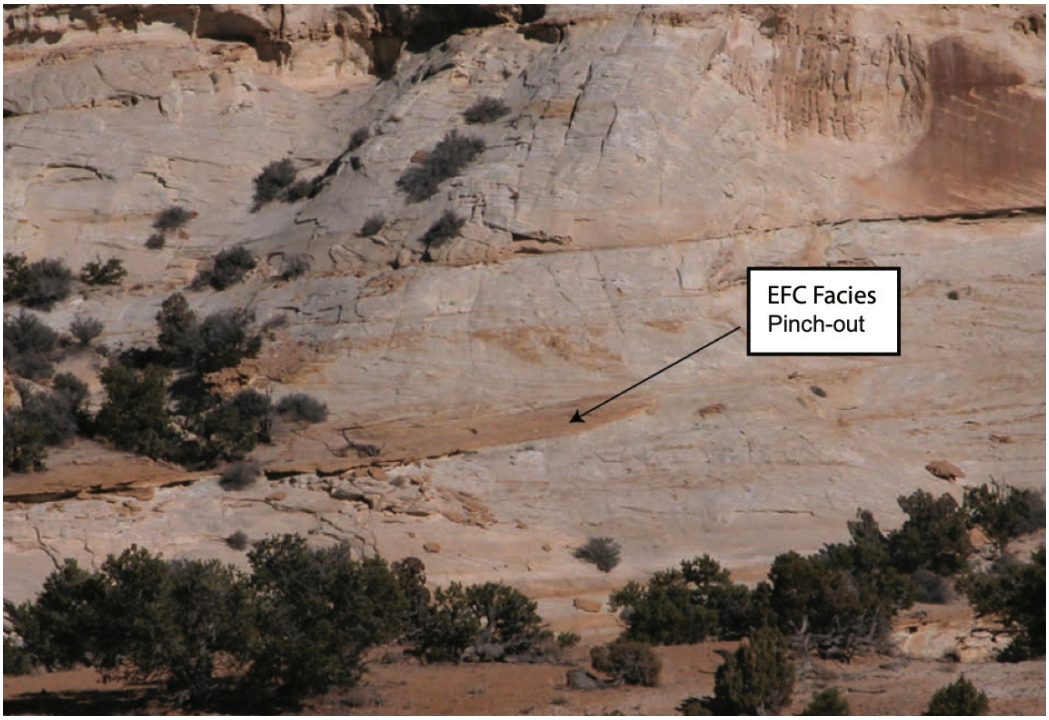

Figure 33. Outcrop view of the pinch-out of the interdune ephemeral fluvial channel (EFC) subfacies, Devils Canyon/Justensen Flats area, west flank of the San Rafael Swell. The EFC subfacies contains planer beds, moderate bioturbation, and can be associated with soft-sediment-deformed beds. Bushy tree in lower left is about 9 feet (3 m) tall. From Chidsey et al. (2020).

are related to the Moab fault (Figure 36A), a major normal northwest-southeast-trending fault in the Paradox fold and fault belt and created by salt withdrawal along a massive salt wall. They are most common where the Moab fault bifurcates near its northwest termination. Chan et al. (2000) postulated that over multiple episodes, reducing brines originating from the dissolution of Pennsylvanian salt at depth by meteoric water, interacted with hydrocarbons, methane, hydrogen sulfide, and organic acids, and then removed iron and manganese near the fault, bleaching the sandstone. As these fluids moved farther away from the fault, they mixed with shallow oxygenated groundwater and precipitated iron and manganese cements where the porosity and permeability of the sandstone was highest, thus creating the pipes and columns.

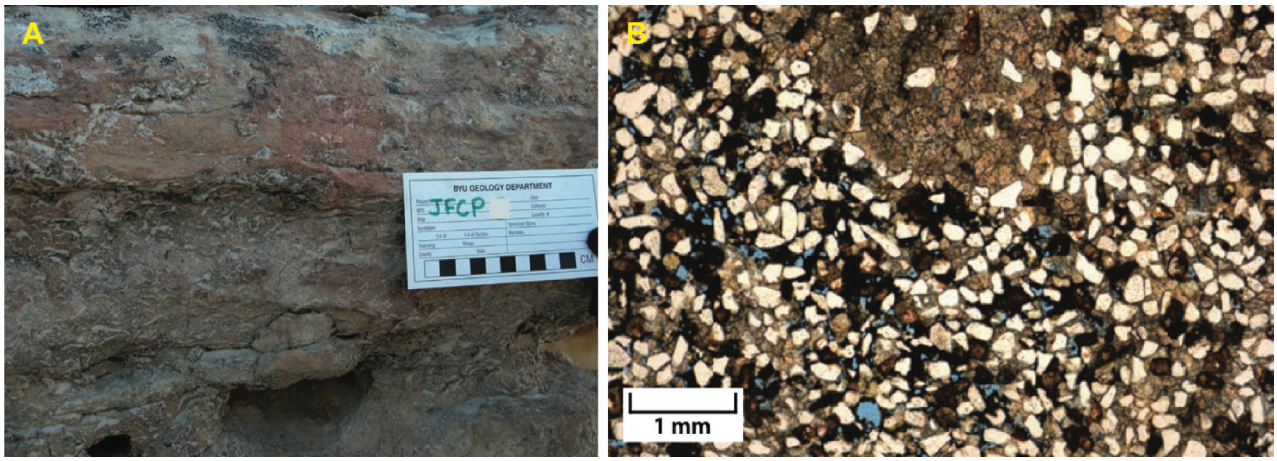

Figure 34. Lithologic and petrologic analysis of the poorly developed interdune (PDI) subfacies, Devils Canyon/Justensen Flats area. (A) Outcrop view of the PDI subfacies displaying inch-scale planer beds to massive beds. (B) Photomicrograph displaying abundant calcite cement and iron/manganese oxides under plane-polarized light. From Chidsey et al. (2020).

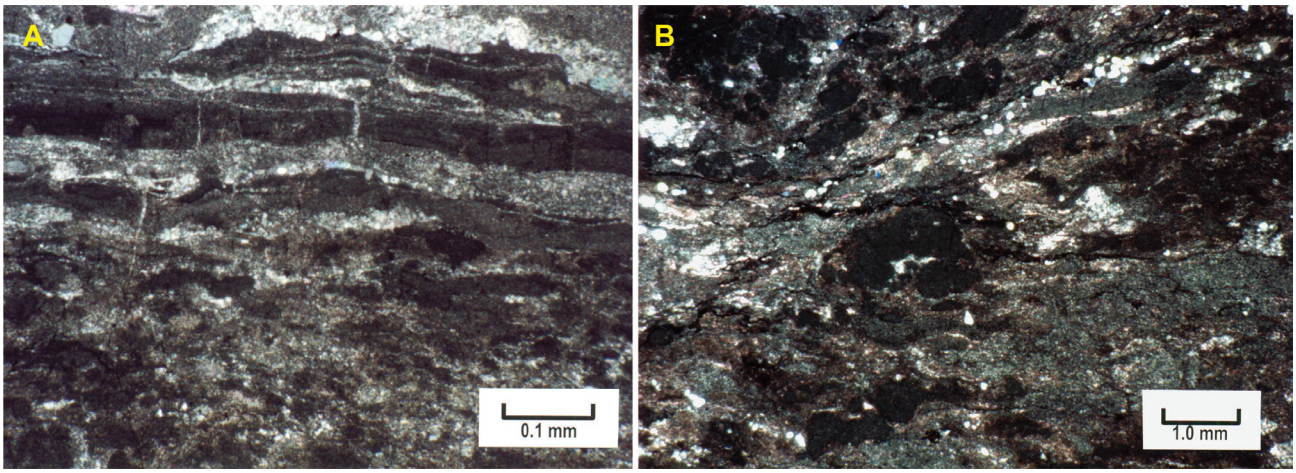

Figure 35. Photomicrographs (crossed nicols) of oasis deposits, Navajo Sandstone, along Lake Powell, Glen Canyon National Recreation Area, Utah. (A) Couplets of alternating cryptalgalaminites and massive microcrystalline layers dominate the upper half of this photomicrograph. The laminated bands are mostly calcitic (limestone) whereas the lighter-colored microcrystalline bands are mostly dolomite. These mm-scale couplets are typical of organic blue-green algal or cyanobacterial mats. The lighter-colored, massive or microcrystalline bands are probably the result of dolomitized storm deposits whereas the microlaminated layers are the result of normal microbial mat trapping and binding activities. The lower half of this image shows a greater concentration of dark-colored rip-up intraclasts. (B) Dark-colored clots and pin cushion-like patches of micrite are surrounded by lighter-colored, partially dolomitized detrital sediments and small, white quartz grains. Several of these lumpy clots can be termed "thrombolites." They were most likely created by coccoid blue-green algal or cyanobacterial processes. Photomicrographs and description by David E. Eby, Eby Petrography & Consulting, Inc., written communication, 2003. From Chidsey et al. (2016).

Iron Concretions

Iron concretions, also commonly called "Moqui Marbles" or "Navajo Berries," weather out of the Navajo Sandstone. They can be prolific in various areas such as the Grand Staircase-Escalante National Monument (Figure 37A), Snow Canyon State Park, and around Lake Powell to name a few. These features consist of a well-cemented limonite, hematite, goethite iron shell

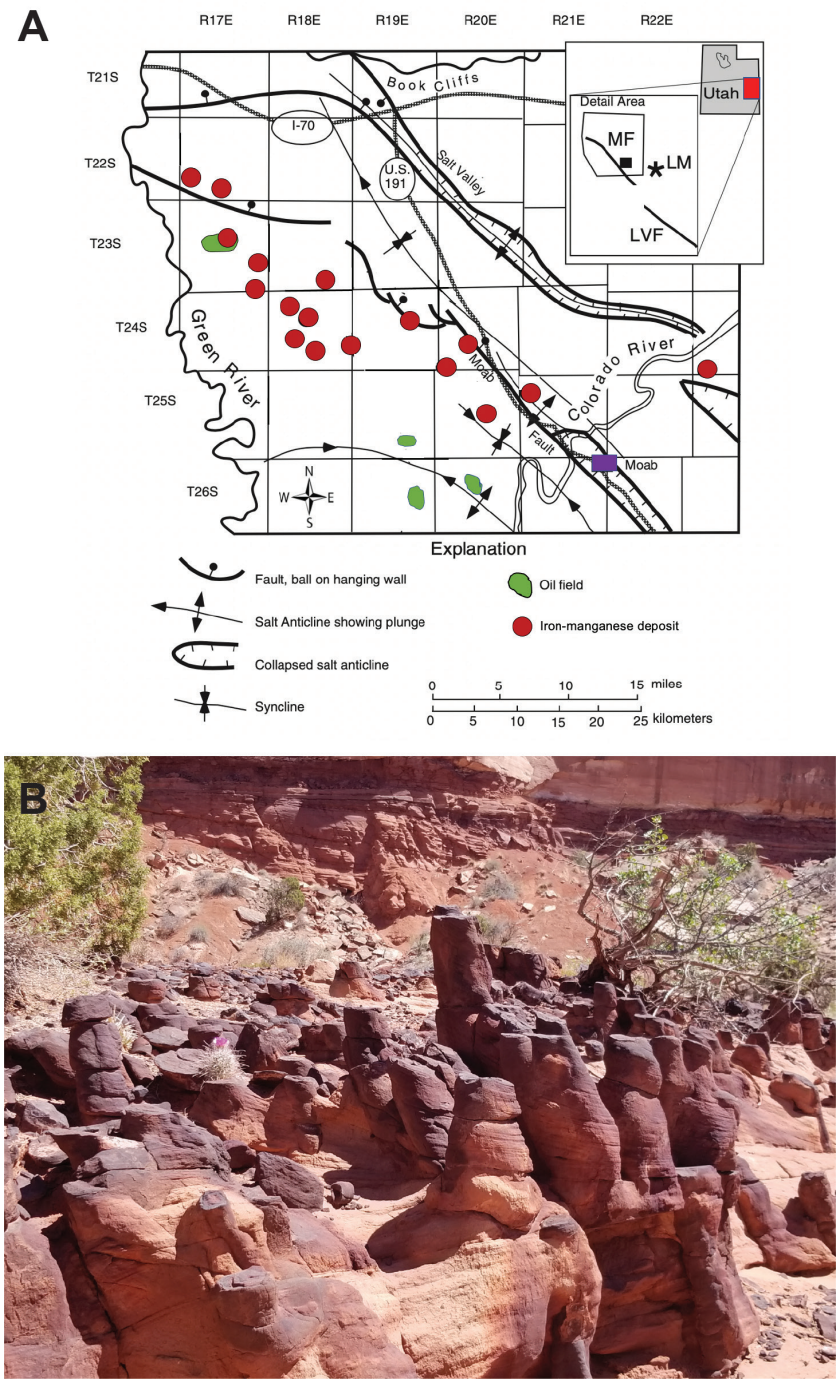

Figure 36 (A) Location of iron-manganese pipes and columns associated with the Moab fault (on inset MF = Moab fault, LM = La Sal Mountains, LVF = Lisbon Valley fault). Modified from Chan et al. (2000). (B) Iron- and manganese-rich pipes and columns in the upper part of the Navajo Sandstone, northwest of Moab in southeastern Utah. Photograph courtesy of Douglas A. Sprinkel, Utah Geological Survey.

around a friable sandstone core (Doelling, 1968, 1975). Most are spherical but can be saucer shaped. They range in size from BB or pea size to as large as baseballs, occurring in great accumulations. These concretions formed when groundwater that may have been acidic or contained hydrocarbons or CO_2 dissolved and transported hematite or other iron-bearing cements between the sand grains (Chan and Parry, 2002). The iron pre-

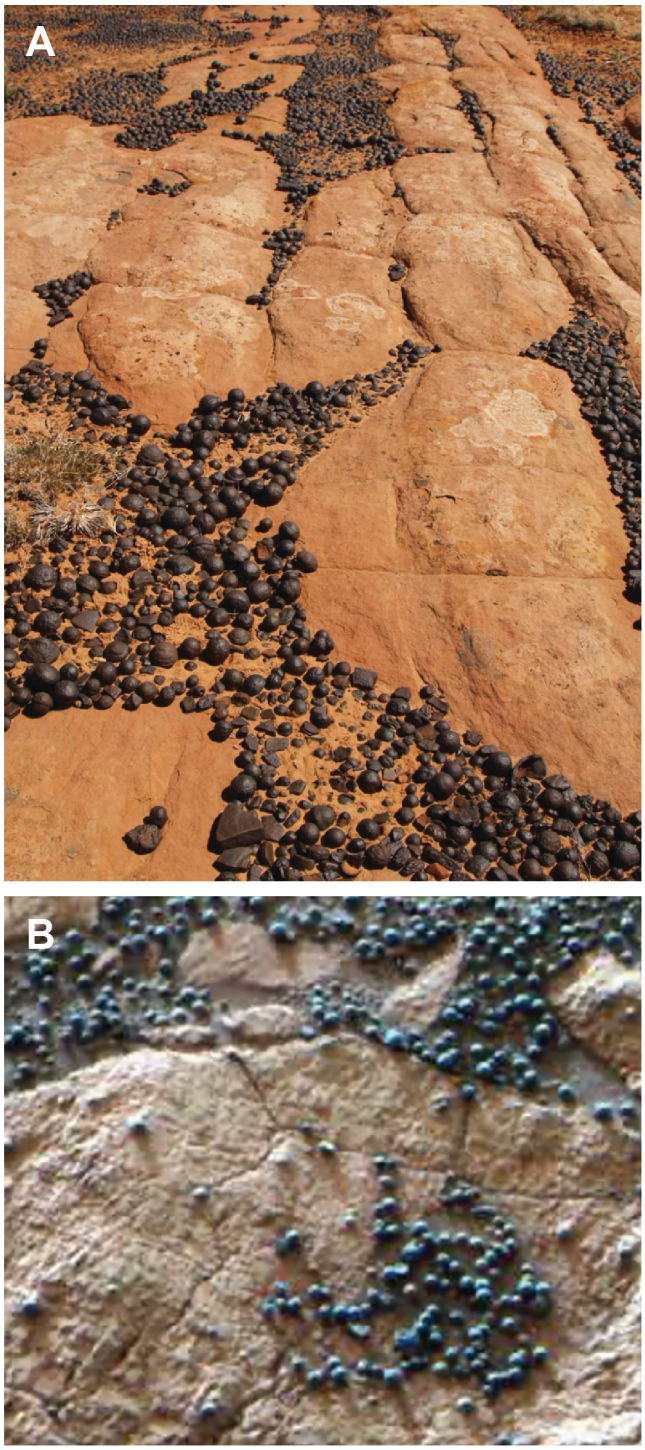

Figure 37. (A) Large iron concretions, "Moqui Marbles" or "Navajo Berries," which weathered out of the Navajo Sandstone, Grand Staircase-Escalante National Monument, south-central Utah. Photograph courtesy of Michael Vanden Berg, Utah Geological Survey. (B) Spherical concretions called "Blueberries" discovered in the Eagle Crater on Mars by the rover Opportunity in 2004. Photograph courtesy of NASA/JPL/Cornell.

cipitated around small impurities when reducing fluids encountered groundwater fluids with slightly increased oxygen (Anderson et al., 2024). They continued to grow as more iron was added. Additionally, the dissolved iron-bearing groundwater can migrate outward toward a precipitation front leaving the core of the concretion weakly cemented in the form of a sphere around a softer center.

Similar spherical concretion-type objects and distributions were discovered on Mars by the rover Opportunity in 2004. Called "blueberries," they are also composed of hematite and provide evidence of groundwater flow during Mars' ancient past (Chan et al., 2005) (Figure 37B). The Navajo Sandstone iron concretions and the processes that created them serve as an analog for understanding these Martian blueberry spherules.

Some of the most distinctive, spectacularly large-sized, and massive populations of these unusual iron concretions have been stolen from federal lands for unscrupulous commercial profit and by selfish or unwitting individuals for their private collections. The most egregious cases occurred in the Grand Staircase-Escalante National Monument where thieves removed vast quantities of large concretions, estimated at 40,000 concretions, using a backhoe in at least one location. Using geologic forensic investigation, Professor M.A. Chan and her colleagues from the University of Utah worked with law enforcement to help charge and convict those responsible with felonies (Chan and Bowen, 2026). Sadly, the Navajo glory of these theft-targeted areas has been diminished for future generations to enjoy and use in scientific studies.

Alcoves and Hanging Gardens

Magnificent alcoves and hanging gardens are found throughout the Navajo Sandstone in southern Utah, especially in the Lake Powell area (Figure 38A). Groundwater percolates down through the pores until encountering a low-permeability boundary such as an interdune oasis or playa deposit. These beds consisting of siltstone, shale, or limestone impede the downward movement of groundwater causing it to flow horizontally along the less resistant flow path in the sandstone and then exiting at a rockface in the form of seeps and

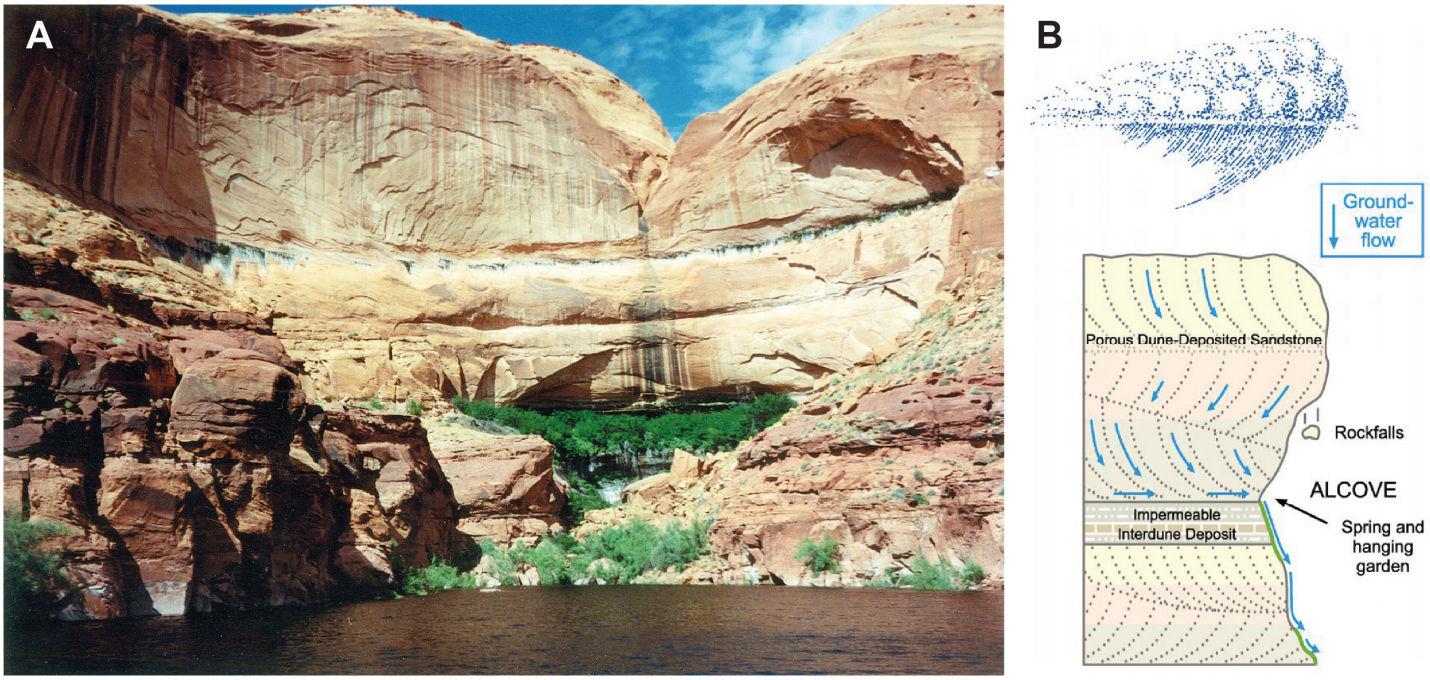

Figure 38. (A) Large alcove with lush hanging garden, Knowles Canyon along Lake Powell, Glen Canyon National Recreation Area. (B) Alcove formation and associated springs. From Chidsey et al., 2012.

springs (Figure 38B). In the process the water dissolves cementing minerals causing the sandstone there to weaken in comparison to elsewhere on the cliff.

Weathering and erosion eventually form a recess or alcove. Increased water discharge and shade are ideal for plant life, which further breaks down the rock and causes the alcoves to enlarge over time. The wet surfaces are often covered with algal mats, ferns such as maidenhair and bracken, grasses, and sedges.

Unusual Soft-Sediment Deformation

Soft-sediment deformation is common in the Navajo Sandstone mostly where the ancient water table was high at the time of deposition, causing the unconsolidated sand to slump and contort (Figure 39). The movement of the sand can be caused by fluctuations in groundwater, gravitational forces, or earthquakes (Morris et al., 2024). Cross-bedding and other sedimentary structures are often destroyed; reservoir/aquifer properties tend to be poor. Massive, homogenous beds with no distinct sedimentary structures or laminations are also recognized in the Navajo and were probably formed by water-saturated sand (Sanderson, 1974; Chidsey, 2013).

The Navajo Sandstone has various types of soft-sediment deformation; however, the most frequent type found in the Navajo Sandstone is convolute bedding (Figure 39A). Jackson (1997) described this as lamina sets that are highly contorted and are bounded above and below by non-contorted lamina. Tight, recumbent folds and flower (pop-up) structures formed by compressional and translational forces while the sand lamina remained unconsolidated as they detached and slid along a finer-grained (interdunal?) basal surface (Figures 39B) (Anderson, et al., 2024; Morris et al., 2024). Convolute bedding in the Navajo tends to trap fluids resulting in precipitation of iron-bearing minerals (Chan and Bruhn, 2014).

An unusual example of soft-sediment deformation is also found in Capitol Reef National Park and is known as "the Elf's Toe" because of the strange curl at the end of thin Navajo bedding (Figure 39C) (see Morris et al., 2024, for location). Morris et al. (2024) offered the following possible explanations for this unique feature: (1) fluid expansion associated with increased water pressure from below curled the beds, which were acting as a permeability barrier to fluid flow; or (2) downslope

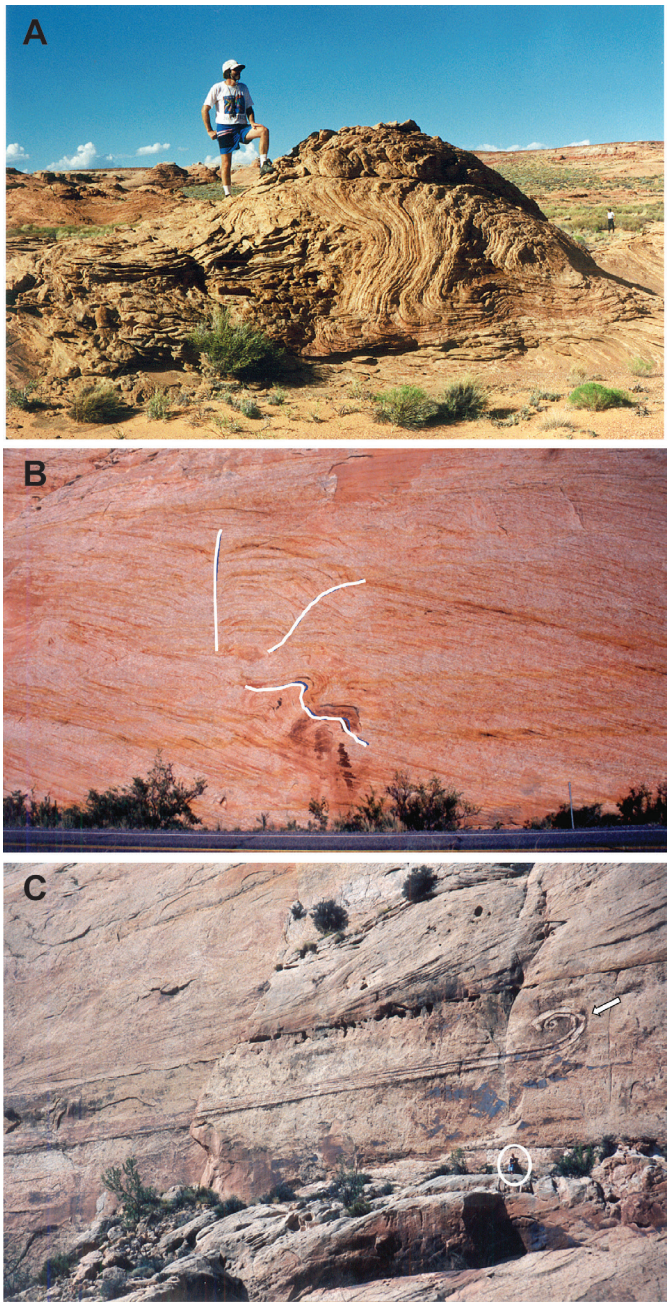

Figure 39. Soft-sediment deformation in the Navajo Sandstone. (A) Spectacular contorted, tight recumbent fold on Antelope Island on the Utah-Arizona border in Lake Powell. (B) Recumbent fold (outlined in lower center) and a flower pop-up like structure (outlined above the fold) indicating soft-sediment deformation and slumping in the upper Navajo Sandstone along Utah Route 24, Capitol Reef National Park, south-central Utah. (C) "The Elf' Toe" (arrow), is an unusual soft-sediment deformation feature in the lower Navajo Sandstone in Spring Canyon, Capitol Reef National Park. Note person for scale (circled). A from Anderson et al. (2024); B and C after Morris et al. (2024).

movement (grainflow) along the dune leeward slipface created a pile of sand ahead of the toe and acting as an abutment caused the upslope sand to curl as movement continued.

Honeycomb Weathering

Another unusual feature in the Navajo Sandstone and other massive sandstone formations on the Colorado Plateau is a honeycomb weathering pattern of small holes called tafoni, formed along cross-beds or bedset boundaries (Figure 40). These holes are created by differential weathering and what is referred to as "case hardening." Groundwater can weaken the cement in the rock, commonly at imperfections or small variations, creating small voids. The voids provide space where water can accumulate and be protected from evaporation. This process further weakens the cement in the surrounding rock and promotes additional growth just like the formation of a mini alcove. In case hardening, the mineral-laced water wicks toward an exposed rock face. Here the water quickly evaporates, depositing cement, which hardens the rock case and preserves the holes that align creating the tafoni pattern (Anderson et al., 2024).

Deformation Bands

Deformation bands are millimeter- to centimeter-thick tabular zones of localized compaction, shear, and/or dilation that develop in highly porous granular rocks such as sandstone (Fossen, 2016; Schultz, 2019). Textbook examples of deformation bands are common in the Navajo Sandstone, as well as the Middle Jurassic Entrada Sandstone, on the Colorado Plateau in southern Utah (Davis, 1999; Fossen et al., 2011). They often form in association with nearby large faults and joint sets (Figure 41). Deformation bands are thicker and have much smaller displacements than fractures. They occur as a single structure, or in clusters and zones (Fossen, 2016). In comparison to the original sandstone, deformation bands consist of much smaller sand grain sizes, poorer sorting, and lower porosity and permeability by the collapse of pore space and the filling of it by crushed grain fragments (Fossen, 2016; Schultz,

Figure 40. Honeycomb weathering in large-scale, high-angle trough cross-beds in the Navajo Sandstone in Spring Canyon, Capitol Reef National Park. The base of the cross-bedded dune set marks the boundary with interdune and soft-sediment deformation deposits below, i.e., an interdune migration surface; see Figure 19. From Morris et al. (2024).

2019). Therefore, they can act as barriers or baffles to fluid flow (i.e., groundwater or oil); fractures or fracture zones generally result in increased porosity and permeability. Finally, deformation bands maintain or increase cohesion, which is lost or reduced in fracturing (Schultz, 2019).

Deformation bands in the Navajo Sandstone are subdivided into compaction, disaggregation, and cataclastic bands depending on variations in mineralogy; grain size, shape, and sorting; cementation; porosity; and the state of stress (Davis, 1999; Fossen et al., 2011). The most important deformation processes affecting these characteristics are granular flow (i.e., grain boundary sliding and grain rotation), cataclasis (grain fracturing), and dissolution and cementation (Fossen et al. 2011; Fossen, 2016). Compaction bands form in very high porosity sandstone like the Navajo when compaction is assisted by dissolution and some grain fracturing. Disaggregation bands in the Navajo develop in very fine grained sandstone and by shear-related disaggregation of sand grains by granular flow. These deformation bands are often so thin that they may only be identified where they cross and offset laminae (Fossen et al. 2011; Fossen, 2016). Cataclastic bands in the Navajo develop where grain fracturing is significant, especially in the core of the band, resulting in grain size reduction, angular grains, and collapse of pore space. They occur in the Navajo that has been buried at depths of 0.9 to 1.9 miles (1.5–3.0 km) (Fossen, 2016). Cataclastic zones can show positive relief due to the amount of grain crushing and

Figure 41. Spectacular weathered out conjugate set (oppositely dipping) of cataclastic deformation bands in the Navajo Sandstone near Mount Carmel Junction and the Sevier fault, a major north-south-trending normal fault in southern Utah and extending to the Grand Canyon in Arizona. Photograph by Douglas A. Sprinkel, Utah Geological Survey.

when well cemented in comparison to the surrounding sandstone (Figure 41).

RESERVOIR FOR HYDROCABONS AND NATURAL CARBON DIOXIDE

Two fields produce oil from the Navajo Sandstone in the central Utah thrust belt – Covenant and Providence in Sevier and Sanpete Counties, respectively (Figure 42). The highly productive Covenant field (almost 34million barrels [bbls] of oil) was discovered in 2004 and the much smaller Providence field (over 824,000 bbls of oil), about 15 miles (24 km) northeast, was discovered in 2008 (Chidsey et al., 2011; Utah Division of Oil, Gas and Mining, 2026). However, the search for other fields in the central Utah thrust belt remains elusive. The Covenant and Providence oil was most likely derived from Mississippian-age marine source beds and migrated primarily along fault planes or through porous Paleozoic and Mesozoic carrier beds within the thrust plates (Wavrek et al., 2007; Chidsey et al., 2007, 2016).

Blaze Canyon (Figure 43), an abandoned one-well field south of the Book Cliffs escarpment in Grand County, produced 38,775 bbls of oil from the Navajo Sandstone (Utah Division of Oil, Gas and Mining, 2026). Discovered in 1974, the trap is a small wedge of the faulted nose of a larger northwest-plunging anticline in the northern Paradox fold and fault belt. The Navajo is about 500 feet (150 m) thick with 22 feet (7 m) being productive; porosity is estimated at 12% (Matheny, 1983).

Farnham Dome field, on the north-plunging nose of the San Rafael Swell, is CO_2 productive in the Navajo Sandstone (Figure 44). Other structures on the Utah part of the Colorado Plateau have tested significant amounts of CO_2 but not from the Navajo, nor have these structures produced (Chidsey and Morgan, 1993). The most likely source of CO_2 in the Plateau is from the thermal decomposition of Paleozoic carbonate rocks, primarily those of the thick Mississippian section. Limestone and dolomitized limestone begin generating CO_2 at temperatures as low as 167°F (75°C) and maximum generation can occur at temperatures as low as 302°F (150°C) (Hunt, 1979). The CO_2 at Farnham Dome and other nearby CO_2-bearing structures was probably sourced and migrating from the Paleozoic rocks deep in the Uinta Basin to the north (Morgan, 2007).

Covenant Oil Field, Sevier County

Field Overview

The trap for Covenant field is a relatively simple northeast- to southwest-trending anticline bounded along the west flank by an east-dipping back thrust off the Gunnison-Salina thrust at depth (Figure 45); other smaller faults dissect the structure. The back thrust creates upper and lower Navajo units but only the upper is productive.

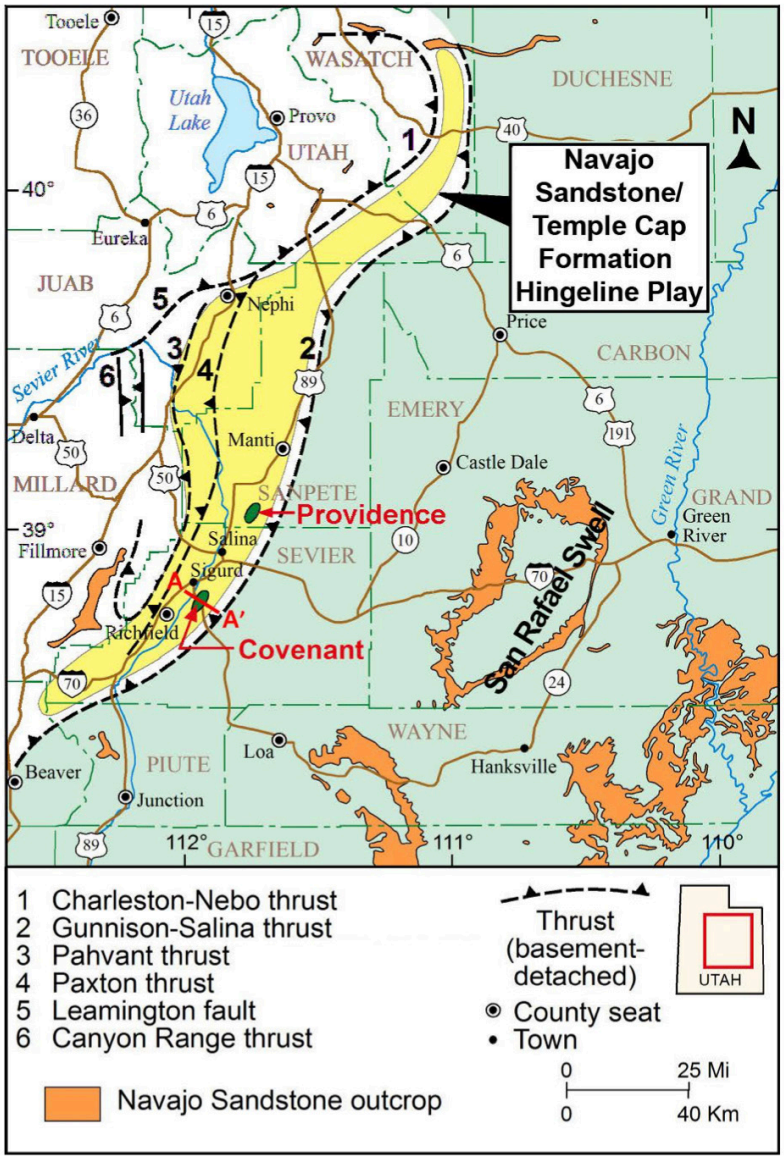

Figure 42. Location of Covenant and Providence fields, potential oil play area, and selected thrust systems of the central Utah thrust belt often referred to as the "Hingeline"), and Navajo Sandstone outcrops in the region. Numbers and sawteeth are on the hanging wall of the corresponding system. The yellow-colored area shows present and potential extent of the Navajo Sandstone/Temple Cap Formation play area. From Chidsey et al. (2020), modified from Hintze (1980). Cross section A–A' shown on Figure 45.

The field is also productive in the White Throne Member of the overlying Temple Cap Formation.

Currently 35 wells in Covenant field are active, with production divided roughly equally between the Navajo Sandstone and White Throne Member. Cumulative production for Covenant as of January 1, 2026, was 33.7 million barrels (bbls) of oil (Utah Division of Oil, Gas and Mining, 2026); the field produces essentially no gas. Covenant production averages about 2540 bbls of oil per day. Original oil in place reserves are estimated at 100 million bbls with 40% to 50% recovery (Chidsey et al., 2007). The reservoir drive mechanism is a strong active water drive.

The initial oil trap for Covenant field formed over 100 million years ago during the late Early Cretaceous through Eocene Sevier orogeny. Primary migration from the source beds occurred 90 to 100 Ma into this paleotrap. However, later back thrusting around 80 to

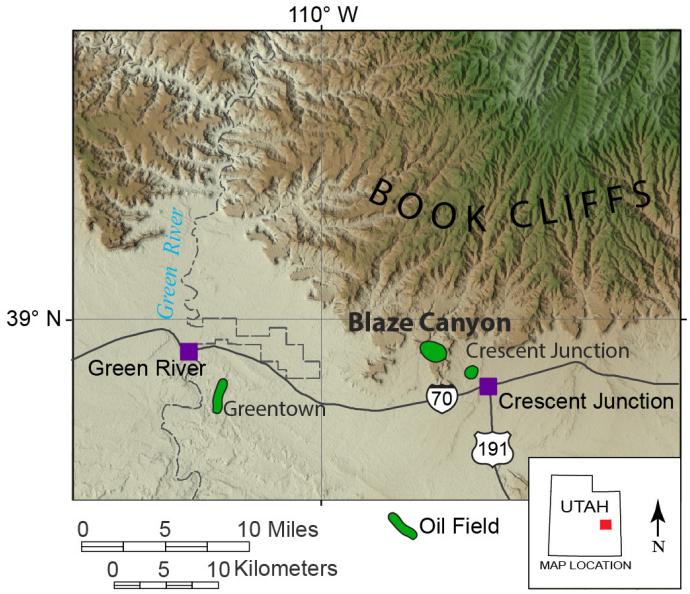

Figure 43. The abandoned Blaze Canyon oil field along the Books Cliffs, east-central Utah.

70 Ma reconfigured the trap and, in the process, remigration stripped the original gas-saturated oil of volatiles (Wavrek et al., 2010), thus accounting for the lack of gas in the field.

The average porosity for the Navajo Sandstone at Covenant field is 12%; the average grain density is 2.651 g/cm^3 based on core-plug analysis. Sandstone exhibits significant secondary porosity in the field from natural fracturing. Permeabilities in the Navajo from the core data are upwards of 100 millidarcys (mD) but range from less than 0.1 to several intervals having over 150 mD (Strickland et al., 2005; Chidsey et al., 2007).

Eolian Dune and Interdune Subfacies

Cores from the Navajo reservoir of Covenant field display many of the same eolian dune and interdune subfacies described from outcrops in the San Rafael Swell to the east (see descriptions above; Chidsey et al., 2020). All dune subfacies described in outcrop are present: large trough cross-stratification (LTC), small trough cross-stratification (STC), and reworked Eolian (RWE). Only two interdune subfacies are recognized in the core: wavy algal mat (WAM) and sandy algal mat (SAM). The following summarizes the findings in Chidsey et al. (2020).

Dune subfacies: The LTC and STC dune subfacies in Covenant cores have well-defined trough cross-beds (Figures 46A and 47A) consisting of (1) foreset beds composed of grainfall laminae, (2) subgraded avalanche laminae, and (3) thin, tightly packed, reworked ripple strata at the dune toe. Petrographically (Figures 46B and 47B), the typical sandstone is 97% white or clear quartz grains (usually frosted) with minor amounts of K-feldspar and a few lithic fragments. Some dissolution has occurred along grain-to-grain contacts of quartz grains. Feldspar grains often appear corroded and/or fractured. There are only minor overgrowths of quartz and very little clay.

The LTC subfacies consists of fine- to medium-grained, well-sorted, subangular to subrounded quartz sand grains and has excellent intergranular porosity with very little clay content (Figures 46A and 46B). In addition, foreset and avalanche laminations can display a bimodal distribution of very fine and fine to upper medium sizes of grains (Figure 46C). Laminations in dune toe deposits are low angle to planar; bedding is thinner than in the foreset and avalanche deposits. In general, the highest reservoir quality is within avalanche and dune toe deposits. Overall, the LTC subfacies has the best reservoir quality in the field with porosity between 13% and 15% and permeability greater than 150 mD. All intervals display oil staining.

The STC subfacies consists of very fine to upper fine, well-sorted sand grains (Figures 47A and 47C). The STC subfacies has good reservoir quality in the field with porosity averaging 12%; however, permeability is highly variable ranging from 2.3 mD to a questionable 1210 mD (fracture) value, based on core plugs. The contacts between the STC and RWE facies are sharp.

The REW subfacies consists of massive, fine- to medium-grained, moderately sorted sandstone (Figures 47B and 47C). Some relict or poorly developed planar laminations in cross-bedding of the STC facies may be present. Porosity is generally good, 12% or more, but permeability is typically low making REW subfacies a baffle or barrier to fluid flow.

Interdune subfacies: The SAM subfacies is well-displayed in Covenant field cores (upper part of Figure 26B). It consists of silt and very fine to upper fine-grained

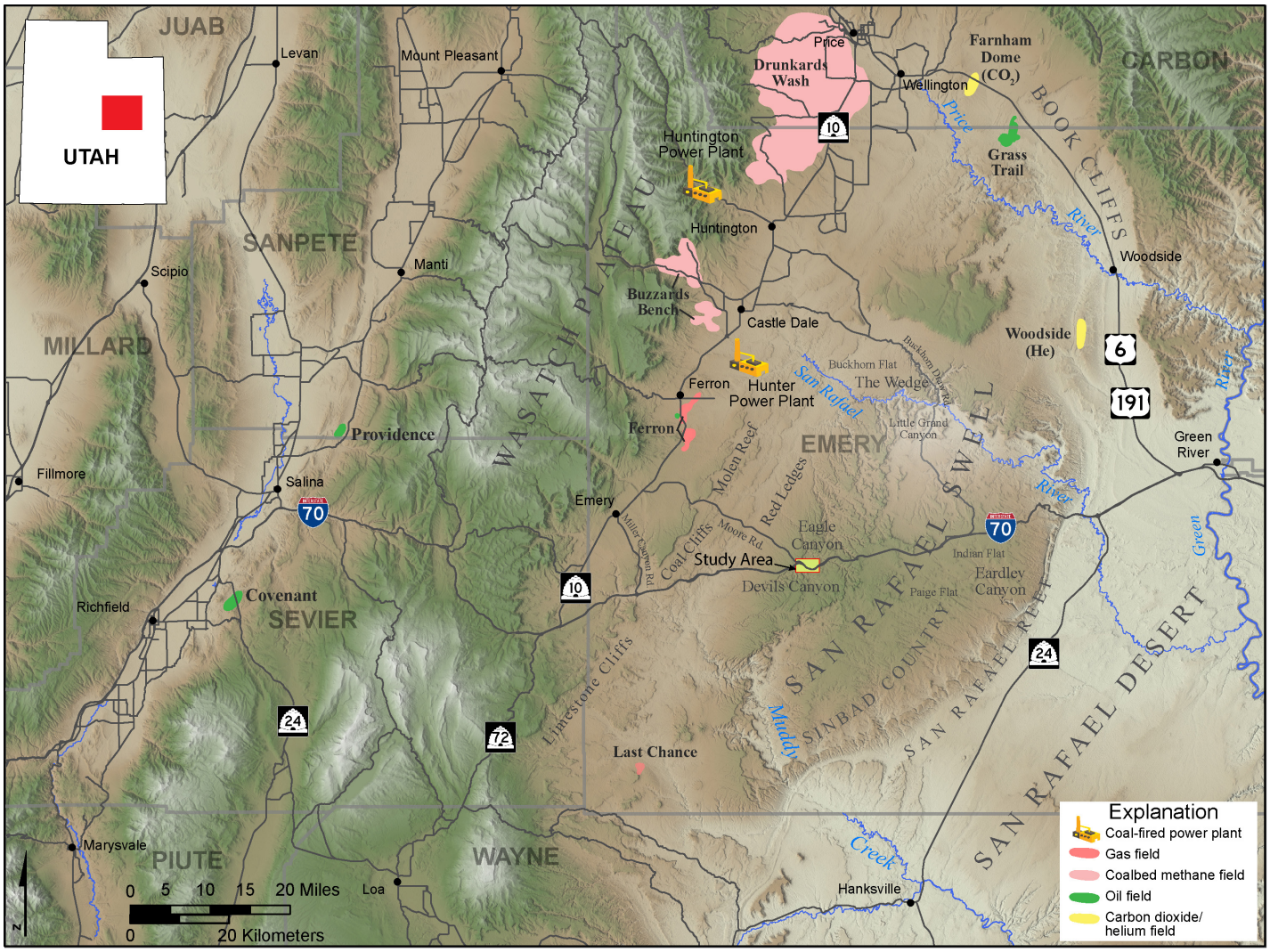

Figure 44. The Navajo Sandstone produces oil at Covenant and Providence fields in the central Utah thrust belt and CO_2 at Farnham Dome field on the north end of the San Rafael Swell. Drunkards Wash field produces coalbed methane from the Ferron Formation of the Upper Cretaceous Mancos Group (Kirkland et al., 2025); the produced water is disposed of in the Navajo. Also shown are the Hunter and Huntington coal-fired power plants. Note the study area (small yellow rectangle) from Chidsey (2020) on the west flank of the San Rafael Swell along Interstate 70.

sand that show medium-angle foreset laminations. The thin wispy or wavy laminations indicate an algal influence. The SAM facies is a barrier or baffle to fluid flow; however, the high silt and sand content can cause it also to be brittle and subject to fracturing. Porosity and permeability averages about 9% and 0.2 mD, respectively.

Only very thin (less than a foot) zones of the Wavy Algal Mat (WAM) subfacies are identified in Covenant cores. The WAM subfacies consists of dark bands of wispy black algal laminae in a light to medium gray silty and muddy matrix. The WAM facies is also a barrier or baffle to fluid flow having porosity and permeability averaging 6% and 0.3 mD, respectively.

Farnham Dome CO_2 Field, Carbon County

Farnham Dome is a subsidiary structure on the north-plunging nose of the Laramide-age (70 to 40 Ma) San Rafael Swell (Figures 44 and 48). It is dissected by a series of small, west-dipping, southwest-north-

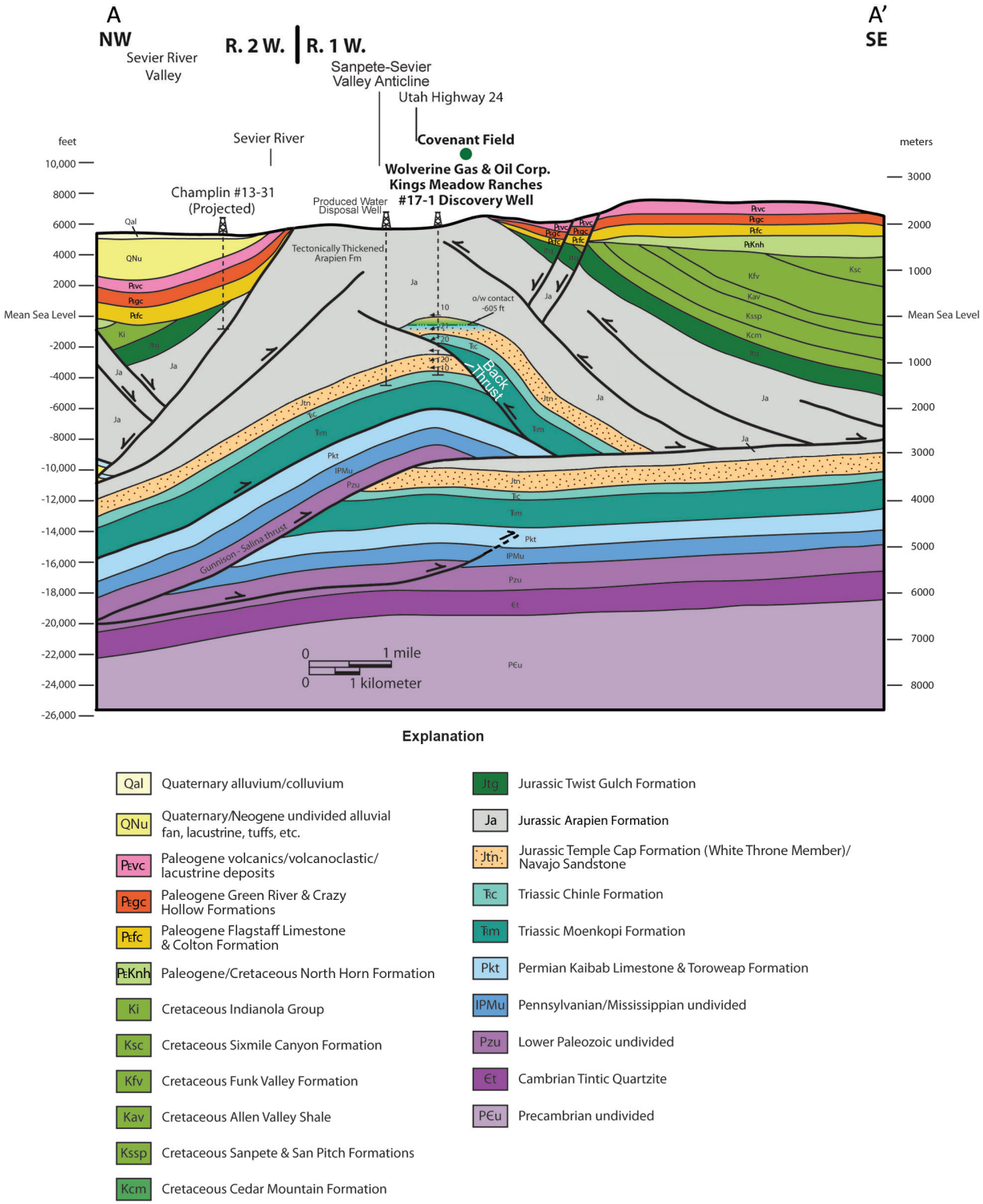

Figure 45. Northwest-southeast structural cross section through Covenant field. Original cross section courtesy of Wolverine Gas & Oil Corporation; modified from Chidsey et al. (2007) and Schelling et al. (2007). Note small back thrust through the anticline that results in a repeated Navajo Sandstone/Temple Cap Formation section; only the upper section is productive. The produced water is injected into the Navajo Sandstone through a disposal well that is off structure to the west of the field. Line of cross section A–A' shown on Figure 42.

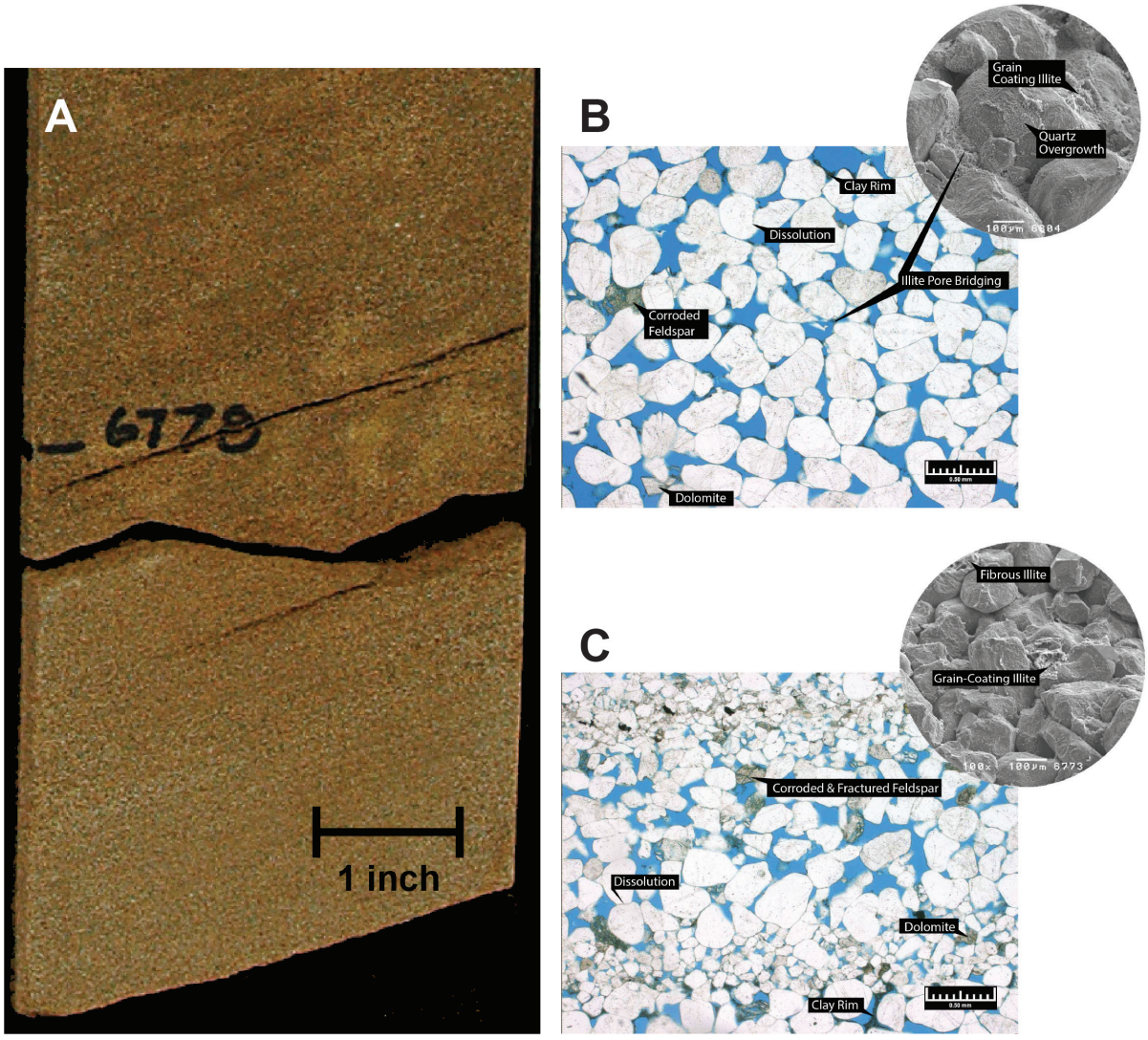

Figure 46. Large trough cross-bedded (LTC) subfacies from the Kings Meadow Ranches No. 17-3 well in Covenant field. (A) Typical large trough cross-bedding in fine-grained sandstone. Slabbed core from 6778 feet (2066 m). Porosity = 14.7%, permeability = 135 mD, based on core-plug analysis. (B and C) Representative LTC thin section photomicrographs (plane-polarized light) and insets of scanning electron microscope images. B shows subangular to subrounded quartz sand and excellent intergranular porosity (blue space) with very little clay content. Porosity = 12.9%, permeability = 213 mD, based on core-plug analysis, 6804 feet (2074 m). C shows bimodal distribution (layered) of subangular to subrounded quartz sand and silt. Note a few fractured and corroded K-feldspar grains are present. Porosity = 14.8%, permeability = 149 mD, based on core-plug analysis, 6773 feet (2064 m). From Chidsey et al. (2020).

east-trending thrust faults mapped on the surface; however, the faults likely die out in the gypsiferous-rich mudstone and siltstone beds of the Winsor Member of the the Middle Jurassic Carmel Formation or a detachment fault within the Winsor (Figure 49). These faults may be similar to the graben structures on the Wasatch Plateau. There, the faults die out in the upper Arapien/Carmel Formations evaporitic beds or sole into a detachment fault in the upper Arapien (Twelvemile Canyon Member) or Carmel (Winsor Member) (Moulton, 1975; Schelling et al., 2007; Anderson, 2008). Also, Neuhauser (1988) documents the possible leading edge of the Sevier thrust belt offsets the Middle Jurassic through Lower Cretaceous rock at Cedar Mountain on

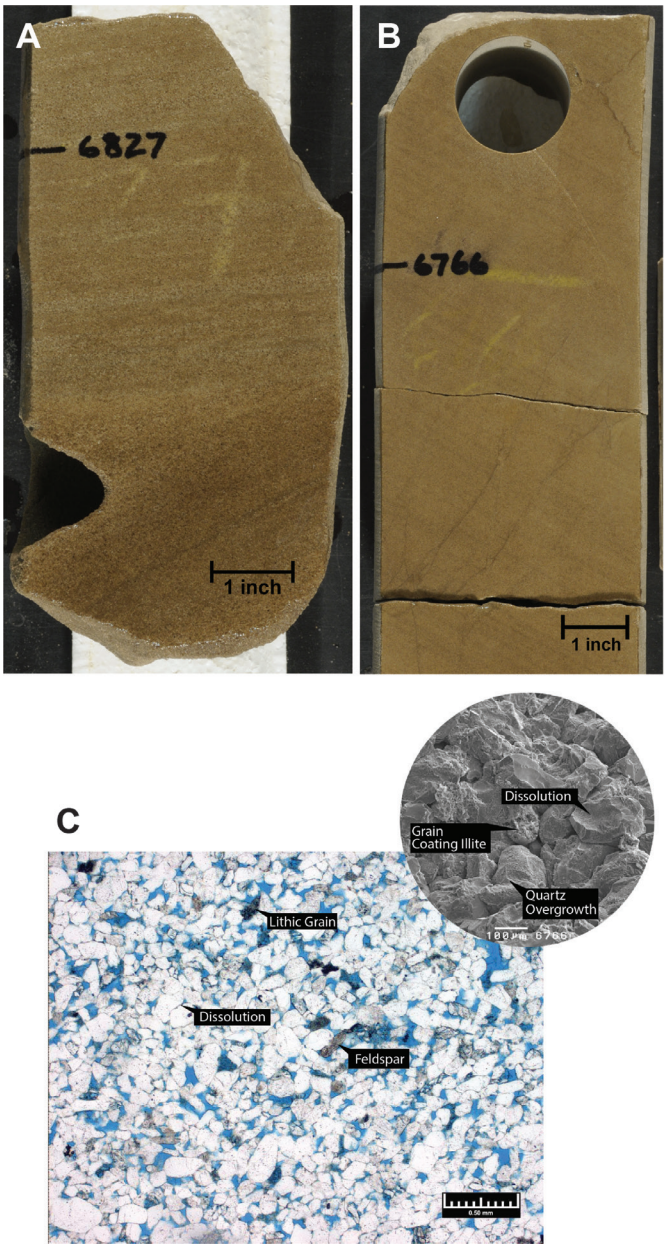

Figure 47. Small trough cross-bedded (STC) and reworked eolian (REW) subfacies from the Kings Meadow Ranches No. 17-3 well in Covenant field. (A) Typical low-angle, small trough cross-bedding representing the dune toe in fine- to medium-grained sandstone of the STC subfacies. Slabbed core from 6827 feet (2081 m). Porosity = 17.6%, permeability = 1210 mD, the highest values for the Navajo Sandstone in the well based on core-plug analysis. (B) Fine-grained sandstone of the RWE subfacies containing possible relict or poorly developed cross-bedding of the STC facies. Slabbed core from 6766 feet (2062 m). Porosity = 12.4%, permeability = 6.3 mD, based on core-plug analysis. (C) Representative STC to REW thin section photomicrograph (plane-polarized light) and inset of scanning electron microscope image of subangular to angular fine quartz sand and silt having some larger subrounded quartz grains. Note the presence of corroded K-feldspar grains and dissolution along grain boundaries of quartz grains. Porosity = 12.4%, permeability = 6.3 mD, based on core-plug analysis, 6766 feet (2062 m). From Chidsey et al. (2020).

the San Rafael Swell just south of Farnham Dome, further evidence that a detachment fault may underlie the field structure as depicted on Figure 49. These structural scenarios leave the Navajo Sandstone at Farnham Dome below largely unfaulted (Figure 50). Blind, high-angle, east-dipping, basement-involved reverse faults helped create the Farnham structure during Laramide time (Morgan, 2007).

The average depth to the Navajo reservoir is 1800 feet (550 m) in Farnham Dome field. The pay zone thickness averages 40 feet (12 m) with about 12% porosity and permeability over 100 mD (Peterson, 1961; Colson, 1993), similar to the petrographic properties found in Navajo outcrops in the San Rafael Swell farther south. The composition of the gas produced from the Navajo is almost 99% CO_2 and about 1% nitrogen, with no hydrocarbons (Moore and Sigler, 1987; Morgan and Chidsey, 1991; Chidsey and Morgan, 1993; Morgan, 2007). Discovered in 1924, CO_2 production first began in 1931, and the field has since produced almost 5.6 billion cubic feet of gas (BCFG). Initially the gas was transported via a pipeline to a dry ice plant just west of

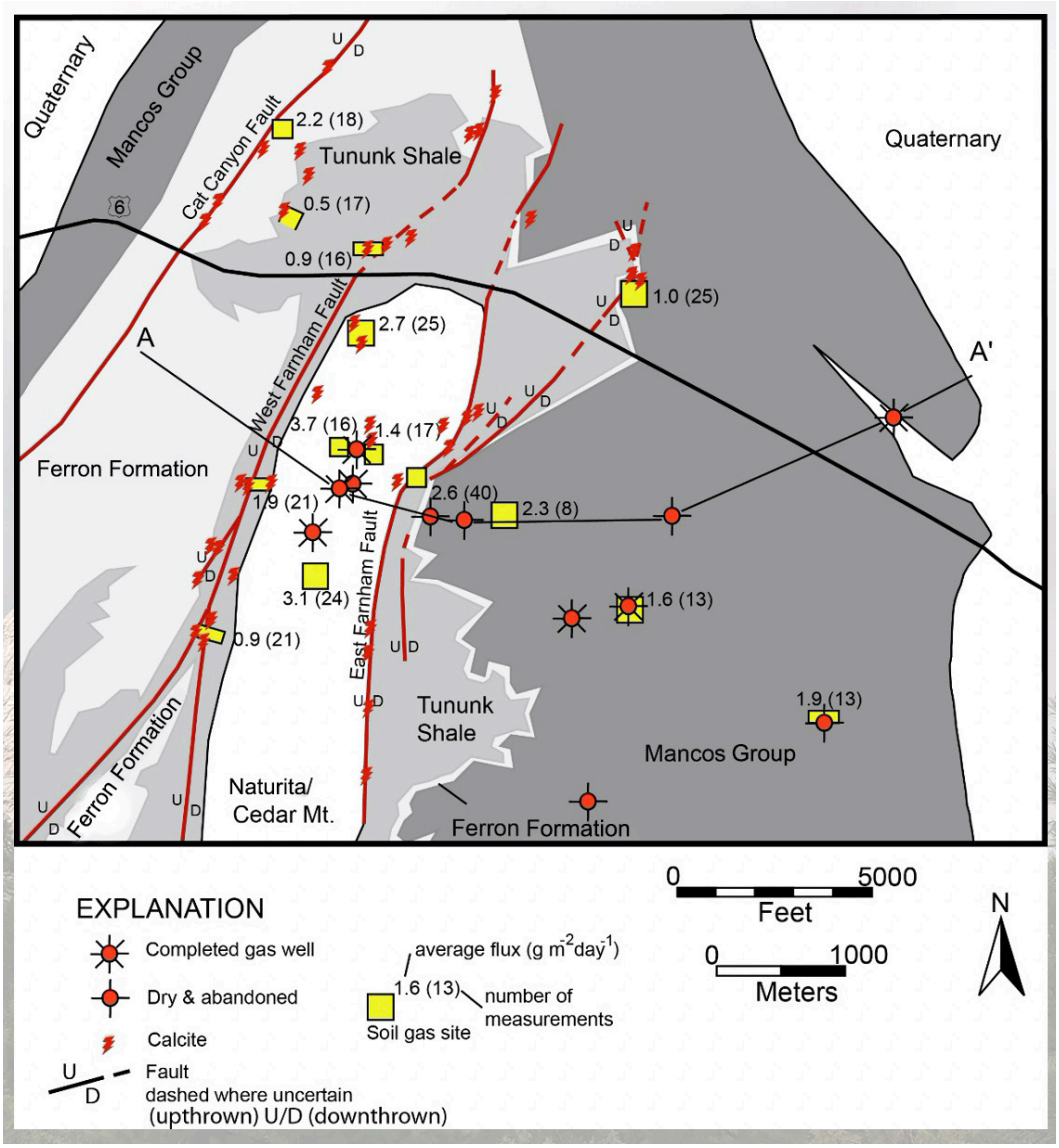

Figure 48. Generalized geologic map of the Farnham Dome field area, east-central Utah, showing faults, calcite locations, and soil-gas survey sites. See Figure 49 for cross section A–A'. After Morgan (2007); soil-gas measurements from Allis et al. (2005).

the field where it was used for food processing. More recently the gas was compressed and trucked north to the Uinta Basin for hydraulic fracturing operations; however, those operations were suspended in 2014 when gas prices crashed. Farnham Dome field currently has one active well that produced 1.16 BCFG in 2025 (Utah Division of Oil, Gas and Mining, 2026).

AQUIFER

Oil and Gas Produced Water Disposal

The Navajo Sandstone is also a major produced water disposal unit at Covenant field, discussed earlier, and Drunkards Wash field just to the northwest of the San Rafael Swell (Figure 44). The Navajo/Nugget Sandstone has the potential for produced water disposal in the Uinta Basin to the north, although in much of the basin this would be very deep (Morgan and Kirby, 2017).

Drunkards Wash Field

Drunkards Wash produces coalbed methane from coal beds in the Ferron Formation of the Upper Cretaceous Mancos Group (Kirkland et al., 2025). Cumulative production as of January 1, 2026, is 1.17 trillion cubic feet of gas (Utah Division of Oil, Gas and Mining, 2026), making it Utah's second largest gas field. There currently are 577 active wells in Drunkards Wash, many

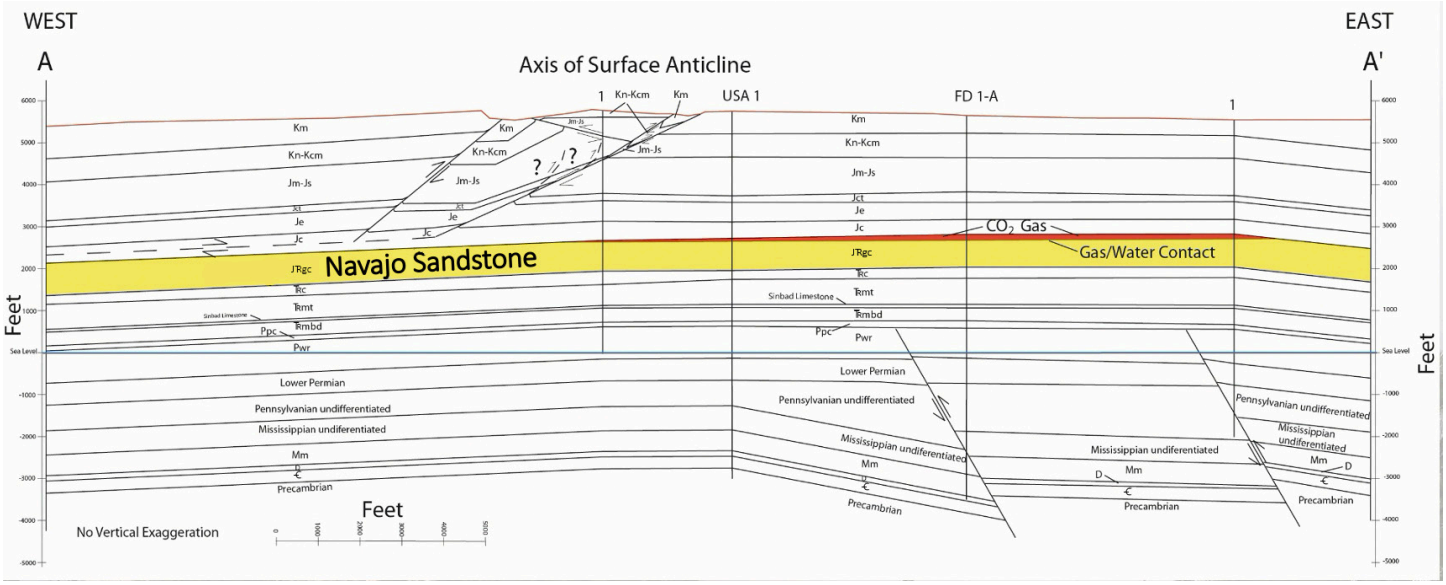

Figure 49. West-to-east cross section A–A' showing a broad Laramide structure providing the trap for CO_2 (light orange) in the Navajo Sandstone at Farnham Dome field. Pwr = Permian White Rim Sandstone; Ppc = Permian Park City Formation; Ṯrmbd = Triassic Moenkopi Formation, Black Dragon Member; Ṯrmt = Triassic Moenkopi Formation, Torrey Member; Ṯrc = Triassic Chinle Formation; JṮrgc = Jurassic Glen Canyon Group (includes Navajo Sandstone); Jc = Carmel Formation; Je = Jurassic Entrada Sandstone; Jct = Curtis Formation; Jm-Js = Jurassic Morrison-Summerville Formations; Kn-Kcm = Cretaceous Naturita (formerly Dakota)-Cedar Mountain Formation; Km = Mancos Shale. After Morgan (2007). Line of cross section A–A' shown on Figures 48 and 50.

of which are used for dewatering the coal zones. This has led to cumulative production of about 297 million bbls of water; 371,000 bbls monthly. The produced water is disposed of by injection into the Navajo Sandstone, with its excellent reservoir properties, through 10 wells.

Covenant Field

The amount of water produced with the oil from the Navajo Sandstone at Covenant field (Figures 42 and 44) has steadily increased since 2010 when it surpassed oil production (Figure 51). Early drilling to define the field's productive limits included a dry hole on the west flank. Although dry, the well helped to reconfigure the structural interpretation of the field. Instead of encountering a repeated Navajo section from a thrust splay, only one Navajo section was penetrated by the well. The resulting interpretation placed a back thrust to the east that created the productive structure (Figure 45). The presence of the back thrust between the west flank dry hole and productive structure set up a secondary nonproductive trap.

Cumulative water production from Covenant field is over 80 million bbls of water as of January 1, 2026 (Figure 51); monthly water production is over 512,000 bbls (Utah Division of Oil, Gas and Mining, 2026). The secondary trap along the west flank of Covenant field has been ideal for disposal of the produced water into the porous and permeable, yet oil-barren, west-dipping Navajo Sandstone using the available dry hole (Figure 45).

Culinary Water

The Navajo Sandstone serves as a major aquifer for culinary water in southern Utah. It is the crucial aquifer for the St. George area (i.e., the Washington County Water Conservatory District) and elsewhere in the Virgin River basin of southwestern Utah (Clyde, 1987; Hurlow, 1998; Heilweil et al., 2000, 2002; Rowley and Dixon, 2004; Rowley et al., 2004) and for the Navajo Nation in the Four Corners area in the southeastern part of the state (Spangler et al., 1996). Wells in the Lamb Point

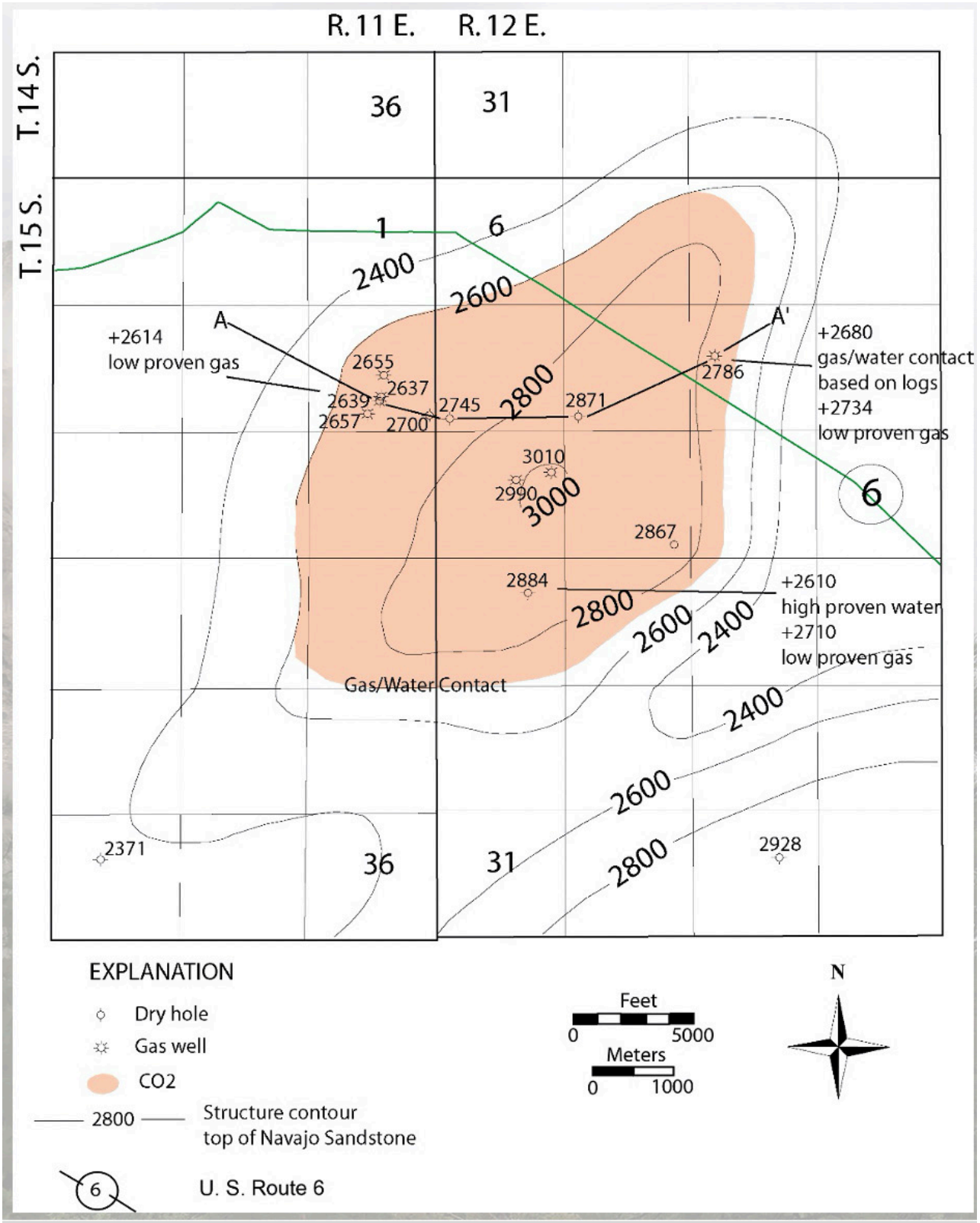

Figure 50. Structure contours on top of the Navajo Sandstone showing the CO_2 gas column (light orange) displaced slightly to the west-northwest. Contour interval = 200 feet; datum is mean sea level. From Morgan (2007). See Figure 49 for cross section A–A'.

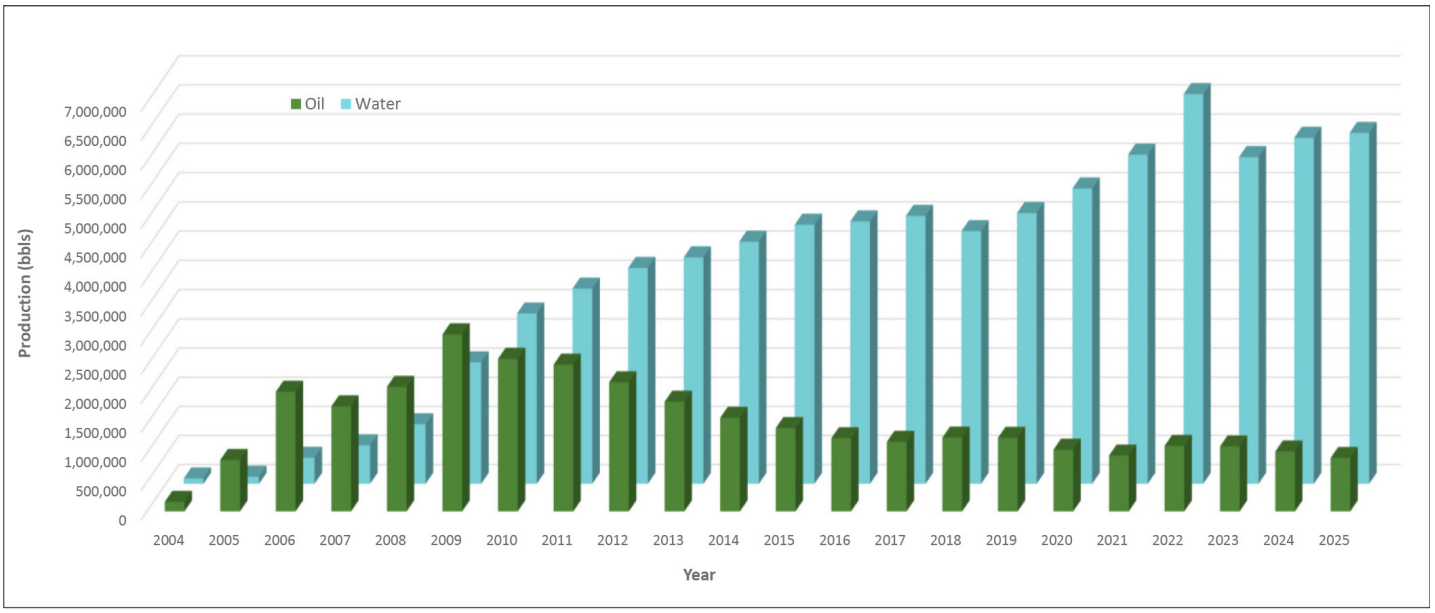

Figure 51. Yearly oil and water production from wells in Covenant field as of January 1, 2026. Data from Utah Division of Oil, Gas and Mining (2026).

Tongue of the Navajo also supply culinary water to the towns of Kanab (east of Zion National Park), Utah, and nearby Fredonia just to the south in Arizona (Doelling et al., 2024).

Washington County Water Conservatory District

St. George is a fast-growing metropolitan community with a population of over 175,000. Most culinary water for this area is supplied by several aquifers in the Washington County Water Conservatory District, the largest being the Navajo Sandstone. The Navajo dips north and is cut by several down-to-the-west, high-angle, north-south-trending normal faults, the largest of which are the Gunlock fault to the west and the enormous Hurricane fault to the east that, along with the erosional extent to the south and west, form the boundaries of the aquifer (Heilweil et al., 2000). Between these faults, the Navajo has large outcrop exposures and a stratigraphic thickness of 2000 to 2300 feet (600–700 m) (Hintze and Kowallis, 2021) (Figures 52 and 53).

Combined with extensive fracture zones and uniform sandstone grain size, the Navajo aquifer is able to receive, store, and move large amounts of water (Heilweil et al., 2000). The horizontal hydraulic conductivity values of the Navajo range from 0.2 to 32 feet (0.06–9.8 m) per day depending on fracturing along the outcrop belt (Heilweil et al., 2000). Recharge is primarily from infiltration of precipitation. Total water moving through the Navajo (including the smaller underlying Kayenta Formation aquifer) is estimated at about 25,000 acre-feet (31 hm^3) per year (Heilweil et al., 2000). The water in the aquifers is low in total dissolved solids (TDS), i.e., Class 1A or pristine aquifer, with two areas having TDS concentrations greater than 500 milligrams per liter (mg/L); i.e., Class II or drinking water aquifer (Figure 52) (Heilweil et al., 2000; Hansen, Allen, & Luce, Inc., 2005).

Navajo Nation in the Four Corners Area

In Four Corners area (i.e., the Navajo Nation, Figure 54) of southeastern Utah where the population is sparse, the Navajo Sandstone is the largest aquifer—equally important as it is for those living in the southwestern part of the state. The Navajo, and other aquifers, is confined in the area and is 200 to 800 feet (60–240 m) thick (Hintze and Kowallis, 2021) with the top averaging about 550 feet (170 m) below the surface. The Navajo aquifer is recharged along the flanks of the Abajo Mountains

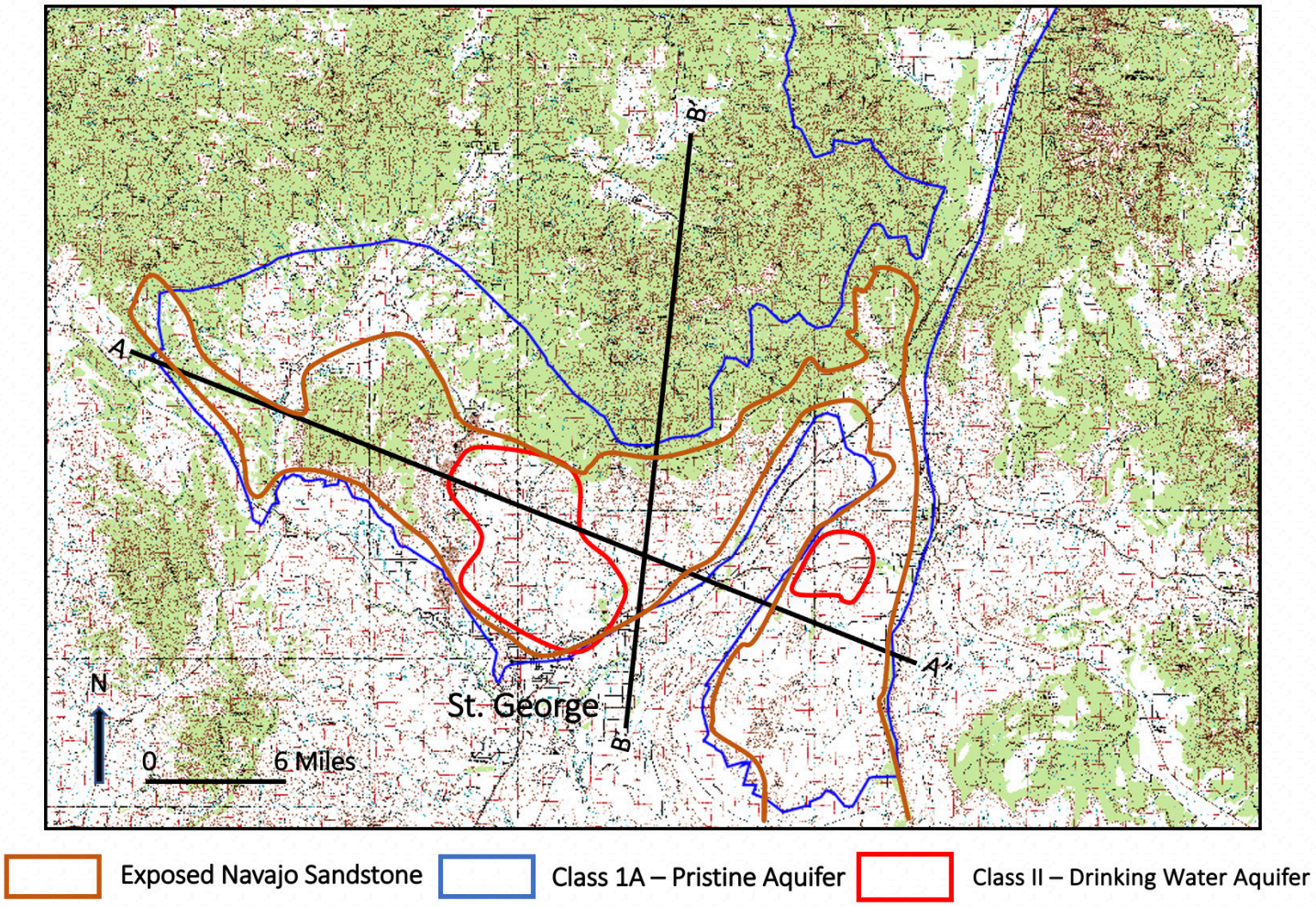

Figure 52. Map of Navajo aquifer classification in Washington County Water Conservatory District. After Hansen, Allen, & Luce, Inc. (2005). See Figure 53 for cross sections A–A' and B–B'.

in Utah, Sleeping Ute Mountain in Colorado, and the Carrizo Mountains in Arizona, to the north, east, and south, respectively (Spangler et al., 1996). Potentiometric contours and increasing hydraulic head with depth indicate that water in the Navajo aquifer moves downgradient from these recharge areas and then migrates upward into the shallow Upper Jurassic Morrison Formation aquifer before discharging into the San Juan River (Figure 55) (Thomas, 1989; Freethey and Cordy, 1991; Weiss, 1991).

Water flow through the Navajo Sandstone also occurs in the Greater Aneth oil field area (Figures 54 and 55), the largest oil field in Utah with over 512 million bbls of oil production from the Pennsylvanian Paradox Formation (Utah Division of Oil, Gas and Mining, 2026) (Figure 55). Water from the Navajo and the other aquifers flows primarily from water wells and abandoned oil wells that were plugged back to the water-bearing formations. Measured discharge from flowing wells has been recorded from less than 1 to as much as 150 gallons (3.8–570 L) per minute, or 600-acre feet (0.7 hm^3) per year (Spangler et al., 1996). The TDS concentrations in water from 56 wells in the Navajo aquifer ranges from 145 mg/L (fresh) to as much as 17,300 mg/L (very saline) (Spangler et al., 1996). Protecting these aquifers from casing leaks in oilfield wells and surface spills is critical for the people who live in the region and use the groundwater for culinary and agriculture purposes.

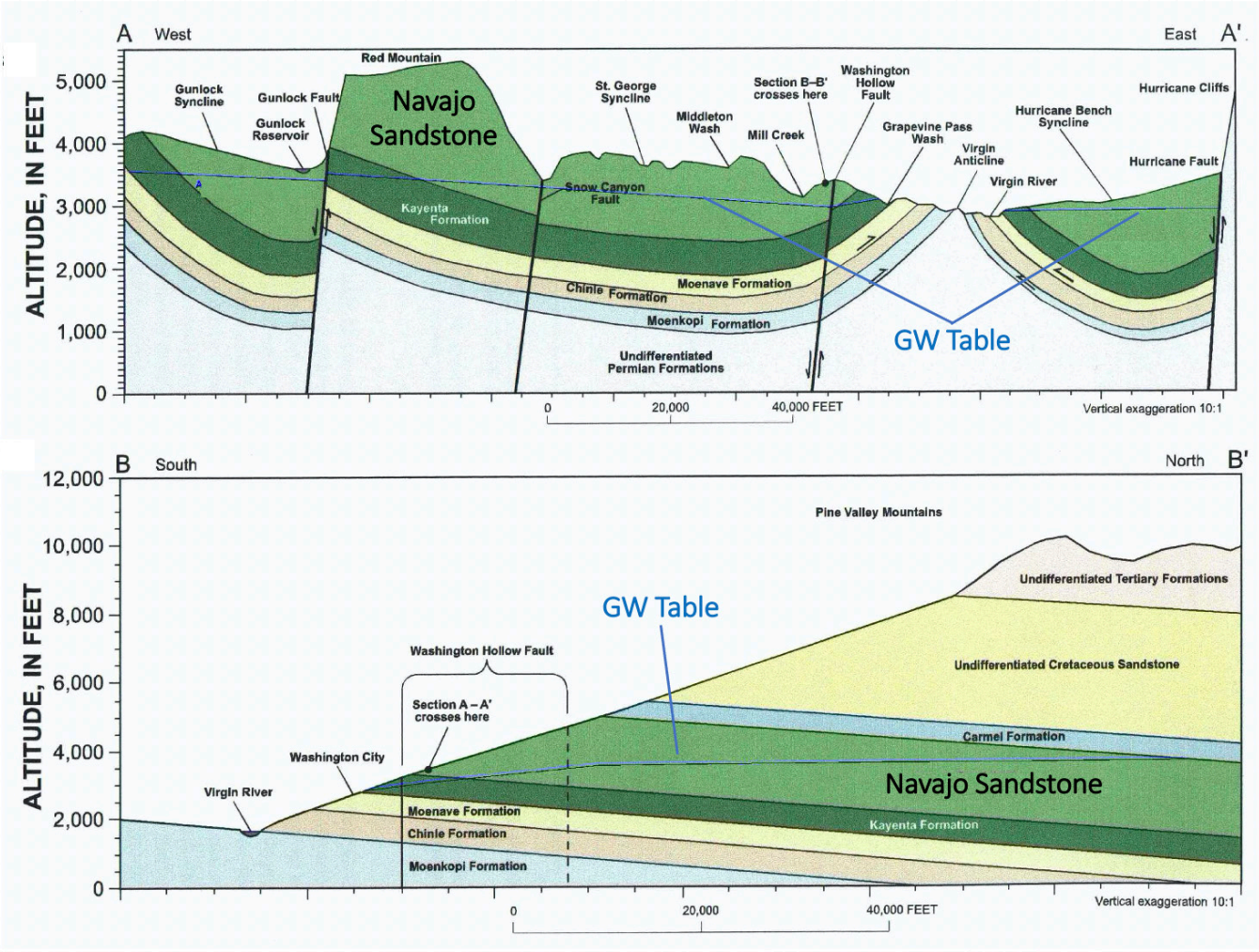

Figure 53. Structural cross sections A–A' and B–B' through the Washington County Water Conservatory District. Note the position of the groundwater table (GW) and recharge area (Navajo Sandstone outcrops). After Heilweil et al. (2000). Line of cross sections A–A' and B–B' shown on Figure 52.

POTENTIAL FOR CARBON SEQUESTRATION

Castle Valley/Eastern Wasatch Plateau Area, East-Central Utah

The Navajo Sandstone has enormous potential as a storage unit for CO_2 that could be captured from the Hunter and Huntington coal-fired power plants just west of the San Rafael Swell in the Castle Valley/eastern Wasatch Plateau area (Figure 44) and has been the subject of several major studies for that purpose (see Allis et al., 2001, 2003, 2005; White et al., 2003, 2005; Parry et al., 2007; Allen et al., 2013; McPherson, 2018; and Steele et al., 2018, Chidsey et al., 2020). These studies included characterization of the reservoir and seal based on Navajo Sandstone and the overlying Temple Cap/Carmel Formation crop out in the nearby San Rafael Swell (Figure 56) and reservoir modeling. The results of the modeling showed CO_2 captured from the power plants could be injected into the Navajo and safely stored as a supercritical fluid at depth along the western flank of the San Rafael Swell (Figure 57).

Furthermore, Farnham Dome on the northern end of the Swell and the natural CO_2 trapped there (see discussion above) in the Navajo Sandstone proved to be

Figure 54. Map of oil fields, including Greater Aneth, and the Navajo Nation boundary and communities in southeastern Utah in the Four Corners area.

an ideal analog. The gas likely migrated into the trap between 50 and 10 Ma. However, no surface leakage of CO_2 was detected over the field area despite the millions of years it has been stored in the Navajo and a significant number of faults associated with the structure (Morgan, 2007). Farnham Dome demonstrates CO_2 can be stored in "empty" Navajo traps elsewhere on the Colorado Plateau.

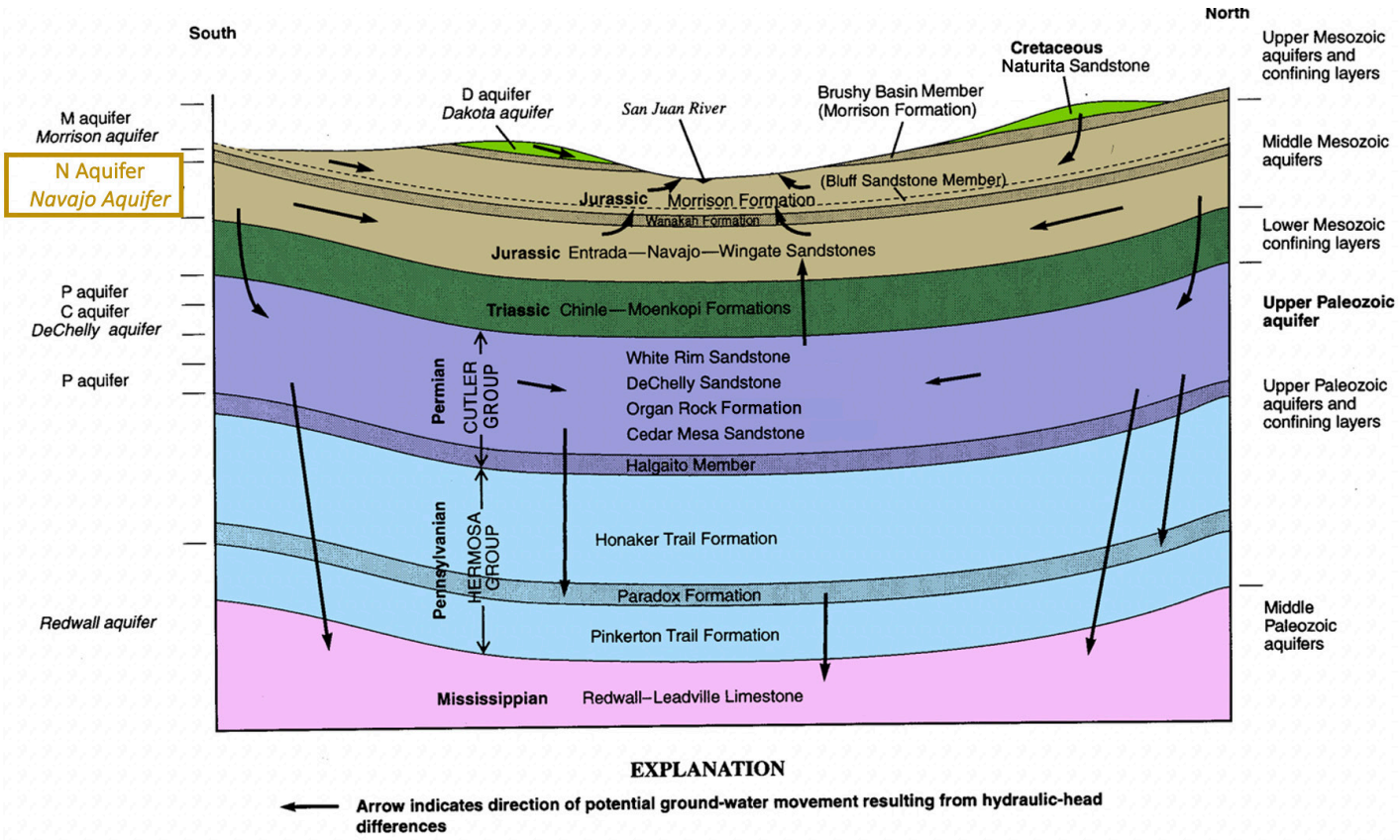

Figure 55. Schematic north-south cross section of the hydrogeologic units in the Greater Aneth oil field area, San Juan County, Utah. Arrows indicate direction of potential groundwater movement from hydraulic head differences. Modified from Spangler et al. (1996).

Iron Springs Mining District, Southwestern Utah

Farther west in the eastern part of the Basin and Range Province near Cedar City, another growing population center in southwestern Utah, the UGS is assessing the carbon sequestration potential in the Iron Springs mining district, one of the largest sources of iron ore in the United States. Steel from this ore is currently manufactured overseas; however, plans are being developed to build a direct-reduced iron ore processing plant that will include a carbon capture and storage site/reservoir in an adjacent area where more than 500,000 metric tons of CO_2 will be injected per year (Smith, et al., 2022; Szymanski, 2022; Szymanski et al., 2022a, 2022b). Once again, the primary target formation for CO_2 storage is the Navajo Sandstone.

The Iron Springs mining district lies at the eastern margin of the Basin and Range Province as it transitions into the Colorado Plateau, an area often referred to as "the Hingeline." This region is characterized by north-northeast-trending, basement-cored uplifts and grabens, typical of the Basin and Range. Extensive faulting involves thick Paleozoic and Mesozoic stratigraphic sequences and extensive Eocene and younger volcanics (Szymanski et al., 2022a, 2022b). The mining district lies within the "Iron Axis" magmatic province that parallels the Iron Springs thrust fault system, which formed during the Sevier orogeny in the Late Cretaceous. Oligocene-Miocene calc-alkalic igneous activity about 35 to 22 Ma included quartz monzonite intrusions (Figure 58), followed by post-volcanic thermal subsidence, and Basin and Range extension that began in the late Miocene around 10 Ma.

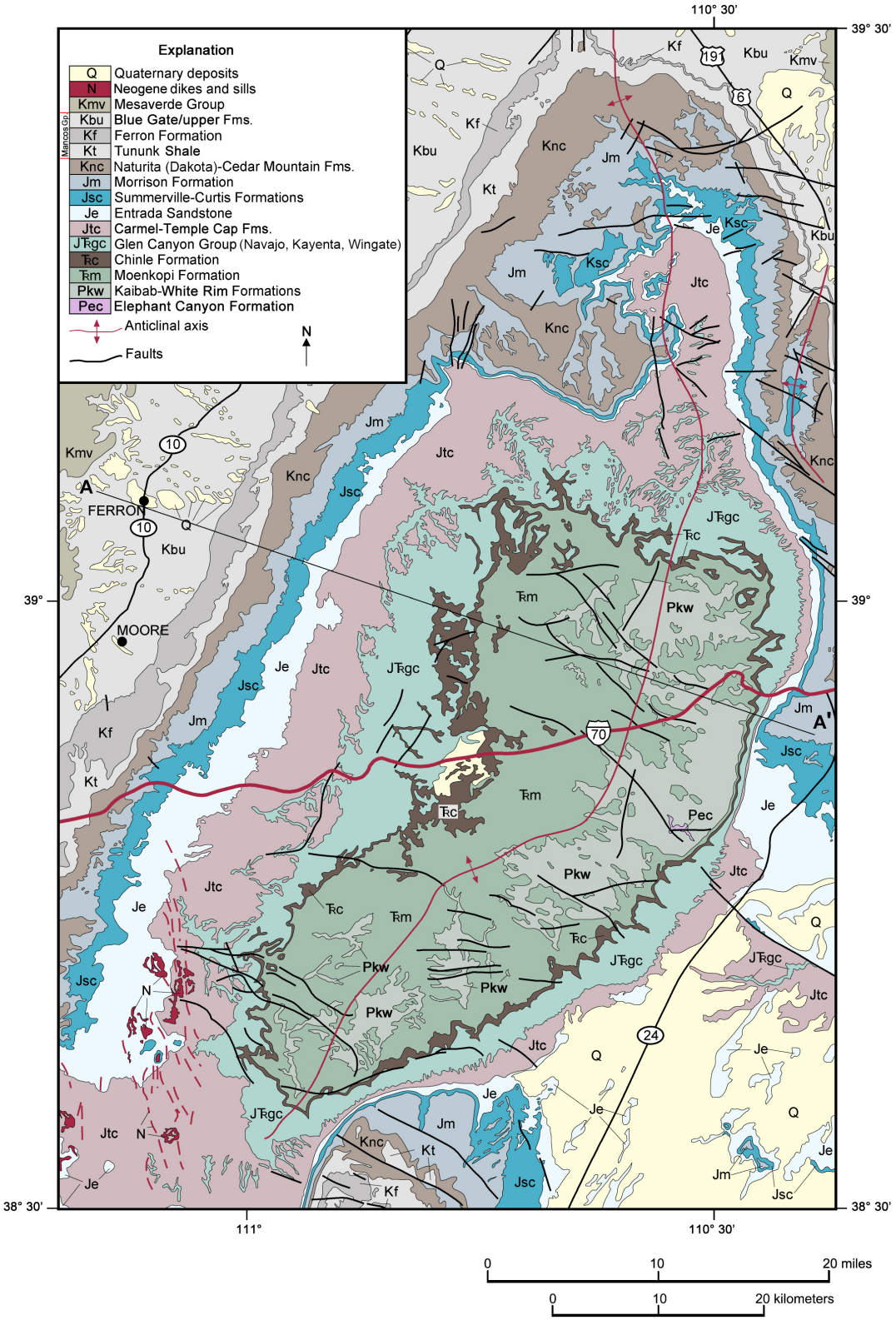

Figure 56. Generalized geologic map of the San Rafael Swell; the Navajo Sandstone is within the Triassic-Jurassic Glen Canyon Group (colored turquoise; see Explanation for unit symbols). After Doelling and Hylland (2002). Cross section A–A' shown on Figure 57.

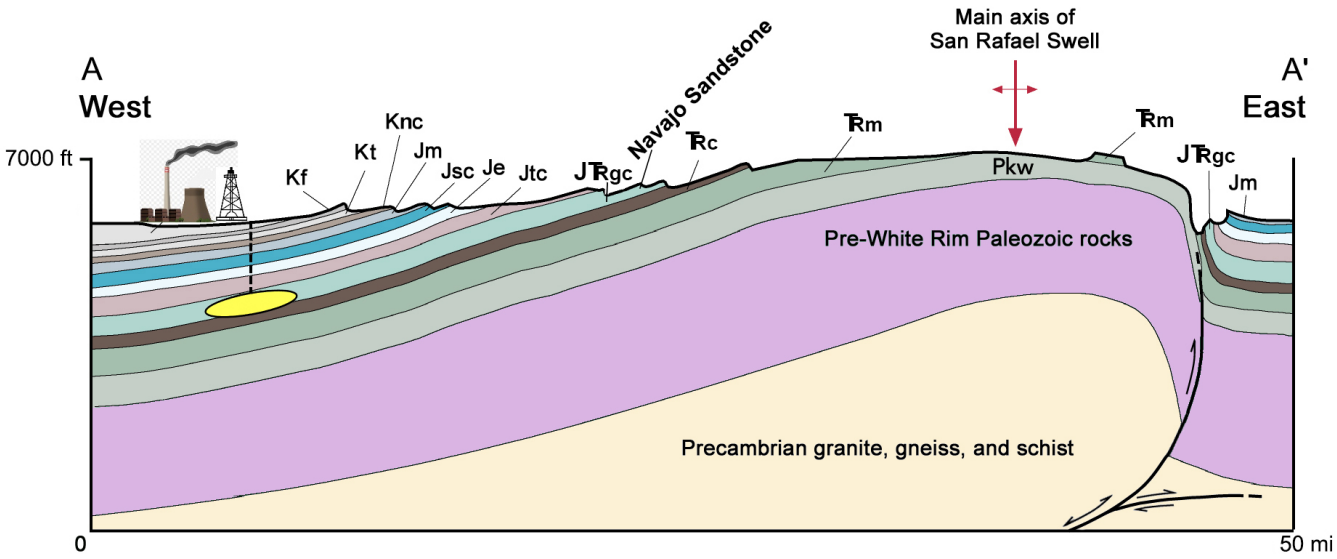

Figure 57. Diagrammatic cross section across the middle of the San Rafael Swell. Shown is CO_2 captured from coal-fired power plants safely stored in the Navajo Sandstone as a supercritical fluid at depth (elongate yellow oval). The cross section is not drawn to scale, but the vertical dimension is exaggerated about eight times relative to the horizontal; the horizontal length of the cross section covers about 50 miles (80 km). Symbols and colors of geologic formations correspond to those shown on Figure 56; cross section A–A' also shown on Figure 56. After Doelling and Hylland (2002).

Within the Iron Springs mining district, the targeted Navajo Sandstone is stratigraphically sealed by overlying gypsiferous shale and gypsum beds of the Middle Jurassic Carmel Formation and, in certain areas, further sealed by the Three Peaks quartz monzonite (Figures 59 and 60), which intruded the Carmel in Oligocene-Miocene time creating a large laccolith (Szymanski et al., 2022a, 2022b). The igneous intrusion has historically been interpreted as a continuous, sheet-like intrusion, but questions remain about the orientation and extent of the laccolith. Furthermore, structural complexities are also unknown at depth and could impact seal integrity (Szymanski et al., 2022a, 2022b).

The UGS study includes site characterization and analysis of Navajo Sandstone's CO_2 storage capacity, risks, and economic options. Planned activities are groundwater/aquifer characterization, chronostratigraphy, structural and tectonic history analysis, an outcrop study of the Navajo, examination of well cuttings from exploration wells in the region to characterize the subsurface Navajo, reevaluation of two-dimensional seismic and new gravity surveys, and appraisal of historical and modern seismicity (Smith, et al., 2022; Szymanski, 2022; Szymanski et al., 2022a, 2022b).

CONCLUSIONS

The Lower Jurassic Navajo Sandstone with its spectacular cross-bedding creates the magnificent cliffs and canyons in Zion and other national parks and public lands on the Colorado Plateau in southern Utah. The Navajo represents the textbook example of an ancient eolian environment. However, the there is more to the scenic beauty of this glorious stratigraphic sandstone formation.

- The Navajo Sandstone was deposited in a great Sahara-like erg that covered much of Utah. Originally sourced, in part, from the northern Appalachian region and Canadian highlands far to the east and northeast, sand was transported by river systems along a circuitous route to the western part of the continent, deposited in a large delta system, and then during times when parts of the delta dried, was blown into the Utah

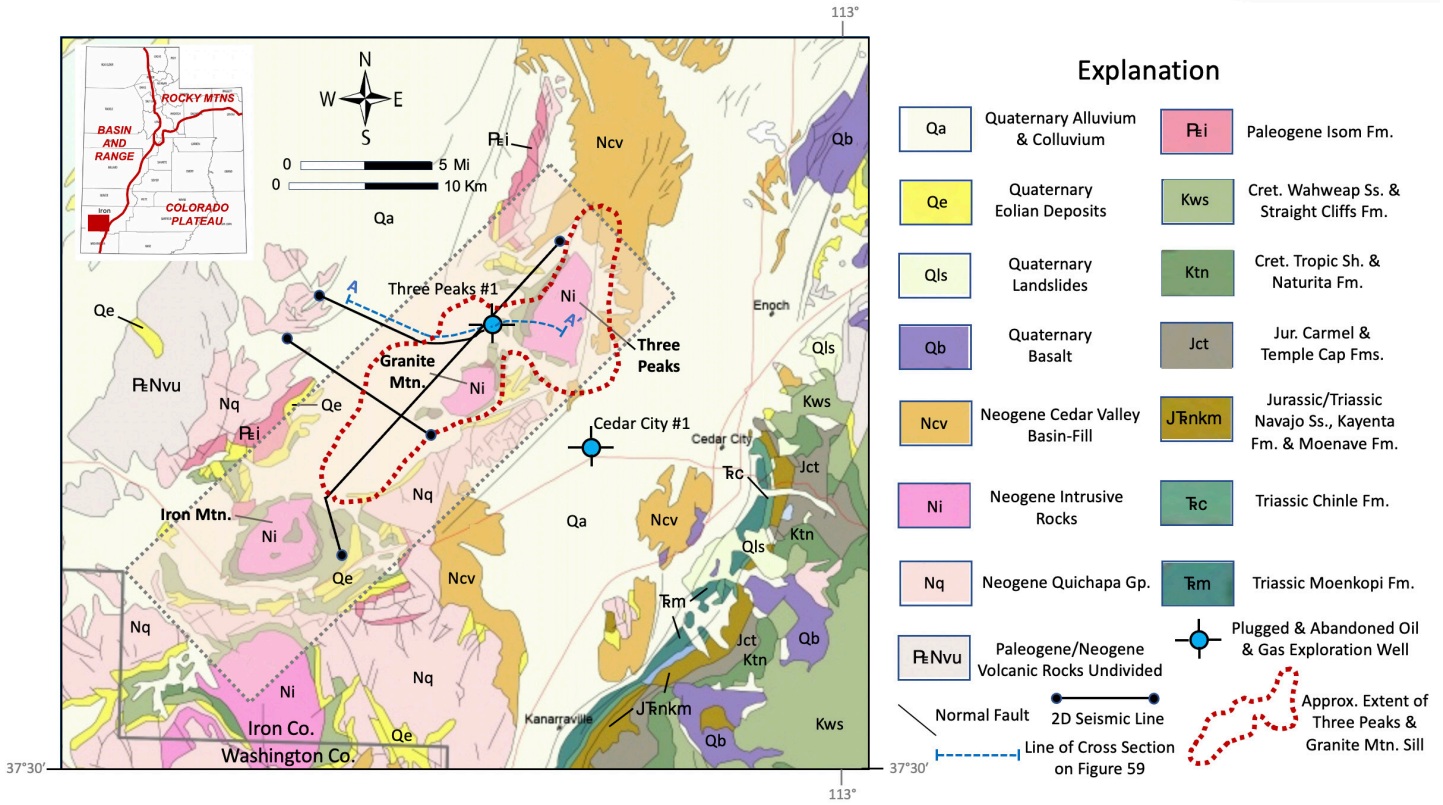

Figure 58. Generalized geologic map of the Iron Springs mining district (shaded rectangle) and surrounding region, Iron County, southwestern Utah. Also shown is the approximate extent of the Three Peaks and Granite Mountain sill/laccolith (dashed red outline) and the location of wells. Cross section A–A' shown on Figure 59. Geologic map modified from Hintze et al. (2000). Other contributions from Blank and Mackin (1967), Bullock (1973), Smith et al. (2022), and Szymanski et al. (2022a, 2022b).

area from the north and northwest. The climate was hot and dry.

- The eolian deposits included large dunes, interdunes oases, wadis, and sand sheets. The springs and lakes in the oases were the result of a climate-controlled high paleo-water table and formed carbonate rocks.
- The Navajo Sandstone preserves most bedding types and sedimentary structures formed and found in modern sand dunes – trough, tabular, and wedge cross-bedding; wind ripples; grainfall, grainflow, and avalanche deposits; and soft-sediment deformation.
- The beautiful White Cliffs of the Grand Staircase in southernmost central Utah are composed of the Navajo Sandstone; the Grand Staircase section was measured and described by Charles D. Walcott in 1879. The Navajo Sandstone extends to central Utah and is stratigraphically equivalent to the upper part of the Nugget Sandstone to the north. The Lower Jurassic Navajo is separated from overlying Middle Jurassic formations by the J-1 unconformity, a time gap of 10 million years, and intertongues with the underlying Kayenta Formation.
- At least eight Navajo Sandstone subfacies are identified: three dune subfacies – large trough cross-bedded, small trough cross-bedded, and reworked Eolian; and five interdune subfacies – wavy algal mat, sandy algal mat, ephemeral fluvial channel, poorly developed interdune, and evolving interdune.

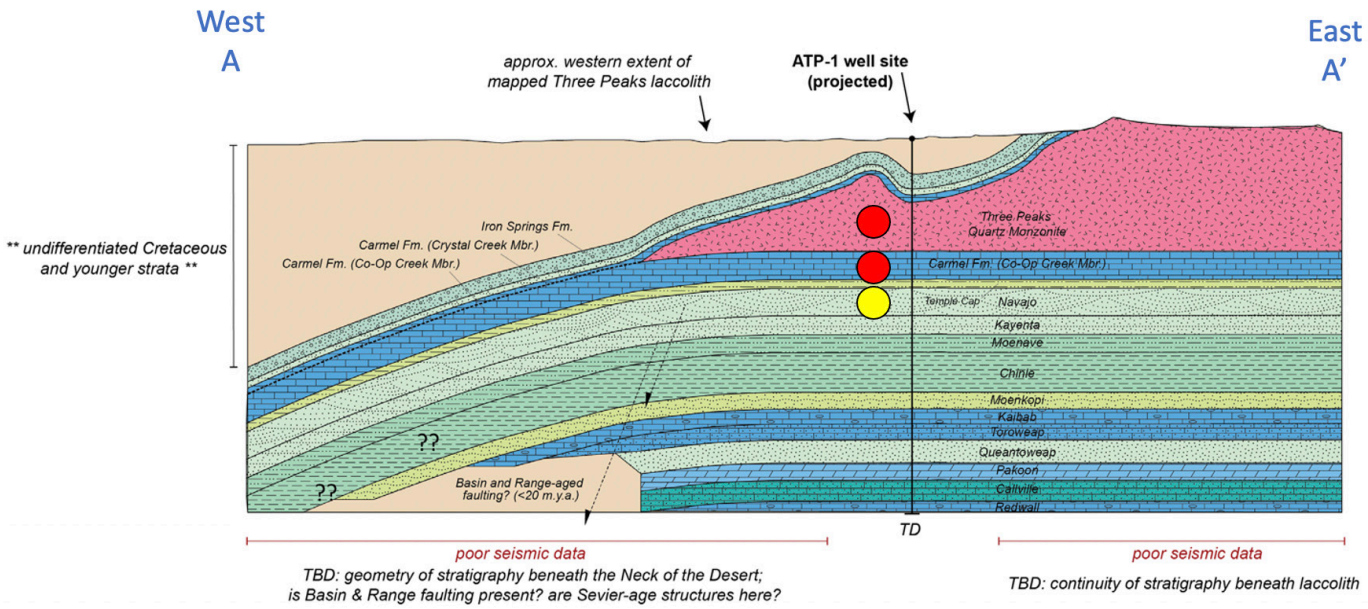

Figure 59. Structural cross section showing the Navajo Sandstone targeted for CO_2 injection (yellow dot) and the potential seals (red dots) consisting of the Carmel Formation and the Three Peaks quartz monzonite laccolith. Also shown is the projected ARCO Three Peaks No. 1 (ATP-1) abandoned exploration well (section 17, T. 35 S., R. 12 W., SLBL&M, Iron County). Inferred location of the monzonite laccolithic intrusion is from Rowley and Barker (1978) and Van Kooten (1988). Figure from Smith et al. (2022) and Szymanski et al. (2022a, 2022b). Line of section show on Figure 58.

- The Navajo Sandstone has unique iron- and manganese-rich diagenetic pipes and columns, alcoves and hanging gardens, weathered-out iron concretions, highly contorted soft-sediment deformation, honeycomb weathering, and deformation bands.
- The Navajo Sandstone serves as a reservoir both for hydrocarbons (Covenant, Providence, and Blaze Canyon fields) and CO_2 (Farnham Dome field). Cores from the Navajo reservoir of Covenant field display many of the same eolian dune and interdune subfacies and other characteristics found in outcrop.
- The Navajo Sandstone is a significant produced water disposal unit at Covenant and Drunkards Wash fields.
- The Navajo Sandstone serves as a major aquifer for culinary water for the St. George area and for the Navajo Nation in the Four Corners area in the southwestern and southeastern parts of the Utah, respectively. The Lamb Point Tongue of the Navajo is the culinary water aquifer for the towns of Kanab, Utah, and Fredonia, Arizona.
- The Navajo Sandstone has great potential as a storage unit for CO_2 that could be captured from coal-fired power plants in the Castle Valley/eastern Wasatch Plateau area and the Iron Springs mining district from a proposed iron ore processing plant, that will include carbon capture, at the eastern margin of the Basin and Range Province in southwestern Utah.

ACKNOWLEDGMENTS

This paper would not be possible were it not for the early U.S. Geological Survey workers, going back to Charles Walcott in 1879, and many others whose pioneering and timeless efforts in the field, their maps and publications, brought to light the geologic glory of the Navajo Sandstone for those following in their footsteps. I would like to thank the following friends, colleagues, and students, for their excellent research on the Navajo included in this paper: Thomas H. Morris, Brigham

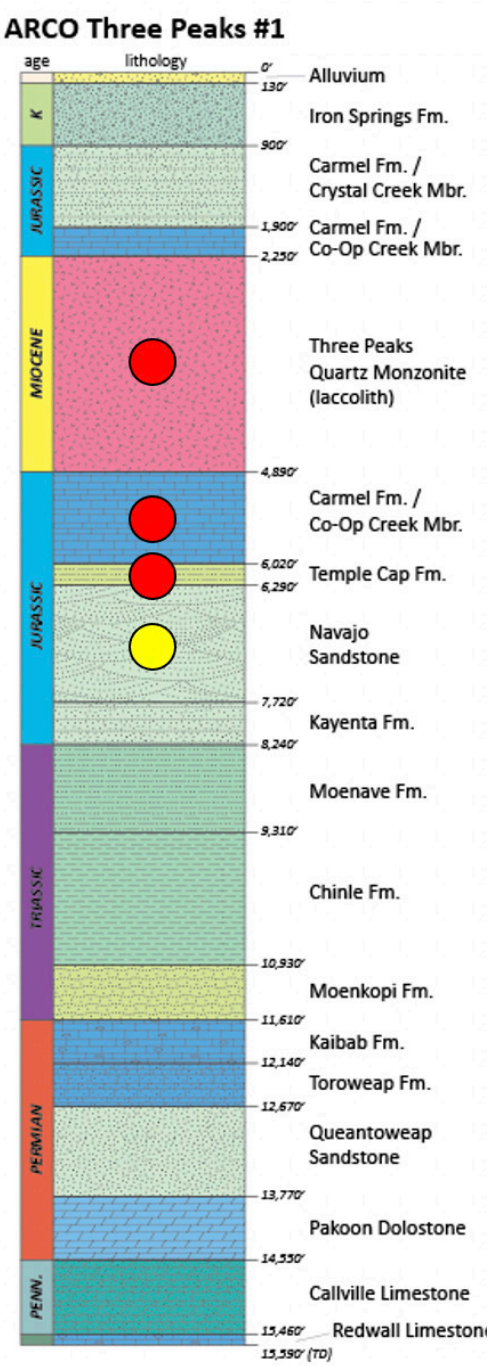

Figure 60. Revised stratigraphy from the ARCO 3 Peaks No. 1 well geophysical well log; location shown on Figure 58. Also shown are the Navajo Sandstone targeted for CO_2 injection (yellow dot) and the potential seals (red dots). Well log stratigraphy originally interpreted by Van Kooten (1988), the Jurassic and Triassic stratigraphy were revised with control from local wells, outcrops, and open mine pits (Douglas A. Sprinkel, Utah Geological Survey, personal communication, 2022); from Smith et al. (2022) and Szymanski et al. (2022a, 2022b).

Young University (BYU); Douglas A. Sprinkel, Azteca Geosolutions/Utah Geological Survey (UGS); the late W. Kenneth Hamblin, BYU; Ashley D. Hansen, Petroleum Systems International, LLC; Stephanie M. Carney, UGS; Craig D. Morgan, UGS; the late Hellmut H. Doelling, UGS; the late Lehi F. Hintze, BYU; Bart J. Kowallis, BYU; David E. Eby, Eby Petrography & Consulting, Inc.; Margorie A. Chan, William Parry, Brenda Bowen, Greg Nielsen, Peter Steele, and Jessica Allen, University of Utah; Stephen P. Phillips, BYU; Eugene Szymanski, UGS; Gerald Waanders, Consulting Palynologist; and Isaac Allred, BYU Idaho. The National Park Service provided access to various parks and the UGS provided drafting assistance and other support. I thank Grant C. Willis, UGS Emeritus; Douglas A. Sprinkel, Azteca Geosolutions; and Willian Lund, UGS Emeritus, for their reviews and constructive criticisms that greatly improved this paper.

REFERENCES

Ahlbrandt, T.S., and Fryberger, S.G., 1982, Introduction to eolian deposits, *in* Scholle, P.A., and Spearing, D., editors, Sandstone depositional environments: American Association of Petroleum Geologists Memoir 31, p. 11–47.

Allen, J., Lee, S., and Potter, S., 2013, Three dimensional geologic model of the eolian Jurassic Navajo Sandstone in central Utah for the evaluation of CO_2 sequestration, *in* Morris, T.H., and Ressetar, R., editors, The San Rafael Swell and Henry Mountains basin—geologic centerpiece of Utah: Utah Geological Association Publication 42, p. 223–260.

Allen, P.A., Verlander, J.E., Burgess, P.M., and Audet, D.M., 2000, Jurassic giant erg deposits, flexure of the United States continental interior, and timing of the onset of Cordilleran shortening: Geology, v. 28, no. 2, p. 159–162.

Allis, R, Chidsey, T, Gywnn, W, Morgan, C, White, S., Adams, M., and Moore, J., 2001, Natural CO_2 reservoirs on the Colorado Plateau and southern Rocky Mountains—candidates for CO_2 sequestration: Proceedings Volume, First National Conference on Carbon Sequestration, May 14–17, 2001, DOE/NETL-2001/1144, Washington, D.C., 19 p.

Allis, R.G., Chidsey, T.C., Jr., Morgan, C.D., Moore, J., and White, S., 2003, CO_2 injection potential beneath large power plants in the Colorado Plateau-Southern Rocky Mountain region, USA: Proceedings Volume, Second

Annual Conference on Carbon Sequestration, May 5–8, 2003, Alexandria, VA, 25 p.

Allis, R.G., Bergfield, D., Moore, J.N., McClure, K., Morgan, C., Chidsey, T.C., Jr., Heath, J., and McPherson, B., 2005, Implications of results from CO_2 systems for long-term monitoring: Proceedings Volume, Fourth Annual Conference on Carbon Capture and Sequestration, May 2-5, 2005, Alexandria, VA, p. 1367–1388.

Allred, I.J., and Blum, M.D., 2021, Early Pennsylvanian sediment routing to the Ouachita Basin (southeastern United States) and barriers to transcontinental sediment transport sourced from the Appalachian orogen based on detrital zircon U-Pb and Hf analysis: Geosphere, v. 18, no. 1, p., 350–369, https://doi.org/10.1130/GES02408.1.

Allred, I.J., and Blum, M.D., 2022, Demarcation of Early Pennsylvanian paleovalleys in depozones of the Appalachian foreland-basin system based on detrital-zircon U-Pb and Hf analysis: Journal of Sedimentary Research, v. 92, no. 10, p. 919–933, https://doi.org/10.2110/jsr.2021.128.

Allred, I.J., Blum, M.D., Frederick, B.C., and Wahbi, A.M., 2023, There and back again—recycling of the Appalachian signature in DZ U-Pb records of Phanerozoic North America: Lithosphere, v. 2023, article ID 8478638, 11 p., https://doi.org/10.2113/2023/8478638.

Anderson, L.W., 2008, Evaluation of the seismogenic potential of the Joes Valley fault zone—Joes Valley Dam, Emery County project, Utah: Bureau of Reclamation Technical Memorandum No. 86-68321-2008-10, 43 p.

Anderson, P.B., Chidsey, T.C., Jr., Sprinkel, D.A, and Willis, G.C., 2024, Geology of Glen Canyon National Recreation Area, Utah-Arizona, *in* Sprinkel, D.A., Chidsey, T.C., Jr., Anderson, P.B., and Willis, G.C., editors, Geology of Utah's parks and monuments (4th edition): Utah Geological Association Publication 28, p. 109–148.

Averitt, P., 1962, Geology and coal resources of the Cedar Mountain quadrangle, Iron County, Utah: U.S. Geological Survey Professional Paper 389, 71 p., 3 plates, scale 1:24,000, https://doi.org/10.3133/pp389.

Averitt, P., Detterman, J.S., Harshbarger, J.W., Repenning, C.A., and Wilson, R.F., 1955, Revisions in correlation and nomenclature in southwestern Utah and Arizona—geologic notes: American Association of Petroleum Geologist Bulletin, v. 39, no. 12, p. 2515–2535.

Averitt, P., and Threet, R.L., 1973, Geologic map of the Cedar City quadrangle, Iron County, Utah: U.S. Geological Survey Geologic Quadrangle Map GQ-1120, 1 plate, scale 1:24,000.

Baker, A.A., 1936, Geology of the Monument Valley-Navajo Mountain region, San Juan County, Utah: U.S. Geological Survey Bulletin 865, 106 p.

Beitler, B., Parry, W.T., and Chan, M.A., 2005, Fingerprints of fluid flow—chemical diagenetic history of the Jurassic Navajo Sandstone, southern Utah, U.S.A.: Journal of Sedimentary Research, v. 75, no. 4, p. 547–561.

Beranek, L.P., Mortensen, J.K., Lane, L.S., Allen, T.L., Fraser, T.A., Hadlari, T., and Zantvoort, W.G., 2010, Detrital zircon geochronology of the Western Ellesmerian clastic wedge, Northwestern Canada—insights on Arctic tectonics and the evolution of the northern Cordilleran miogeocline: Geological Society of America Bulletin, v. 122, nos. 11–12, p. 1899–1911.

Biek, R.F., and Hayden, J.M., 2016, Geologic map of the Kanarraville quadrangle, Iron County, Utah: Utah Geological Survey Map 276DM, 21 p., 2 plates, scale 1:24,000, https://doi.org/10.34191/M-276dm.

Biek, R.F., Willis, G.C., Hylland, M.D., and Doelling, H.H., 2024, Geology of Zion National Park, Utah, *in* Sprinkel, D.A., Chidsey, T.C., Jr., Anderson, P.B., and Willis, G.C., editors, Geology of Utah's parks and monuments (4th edition): Utah Geological Association Publication 28, p. 391–433.

Blakey, R.C., 1994, Paleogeographic and tectonic controls on some Lower and Middle Jurassic erg deposits, Colorado Plateau, *in* Caputo, M.V., Peterson, J.A., and Franczyk, K.J., editors, Mesozoic systems of the Rocky Mountain region, USA: Society for Sedimentary Geology (SEPM), Rocky Mountain Section Guidebook, p. 273–298.

Blakey, R.C., 2013, Using paleogeographic maps to portray Phanerozoic geologic and paleotectonic history of Western North America [abs.]: American Association of Petroleum Geologists Search and Discovery, article no. 30267, 61 p.

Blakey, R., and Ranney, W., 2008, Ancient landscapes of the Colorado Plateau: Grand Canyon, Arizona, Grand Canyon Association, 156 p.

Blank, H.R., Jr., and Mackin, J.H., 1967, Geologic interpretation of an aeromagnetic survey of the Iron Springs district, Utah: U.S. Geological Survey Professional Paper 516-B, p. B1–B14.

Britt, B.B., Chure, D.J., Engelmann, G.F., and Shumway, J.D., 2016, Rise of the erg—paleontology and paleoenvironments of the Triassic-Jurassic transition in northeastern Utah: Geology of the Intermountain West, v. 3, p. 1–32.

Bullock, K.C., 1973, Geology and iron deposits of Iron Springs district, Iron County, Utah: Brigham Young University Geology Studies, v. 20, pt. 1, p. 27–64.

Busby, C.J., Schermer, E.R., and Mattinson, J.M., 2002, Extensional arc setting and ages of Middle Jurassic eolianites, Cowhole Mountains (eastern Mojave Desert block, California), *in* Glazner, A.F., Walker, J.D., and Bartley, J.M., editors, Geologic evolution of the Mojave Desert and southwestern Basin and Range: Geological Society of America Memoir 195, p. 79–91.

Chan, M.A., and Bowen, B.B., 2026, The case of the missing marbles—forensics for geoheritage: Geoheritage, v. 18, article 17, 11 p., https://doi.org/10.1007/s12371-025-01252-9.

Chan, M.A., and Bruhn, R., 2014, Dynamic liquefaction of Jurassic sand dunes—processes, origins, and implications: Earth Surfaces, Processes and Landforms, v. 39, p. 1478–1491.

Chan, M.A., and Parry, W.T., 2002, Rainbow of rocks—mysteries of sandstone colors and concretions in Colorado Plateau canyon country: Utah Geological Survey Public Information Series 77, 17 p.

Chan, M.A., Parrish, J.T., and Hasiotis, S.T., 2023, An erg landscape mystery—an exotic boulder in Jurassic aeolian-fluvial deposits, Grand Staircase Escalante National Monument, Utah, USA: Geological Journal, p. 1–14.

Chan, M.A., Parry, W.T., and Bowman, J.R., 2000, Diagenetic hematite and manganese oxides and fault-related fluid flow in Jurassic sandstones, southeastern Utah: American Association of Petroleum Geologists Bulletin, v. 84, no. 9, p. 1281–1310.

Chan, M.A., Beitler, B., Parry, W.T., Ormo, J., and Komatsu, G., 2005, Analogs of Earth marbles to Mars blueberries—records of groundwater history from red rock to Red Planet: American Association of Petroleum Geologists Search and Discovery, article no. 110028, 32 p.

Chandonia, W.J., and Hogan, J.P., 2023, The Kanarra fold-thrust structure—the leading edge of the Sevier fold-thrust belt, southwestern Utah: Geology of the Intermountain West, v. 10, p. 1–64, https://doi.org/10.31711/giw.v10.pp1-64.

Chidsey, T.C., Jr., 2013, Geology of the San Rafael Swell, east-central Utah, *in* Morris, T.H., and Ressetar, R., editors, The San Rafael Swell and Henry Mountains basin—geologic centerpiece of Utah: Utah Geological Association Publication 42, p. 1–73.

Chidsey, T.C., Jr., 2023, Potential drilling hazards for wells targeting the Cane Creek shale, Pennsylvanian Paradox Formation, Paradox fold and fault belt, southeastern Utah and southwestern Colorado: Geology of the Intermountain West, v. 10, p. 131–167, appendix, https://doi.org/10.31711/giw.v10.pp131-167.

Chidsey, T.C., Jr., DeHamer, J.S., Hartwick, E.E., Johnson, K.R., Schelling, D.D., Sprinkel, D.A., Strickland, D.K., Vrona, J.P., and Wavrek, D.A., 2007, Petroleum geology of Covenant oil field, central Utah thrust belt, *in* Willis, G.C., Hylland, M.D., Clark, D.L., and Chidsey, T.C., Jr., editors, Central Utah—diverse geology of a dynamic landscape: Utah Geological Association Publication 36, p. 273–296.

Chidsey, T.C., Jr., Doelling, H.H., Morgan, C.D., Sprinkel, D.A., Willis, G.C., and Eby, D.E., 2016, Chapter 11—outcrop analogs for major reservoirs, *in* Chidsey, T.C., Jr., editor, Major oil plays in Utah and vicinity: Utah Geological Survey Bulletin 137, p. 207–266.

Chidsey, T.C., Jr., Hartwick, E.E., Johnson, K.R., Schelling, D.D., Sbarra, R., Sprinkel, D.A., Vrona, J.P., and Wavrek, D.A., 2011, Petroleum geology of Providence oil field, central Utah thrust belt, *in* Sprinkel, D.A., Yonkee, W.A., and Chidsey, T.C., Jr., editors, The Sevier orogen—hinterland to foreland evolution of a classic fold and thrust belt: Utah Geological Association Publication 40, p. 213–231.

Chidsey, T.C., Jr., and Morgan, C.D., 1993, Low-BTU gas in Utah, *in* Hjellming, C.A., editor, Atlas of major Rocky Mountain gas reservoirs: New Mexico Bureau of Mines and Mineral Resources, p. 171.

Chidsey, T.C., Jr., Morris, T.H., Carney, S.M., Hansen, A.D., McBride, J.H., and Morgan, C.D., 2020, Surface to subsurface reservoir/aquifer characterization and facies analysis of the Jurassic Navajo Sandstone, central Utah: Utah Geological Survey Special Study 167, 102 p., 3 appendices, 1 plate.

Chidsey, T.C., Jr., and Sprinkel, D.A., 2016, Chapter 3—Triassic-Jurassic Nugget Sandstone thrust belt play, *in* Chidsey, T.C., Jr., editor, Major oil plays in Utah and vicinity: Utah Geological Survey Bulletin 137, p. 35–57.

Chidsey, T.C., Jr., Sprinkel, D.A., Willis, G.C., and Ander-

son, P.B., 2012, Geologic guide along Lake Powell, Glen Canyon National Recreation Area and Rainbow Bridge National Monument, Utah-Arizona, *in* Anderson, P.B., and Sprinkel, D.A., editors, Geologic road, trail, and lake guides to Utah's parks and monuments (2nd edition): Utah Geological Association Publication 29, 76 p.

Chidsey, T.C., Jr, Sprinkel, D.A., Vrona, J.P., Hartwick, E.E., Lester, M., and Sbarra, R., 2014, Covenant oil field, central Utah thrust belt—new interpretation of the reservoir stratigraphy: Rocky Mountain Association of Geologists, The Outcrop, v. 63, no. 12, p. 10–12, 14–17.

Chidsey, T.C., Jr., Willis, G.C., Sprinkel, D.A., and Anderson, P.B., 2024, Geology of Rainbow Bridge National Monument, Utah, *in* Sprinkel, D.A., Chidsey, T.C., Jr., Anderson, P.B., and Willis, G.C., editors, Geology of Utah's parks and monuments (4th edition): Utah Geological Association Publication 28, p. 337–350.

Clyde, C.G., 1987, Groundwater resources of the Virgin River basin in Utah: Logan, Utah State University, Utah Water Research Laboratory, 104 p.

Colson, C.T., 1993, Farnham Dome, *in* Hill, B.G., and Bereskin, S.R., editors, Oil and gas fields of Utah: Utah Geological Association Publication 22, non-paginated.

Cornet, B., and Waanders, G., 2006, Palynomorphs indicate Hettangian (Early Jurassic) age for middle Whitmore Point Member of the Moenave Formation, Utah and Arizona, *in* Harris, J.D., Lucas, S.G., Spielmann, J.A., Lockley, M.G., Milner, A.R.C., and Kirkland, J.I., editors, Terrestrial Triassic-Jurassic transition: New Mexico Museum of Natural History and Science Bulletin 37, p. 1–17.

Cross, W., 1908, The Triassic portion of the Shinarump Group, Powell: Journal of Geology 16, p. 97–123.

Dalrymple, A., and Morris, T.H., 2007, Facies analysis and reservoir characterization of outcrop analogs of the Navajo Sandstone in the central Utah thrust belt exploration play, *in* Willis, G.C., Hylland, M.D., Clark, D.L., and Chidsey, T.C., Jr., editors, Central Utah—diverse geology of a dynamic landscape: Utah Geological Association Publication 36, p. 311–322.

Dames & Moore, 1972, Geological and structural evaluation of Rainbow Bridge, Rainbow Bridge National Monument, Utah: Unpublished consultant's report for the Upper Colorado River Commission, 39 p., 4 appendices.

Davis, G.H., 1999, Structural geology of the Colorado Plateau region of southern Utah, with special emphasis on deformation bands: Geological Society of America Special Paper 342, 157 p.

Dickinson, W.R., and Gehrels, G.E., 2003, U-Pb ages of detrital zircons from Permian and Jurassic eolian sandstones of the Colorado Plateau, USA—paleogeographic implications: Sedimentary Geology, v. 163, issues 1-2, p. 29–66.

Dickinson, W.R., and Gehrels, G.E., 2009, U-Pb ages of detrital zircons in Jurassic eolian and associated sandstones of the Colorado Plateau—evidence for transcontinental dispersal and intraregional recycling of sediment: Geological Society of America Bulletin, v. 121, no. 3-4, p. 408–433, https://doi.org/10.1130/b26406.1.

Dickinson, W.R., and Gehrels, G.E., 2010, Synoptic record in space and time of provenance relations for Mesozoic strata in south-central Utah from U-Pb ages of detrital zircons, *in* Carney, S.M., Tabet, D.E., and Johnson, C.L., editors, Geology of south-central Utah: Utah Geological Association Publication 39, p. 178–193.

Doe, T.W., and Dott, R.H., 1980, Genetic significance of deformed cross bedding—with examples from the Navajo and Weber Sandstones of Utah: Journal of Sedimentary Petrology, v. 50, no. 3, p. 793–812.

Doelling, H.H., 1968, Southern Utah oddities lure rock hounds: Utah Geological Survey Quarterly Review, v. 2, no. 3., p. 7.

Doelling, H.H., 1975, Geology and mineral resources of Garfield County, Utah: Utah Geological and Mineral Survey Bulletin 107, 175 p., 1 plate, scale 1:250,000.

Doelling, H.H., and Davis, F.D., 1989, The geology of Kane County, Utah—geology, mineral resources, geologic hazards: Utah Geological and Mineral Survey Bulletin 124, 192 p.

Doelling, H.H., and Hylland, M.D., 2002, San Rafael Swell proposed as site of new national monument: Utah Geological Survey, Survey Notes, v. 34, no. 2, p. 9–11.

Doelling, H.H., and Chidsey, T.C., Jr., 2012, Dead Horse Point State Park and vicinity geologic road logs, Grand and San Juan Counties, Utah, *in* Anderson, P.B., and Sprinkel, D.A., editors, Geologic road, trail, and lake guides to Utah's parks and monuments (2nd edition): Utah Geological Association Publication 29, 38 p.

Doelling, H.H., Blackett, R.E., Hamblin, A.H., Powell, J.D., Pollock, G.L., Sprinkel, D.A., and Titus, A.L., 2024, Geology of Grand Staircase-Escalante National Monument,

Utah, *in* Sprinkel, D.A., Chidsey, T.C., Jr., Anderson, P.B., and Willis, G.C., editors, Geology of Utah's parks and monuments (4th edition): Utah Geological Association Publication 28, p. 251–297.

Doelling, H.H., Sprinkel, D.A., Kowallis, B.J., and Kuehne, P.A., 2013, Temple Cap and Carmel Formations in the Henry Mountains basin, Wayne and Garfield Counties, Utah, *in* Morris, T.H., and Ressetar, R., editors, The San Rafael Swell and Henry Mountains basin—geologic centerpiece of Utah: Utah Geological Association Publication 42, p. 279–318.

Dubiel, R.F., 1994, Triassic depositional systems, paleogeography, and paleoclimate of the Western Interior, *in* Caputo, M.V., Peterson, J.A., and Franczyk, K.J., editors, Mesozoic systems of the Rocky Mountain region, USA: Society for Sedimentary Geology (SEPM), Rocky Mountain Section Guidebook, p. 133–168.

Elder, J., unpublished date, Aeolian dunes and sandstone—overview and terminology, *in* Geology—sand and dunes: online, https://smallpond.ca/jim/sand/index.html, accessed April 2025.

Ford, R.L., Wilkins, D.E., Clement, W.P., Nicoll, K., and Gillman, S.L., 2024, Geology and geomorphology of Coral Pink Sand Dunes State Park, Utah, *in* Sprinkel, D.A., Chidsey, T.C., Jr., Anderson, P.B., and Willis, G.C., editors, Geology of Utah's parks and monuments (4th edition): Utah Geological Association Publication 28, p. 517–544.

Fossen, H., 2016, Structural geology, chapter 7 – deformation bands and fractures in porous rocks: Cambridge University Press, p. 143–149.

Fossen, H., Schultz, R.A., and Torabi, A., 2011, Conditions and implications for compaction band formation in the Navajo Sandstone, Utah: Journal of Structural Geology, v. 33, p. 1477–1490.

Freeman, W.E., and Visher, G.S., 1975, Stratigraphic analysis of the Navajo Sandstone: Journal Sedimentary Petrology, v. 45, no. 3, p. 651–668.

Freethey, G.W., and Cordy, G.E., 1991, Geohydrology of Mesozoic rocks in the Upper Colorado River Basin in Arizona, Colorado, New Mexico, Utah, and Wyoming, excluding the San Juan Basin: U.S. Geological Survey Professional Paper 1411-C, 118 p.

Gregory, H.E., 1917, Geology of the Navajo Country—a reconnaissance of parts of Arizona, New Mexico, and Utah: U.S. Geological Survey Professional Paper 93, 161 p.

Gregory, H.E., 1948, Geology and geography of central Kane County, Utah: Geological Society of America Bulletin, v. 59, p. 211–247.

Gregory, H.E., 1950, Geology and geography of the Zion National Park region, Utah and Arizona: U.S. Geological Survey Professional Paper 220, 200 p.

Gregory, H.E., and Moore, R.C., 1931, The Kaiparowits region, a geographic and geologic reconnaissance of parts of Utah and Arizona: U.S. Geological Survey Professional Paper 164, 161 p.

Hamblin, W.K., 2004, Beyond the visible landscape—aerial panoramas of Utah's geology: Provo, Utah, Brigham Young University Department of Geology, 300 p.

Hanson, A.D., 2007, Reservoir characteristics and outcrop analogs of the Navajo Sandstone in the central Utah thrust exploration belt play: Provo, Utah, Brigham Young University, M.S. thesis, 110 p.

Hansen, Allen, & Luce, Inc., 2005, Washington County Water Conservancy District—petition for classification of the Navajo/Kayenta and Upper Ash Creek aquifers, final report: Online, https://www.wcwcd.gov/wp-content/themes/wcwcd/pdf/Classification%20Petition_2005.pdf, accessed February 2025.

Hartwick, E.E., 2010, Eolian architecture of sandstone reservoirs in the Covenant field, Sevier County, Utah: American Association of Petroleum Geologists Search and Discovery, article no. 20091, 23 p.

Hasiotis, S.T., Chan, M.A., and Parrish, J.T, 2021, Defining bounding surfaces within and between eolian and non-eolian deposits, Lower Jurassic Navajo Sandstone, Moab area, Utah, U.S.A.—implications for subdividing erg system strata: Journal of Sedimentary Research, v. 91, p. 1275–1304, https://doi.org/10.2110/jsr.2021.027.

Heilweil, V.M., Freethey, G.W., Wilkowske, C.D., Stolp, B.J., and Wilberg, D.E. 2000, Geohydrology and numerical simulation of groundwater flow in the central Virgin River basin of Iron and Washington Counties, Utah: Utah Department of Natural Resources, Division of Water Rights, Technical Publication No. 116, 139 p.

Heilweil, V.M., Watt, D.E., Solomon, D.K., and Goddard, K.E., 2002, The Navajo aquifer system of southwestern Utah, *in* Lund, W.R., editor, Field guide to geologic excursions in southwestern Utah and adjacent areas of Arizona and Nevada: U.S. Geological Survey Open-File Report 02-172, p. 105–130.

Hintze, L.F., 1980, Geologic map of Utah: Utah Geological Survey Map M-A-1, 2 sheets, scale 1:500,000, https://doi.org/10.34191/M-A1.

Hintze, L.F., and Kowallis, B.J., 2021, Geologic history of Utah: Provo, Utah, Brigham Young University Department of Geological Sciences Special Publication 10, 266 p.

Hintze, L.F., Willis, G.C., Laes, D.Y.M., Sprinkel, D.A., and Brown, K.K.D., 2000, Digital geologic map of Utah: Utah Geological Survey Map 179DM, scale 1:500,000.

Hintze, L.F., and Yochelson, E., 2009, The Grand Staircase at Kanab Creek in 1879—its remarkable first measurement by C.D. Walcott: Brigham Young University Geology Studies Special Publication 10, 55 p.

Hunt, J.M., 1979, Petroleum geochemistry and geology: San Francisco, California, W.H. Freeman and Company, 616 p.

Hurlow, H.A., 1998, The geology of the central Virgin River basin, southwestern Utah, and its relation to ground-water conditions: Utah Geological Survey Water-Resources Bulletin 26, 53 p., 6 plates.

Jackson, J.A., 1997, Glossary of geology (4th edition): American Geologic Institute, p. 769.

Kirkland, J.I., King, M.R., and Bylund, K.G., 2025, Revisiting the Cretaceous Mancos Group in Utah—problems, previous methods, and new perspectives on a world-class Cretaceous marine section: Geology of the Intermountain West, v. 12, p. 75–154, https://doi.org/10.31711/giw.v12.pp75-154.

Knudsen, T.R., 2024, Geologic map of the Cedar City 7.5-minute quadrangle, Iron County, Utah: Utah Geological Survey Map 302DM, 18 p., 2 plates, scale 1:24,000, https://doi.org/10.34191/M-302DM.

Kocurek, G., and Dott, R.H., 1983, Jurassic paleogeography and paleoclimate of the central and southern Rocky Mountains region, *in* Reynolds, M.W., and Dolly, E.D., editors, Mesozoic paleogeography of the west-central United States: Society for Sedimentary Geology (SEPM), Rocky Mountain Section, p. 101–116.

Kowallis, B.J., Christiansen, E.H., Deino, A.L., Zhang, C., and Everett, B.H., 2001, The record of Middle Jurassic volcanism in the Carmel and Temple Cap Formations of southwestern Utah: Geological Society of America Bulletin, v. 113, no. 3, p. 373–387.

Leary, R.J., Umhoefer, P., Smith, M.E., Tyson M., Smith, T.M., Saylor, J.E., Riggs, N., Burr, G., Lodes, E., Foley, D., Licht, A., Mueller, M.A., and Baird, C., 2020, Provenance of Pennsylvanian–Permian sedimentary rocks associated with the Ancestral Rocky Mountains orogeny in southwestern Laurentia—implications for continental-scale Laurentian sediment transport systems: Lithosphere, v. 12, no. 1, p. 88–121.

Lindquist, S.J., 1988, Practical characterization of eolian reservoirs for development—Nugget Sandstone, Utah-Wyoming thrust belt: Sedimentary Geology, v. 56, p. 315–339.

Lockley, M.G., Farlow, J.O., Milner, A.R.C., and Davidson, J., 2026, *Eubrontes* out west (and beyond)—distribution, morphology, ichnotaxonomy, and associated ichnofauna of footprints of large, Early Jurassic theropod trackmakers: Geology of the Intermountain West, v. 13, v. 13, p. 1–51, https://doi.org/10.31711/giw.v13.pp1-51.

Lockley, M.G., Hunt, A.P, Meyer, C., Rainforth, E.C., and Schultz, J.J., 1998, A survey of fossil footprint sites at Glen Canyon National Recreation Area (Western USA)—a case study in documentation of trace fossil resources at a national preserve: Ichnos, v. 5, p. 177–211.

Loope, D., Rowe, C., and Joeckel, M., 2001, Annual monsoon rains recorded by Jurassic dunes: Nature, v. 412, p. 64–66.

Lynds, R., and Hajek, E., 2006, Conceptual model for predicting mudstone dimensions in sandy braided-river reservoirs: American Association of Petroleum Geologists Bulletin, v. 90, no. 8, p. 1273–1288.

Marzolf, J.E., 1994, Reconstruction of the early Mesozoic Cordilleran cratonal margin adjacent to the Colorado Plateau, *in* Caputo, M.V., Peterson, J.A., and Franczyk, K.J., editors, Mesozoic systems of the Rocky Mountain region, USA: Society for Sedimentary Geology (SEPM), Rocky Mountain Section Guidebook, p. 181–216.

Matheny, J.P, 1983, Blaze Canyon, *in* Fassett, J.E., editor, Oil and gas fields in the Four Corners area: Four Corners Geological Society Guidebook, v. III, p. 1067–1069.

McPherson, B., editor, 2018, CarbonSafe Rocky Mountain Phase I—ensuring safe subsurface storage of carbon dioxide in the Intermountain West, Final Report, reporting period March 1, 2017–August 31, 2018: U.S. Department of Energy, DE-FE0029280, 558 p., 14 appendices, CarbonSAFE Rocky Mountain Phase I: Ensuring Safe Subsurface Storage of Carbon Dioxide in the Intermountain West (Technical Report) | OSTI.GOV.

Moore, B.J., and Sigler, S., 1987, Analyses of natural gases, 1917–85: U.S. Bureau Mines Information Circular 9129, p. 847–948.

Morgan, C.D, 2007, Structure, reservoir characterization, and carbon dioxide resources of Farnham Dome field, Carbon County, Utah, *in* Willis, G.C., Hylland, M.D., Clark, D.L., and Chidsey, T.C., Jr., editors, Central Utah—diverse geology of a dynamic landscape: Utah Geological Association Publication 36, p. 297–310.

Morgan, C.D., and Chidsey, T.C., Jr., 1991, Gordon Creek, Farnham Dome, and Woodside fields, Carbon and Emery Counties, Utah, *in* Chidsey, T.C., Jr., editor, Geology of east-central Utah: Utah Geological Association Publication 19, p. 301–309.

Morgan, C.D., and Kirby, S.M., 2017, Uinta Basin reservoirs/aquifers—Triassic-Jurassic Glen Canyon Group through the Cretaceous Cedar Mountain and Dakota Formations, *in* Chidsey, T.C., Jr., compiler and editor, Produced water in the Uinta Basin, Utah—evaluation of reservoirs, water storage aquifers, and management options: Utah Geological Survey Bulletin 138, p. 59–139.

Morris, T.H., Manning, V.W., and Ritter, S.M., 2024, Geology of Capitol Reef National Park, Utah, *in* Sprinkel, D.A., Chidsey, T.C., Jr., Anderson, P.B., and Willis, G.C., editors, Geology of Utah's parks and monuments (4th edition): Utah Geological Association Publication 28, p. 87–109.

Moulton, F.C., 1975, Lower Mesozoic and Upper Paleozoic petroleum potential of the hingeline area, *in* Boylard, D.W., editor, Symposium on deep drilling frontiers in the central Rocky Mountains: Rocky Mountain Association of Petroleum Geologists Guidebook, p. 87–97.

Neuendorf, K.E., Mehl, J.P, Jr., and Jackson, J.A., 2011, Glossary of geology (5th edition): American Geosciences Institute, 800 p.

Neuhauser, K.R., 1988, Sevier-age ramp-style thrust faults at Cedar Mountain, northwest San Rafael Swell (Colorado Plateau), Emery County, Utah: Geology, v. 16, no. 4, p. 299–302.

Nielsen, G.B., 2010, Geologic map and coloration facies of the Jurassic Navajo Sandstone, Snow Canyon State Park and areas of the Red Cliffs Desert Reserve, Washington County, Utah: Utah Geological Survey Open-File Report 561, 15 p., 2 plates.

Nielsen, G.B., and Chan, M.A., 2009, Mapping and correlation of diagenetic coloration facies, Jurassic Navajo Sandstone, Snow Canyon State Park, Utah, *in* Tripp, B.T., Krahulec, K., and Jordan, L.J., editors, Geology and geologic resources and issues of western Utah: Utah Geological Association Publication 38, p. 67–96.

Nielsen, G.B., Chan, M.A., and Petersen, E.U., 2009, Diagenetic coloration facies and alternation history of the Jurassic Navajo Sandstone, Zion National Park and vicinity, southwestern Utah, *in* Tripp, B.T., Krahulec, K., and Jordan, L.J., editors, Geology and geologic resources and issues of western Utah: Utah Geological Association Publication 38, p. 97–123.

Parris, J.T., 1993, Climate of the supercontinent Pangea: Journal of Geology, v. 101, issue 2, p. 215–233.

Parrish, J.T., Hasiotis, S.T., and Chan, M.A., 2017, Carbonate deposits in the Lower Jurassic Navajo Sandstone, southern Utah and northern Arizona, U.S.A.: Journal of Sedimentary Research, v. 87, p. 740–762.

Parrish, J.T., Rasbury, E.T., Chan, M.A., and Hasiotis, S.T., 2019, Earliest Jurassic U-Pb ages from carbonate deposits in the Navajo Sandstone, southeastern Utah, USA: Geology, v. 47, no. 11, p. 1015–1019, https://doi.org/10.1130/G46338.1.

Parry, W.T., Forster, C.B., Evans, J.P., Bowen, B.B., and Chan, M.A., 2007, Geochemistry of CO_2 sequestration in the Jurassic Navajo Sandstone, Colorado Plateau, Utah: Environmental Geoscience, v. 14, no. 2, p. 91–109.

Peterson, F., 1988, Pennsylvanian to Jurassic eolian transportation systems in the Western United States: Sedimentary Geology, v. 56, no. 1/4, p. 207–260.

Peterson, F., 1994, Sand dunes, sabkhas, streams, and shallow seas—Jurassic paleogeography in the southern part of the Western Interior basin, *in* Caputo, M.V., Peterson, J.A., and Franczyk, K.J., editors, Mesozoic systems of the Rocky Mountain region, USA: Society for Sedimentary Geology (SEPM), Rocky Mountain Section Guidebook, p. 233–272.

Peterson, F., and Pipiringos, G.N., 1979, Stratigraphic relationships of the Navajo Sandstone to Middle Jurassic formations in parts of southern Utah and northern Arizona, *in* Unconformities, correlations, and nomenclature of some Triassic and Jurassic rocks, Western Interior United States: U.S. Geological Survey Professional Paper, 1035-B, p. B1-B43.

Peterson, V.E., 1961, Farnham Dome and Gordon Creek fields, Carbon County, Utah, *in* Preston, D., editor, A symposium of the oil and gas fields of Utah: Intermountain Association of Petroleum Geologists, unpaginated.

Phillips, S.P., 2012, Discriminant analysis of XRF data from sandstones of like facies and appearance—a method for

identifying a regional unconformity, paleotopography, and diagenetic histories: Provo, Utah, Brigham Young University, M.S. thesis, 121 p.

Phillips, S.P., and Morris, T.H., 2013, Identification of an extensive paleotopographic high on the Navajo Sandstone by surface to subsurface correlation of the Temple Cap Formation and time-equivalent portions of the Page Sandstone, *in* Morris, T.H., and Ressetar, R., editors, The San Rafael Swell and Henry Mountains basin—geologic centerpiece of Utah: Utah Geological Association Publication 42, p. 261–278.

Phillips, S.P., Morris, T.H., Tingey, D.G., Eggett, D.L., and Zhou, W., 2015, Discriminant analysis of elemental data to differentiate formations of like facies vertically across an unconformity and laterally across a paleotopographic divide: Journal of Sedimentary Research, v. 85, no. 11, p. 1293–1309.

Picard, M.D., 1975, Facies, petrography and petroleum potential of Nugget Sandstone (Jurassic), southwestern Wyoming and northeastern Utah, *in* Bolyard, D.W., editor, Symposium on deep drilling frontiers of the central Rocky Mountains: Rocky Mountain Association of Petroleum Geologists Guidebook, p. 109–127.

Pipiringos, G.N., and O'Sullivan, R.B., 1978, Principal unconformities in Triassic and Jurassic rocks, Western Interior United States—a preliminary survey: U.S. Geological Survey Professional Paper 1035-A, 29 p.

Rahl, J.M., Reiners, P.W., Campbell, I.H., Nicolescu, S., and Allen, C.M., 2003, Combined single-grain (U-Th)/He and U/Pb dating detrital zircons from the Navajo Sandstone, Utah: Geology, v. 31, no. 9, p. 761–764.

Riese, D. J., Hasiotis, S.T., and Odier, G.P., 2011, Synapsid burrows and associated trace fossils in the Lower Jurassic Navajo Sandstone, southeastern Utah, U.S.A., indicates a diverse community living in a wet desert ecosystem: Journal of Sedimentary Research, v. 81, no. 3-4, https://doi.org/10.2110/jsr.2011.25.

Rowley, P.D., and Barker, D.S., 1978, Geology of the Iron Springs mining district, Utah, *in* Shawe, D.R., editor, Guidebook to mineral deposits of southwestern Utah: Utah Geological Association Publication 7, p. 49–58.

Rowley, P.D., and Dixon, G.L., 2004, The role of geology in increasing Utah's ground-water resources from faulted terranes—lessons from the Navajo Sandstone, Utah, and the Death Valley flow system, Nevada-California, *in* Spangler, L.E., editor, Groundwater in Utah—source, protection, and remediation: Utah Geological Association Publication 31, p. 27–41.

Rowley, P.D., Dixon, G.L., D'Agnese, F.A., O'Brien, G.M., and Brickney, D.W., 2004, Geology and hydrology of the Sand Hollow Reservoir and well field area, Washington County, Utah: St. George, Utah, Washington County Water Conservancy District Report WCWCD-01, 14 p.

Rowley, P.D., Williams, V.S., Vice, G.S., Maxwell, D.J., Hacker, D.B., Snee, L.W., and Mackin, J.H., 2006, Interim geological map of the Cedar City 30' x 60' quadrangle, Iron and Washington Counties, Utah: Utah Geological Survey Open-File Report 476DM, 23 p., 2 plates, scale 1:100,000, https://ugspub.nr.utah.gov/publications/open_file_reports/OFR-476.pdf.

Sanderson, I.D., 1974, Sedimentary structures and their environmental significance in the Navajo Sandstone, San Rafael Swell, Utah: Brigham Young University Geology Studies, v. 21, pt. 1, p. 215–246.

Sansom, P.J., 1992, Sedimentology of the Navajo Sandstone, southern Utah, USA: Oxford, England, Department of Earth Sciences and Wolfson College, Ph.D. dissertation, 291 p.

Santucci, V.L., and Kirkland, J.I., 2010, An overview of the National Park Service paleontological resources from the parks and monuments in Utah, *in* Sprinkel, D.A., Chidsey, T.C., Jr., and Anderson, P.B., editors, Geology of Utah's parks and monuments (3rd edition): Utah Geological Association Publication 28, p. 589–623.

Schelling, D.D., Strickland, D.K., Johnson, K.R., and Vrona, J.P., 2007, Structural geology of the central Utah thrust belt, *in* Willis, G.C., Hylland, M.D., Clark, D.L., and Chidsey, T.C., Jr., editors, Central Utah—diverse geology of a dynamic landscape: Utah Geological Association Publication 36, p. 1–29.

Schultz, R.A., 2019, Geologic fracture mechanics, chapter 7 – deformation bands: Cambridge University Press, p. 265–331.

Sertich, J.J.W., and Loewen, M.A., 2010, A new basal sauropodomorph dinosaur from the Lower Jurassic Navajo Sandstone of southern Utah: PLos One, v. 5, no. 3, paper e9789, https://doi.org/10.1371/journal.pone.0009789.

Smith, K.D., Szymanski, E., Hardwick, C., and Hurlbut, W., 2022, Reducing geologic risk uncertainty for carbon sequestration using modern gravity surveys and modelling

in Iron County, Utah [abs.]: Geological Association of America, Rocky Mountain Section Meeting (Denver, Colorado), paper no. 204-5, https://doi.org/10.1130/abs/2022AM-382816.

Spangler, L.E., Naftz, D.L., and Peterman, Z.E., 1996, Hydrology, chemical quality, and characterization of salinity in the Navajo aquifer in and near the Greater Aneth oil field, San Juan County, Utah: U.S. Geological Survey Water-Resources Investigations Report 96–4155, 90 p.

Sprinkel, D.A., Kowallis, B.J., Waanders, G., Doelling, H.H., and Kuehne, P.A., 2009, The Middle Jurassic Temple Cap Formation, southern Utah—radiometric age, palynology, and correlation with the Gypsum Spring Member of the Twin Creek Limestone and Harris Wash Member of the Page Sandstone [abs.]: Geological Society of America Abstracts with Programs, v. 41, no. 7, p. 690.

Sprinkel, D.A., Doelling, H.H., Kowallis, B.J., Waanders, G., and Kuehne, P.A., 2011a, Early results of a study of Middle Jurassic strata in the Sevier fold and thrust belt, Utah, *in* Sprinkel, D.A., Yonkee, W.A., and Chidsey, T.C., Jr., editors, Sevier thrust belt—northern and central Utah and adjacent areas: Utah Geological Association Publication 40, p. 151–172.

Sprinkel, D.A., Kowallis, B.J., and Jensen, P.H., 2011b, Correlation and age of the Nugget Sandstone and Glen Canyon Group, Utah, *in* Sprinkel, D.A., Yonkee, W.A., and Chidsey, T.C., Jr., editors, Sevier thrust belt—northern and central Utah and adjacent areas: Utah Geological Association Publication 40, p. 131–149.

Sprinkel, D.A., Doelling, H.H., Kowallis, B.J., Waanders, G.L., and Kuehne, P.A., 2024, Stratigraphy, correlation, and age of the Gypsum Spring, Temple Cap, Arapien, Carmel, and Twin Creek Formations (Early and Middle Jurassic) of Utah and surrounding states: Contract Deliverable 18 to the Utah Geological Survey, 220 p., 2 appendices.

Steele, P.A., Chan, M.A., and Wheatley, D.F., 2018, Characterization of the Jurassic Navajo Sandstone of central Utah—a potential carbon capture and sequestration reservoir [abs.]: American Association of Petroleum Geologists Search and Discovery, article no. 90323, 1 p.

Stewart, J.H., and Suczek, C.A., 1977, Cambrian and latest Precambrian paleogeography and tectonics in the Western United States, *in* Stewart, I.J.H., Stevens, C.H., and Fritsche, A.E., editors, Paleozoic paleogeography of the Western United States: Society for Sedimentary Geology (SEPM), Pacific Section, Pacific Coast Paleogeography Symposium, p. 1–18.

Stokes, W.L., 1991, Petrified mini-forests of the Navajo Sandstone, east-central Utah: Utah Geological Survey, Survey Notes, v. 25, no. 1, p. 14–19.

Strickland, D., Johnson, K.R., Vrona, J.P., Schelling, D.D., and Wavrek, D.A., 2005, Structural architecture, petroleum systems, and geological implications for the Covenant field discovery, Sevier County, Utah [abs.]: American Association of Petroleum Geologists Search and Discovery, article no. 110014.

Szymanski, E., 2022, Assessing geologic carbon sequestration opportunities in Utah: Utah Geological Survey, Survey Notes, v. 54, no. 2, p. 1–3.

Szymanski, E., Vanden Berg, M.D., Jagniecki, E.A., Jensen, A. and Moodie, N., 2022a, Mitigating geologic risk uncertainty for carbon (CO_2) sequestration in multiple subsurface targets in the Iron Springs district, Iron County, Utah [abs.]: American Association of Petroleum Geologists, Rocky Mountain Section Meeting Search and Discovery, article no. 91201.

Szymanski, E., Vanden Berg, M.D., Moodie, N., Jagniecki, E.A., Hardwick, C., Jensen, A., Hurlbut, W., and Smith, K., 2022b, Assessing the geologic carbon (CO_2) sequestration potential of multiple subsurface targets in the Iron Springs district, Iron County, Utah [abs.]: Geological Society of America Abstracts with Programs, v. 54, no. 2, https://doi: 10.1130/abs/2022CD-373696.

Thomas, B.E., 1989, Simulation and analysis of the ground-water system in Mesozoic rocks in the Four Corners area, Utah, Colorado, Arizona, and New Mexico: U.S. Geological Survey Water-Resources Investigations Report 88-4086, 89 p.

Thorman, C.H., 2011, The Elko orogeny—a major tectonic event in eastern Nevada-western Utah, *in* Sprinkel, D.A., Yonkee, W.A., and Chidsey, T.C., Jr., editors, Sevier thrust belt—northern and central Utah and adjacent areas: Utah Geological Association Publication 40, p. 117–129.

Thorman, C.H., Sandberg, C.A., Henry, C.D., Zuza, A.V., and Ressel, M.W., 2020, The Late Middle Jurassic Elko orogeny—an update [abs.], *in* Koutz, F.R., and Pennell, W.M., editors, Geology and ore deposits of the Basin and Range—Volume 2: Geological Society of Nevada, p. 1403–1407.

Tran, T., Milner, A.R.C., Tweet, J.S., DeBlieux, D.D., Hunt-Foster, R., Shaffer, A.B., Kirkland, J.I., Warner-Cowgill, E., and Santucci, V.L., 2025, A visual paleontological inventory of Utah's National Park Service areas: Geology of the Intermountain West, v. 12, p. 221–292, https://doi.org/10.31711/giw.v12.pp221-292.

Trettin, H.P., 1991, Silurian–early Carboniferous deformational phases and associated Metamorphism and Plutonism, Arctic Islands, *in* Trettin, H.P., editor, Geology of the Innuitian Orogen and Arctic platform of Canada and Greenland: Geological Survey of Canada, Geology of Canada, p. 295–341.

Tuesink, M.F., 1989, Depositional analysis of an eolian-fluvial environment—the intertonguing of the Kayenta Formation and Navajo Sandstone (Jurassic) in southwestern Utah: Flagstaff, Northern Arizona University, M.S. thesis, 189 p.

Utah Division of Oil, Gas and Mining, 2026, Oil and gas production report by field, December 2025: Online, https://oilgas.ogm.utah.gov/pub/Publications/Reports/Prod/Field/fld_dec_2025.pdf, accessed March 2026.

Van Kooten, G.K., 1988, Structure and hydrocarbon potential beneath the Iron Springs laccolith, southwestern Utah: Geological Society of America Bulletin, v. 100, no. 10, p. 1533–1540.

Walcott, C.D., 1879, Unpublished records pertaining to his Kanab Creek work are kept in the Smithsonian Institution Archives under Walcott Collection, Record Unit 7004; his daily diary from July 21 to November 27, 1879, is in the Collection Division 5, box 11, folder 2; his field notebook is in box 29, folder 26; his 1880 transcriptions of his field notes are in box 29, folders 16 and 25.

Wavrek, D.A., Ali-Adeeb, J., Chao, J.C., Santon, L.E., Hardwick, E.A., Strickland, D.K., and Schelling, D.D., 2007, Paleozoic source rocks in the central Utah thrust belt—organic facies response to tectonic and paleoclimatic variables [abs.]: American Association of Petroleum Geologists, Rocky Mountain Section Meeting Official Program, p. 58–59.

Wavrek, D.A., Schelling, D.D., Sbarra, R., Vrona, J.P., and Johnson, K.R., 2010, Central Utah thrust belt discoveries—a tale of two hydrocarbon charges [abs.]: American Association of Petroleum Geologists, Rocky Mountain Section Meeting, Official Program with Abstracts, p. 72–73.

Webster, D., 2002, Alashan—China's unknown Gobi: National Geographic, v. 201, no. 1, p. 48-76.

Weiss, E., 1991, Regional ground-water flow in Upper and Middle Paleozoic rocks in southeastern Utah and adjacent parts of Arizona, Colorado, and New Mexico: U.S. Geological Survey Water-Resources Investigations Report 90-4079, 57 p.

White, S., Allis, R.G., Moore, J., Chidsey, T.C., Jr., Morgan, C.D., Gwynn, W., and Adams, M., 2003, Injection of CO_2 into an unconfined aquifer located beneath the Colorado Plateau, central Utah, USA: Proceedings Volume, Second Annual Conference on Carbon Sequestration, May 5–8, 2003, Alexandria, Virginia, 15 p.

White, S.P., Allis, R.G., Moore, J., Chidsey, T.C., Jr., Morgan, C., Gwynn, W., and Adams, M., 2005, Simulation of reactive transport of injected CO_2 on the Colorado Plateau, Utah, USA: Chemical Geology, v. 217, issues 3-4, p. 387–405.

Wikipedia, 2025, Charles Doolittle Walcott: Online, https://en.wikipedia.org/wiki/Charles_Doolittle_Walcott, accessed November 19, 2025.

Wilbur, J.H., 2007, The dimensions of Rainbow Bridge: Online, The Natural Arch and Bridge Society, https://www.naturalarches.org/archinfo/rainbow.htm, accessed January 14, 2025.

Willis, G.C., and Hayden, J.M., 2015, Geologic map of the Santa Clara quadrangle, Washington County, Utah: Utah Geological Survey Map 271DR, 23 p., appendix, 2 plates, scale 1:24,000, https://doi.org/10.34191/M-271DM.

Wikipedia, 2026, Teepee structure: Online, https://en.wikipedia.org/wiki/Teepee_structure, accessed March 2026.